A PREPARATIVE AND KINETIC STUDY OF SELENITE SUBSTITUTION WITH AQUO TRANSITION METAL COMPLEXES

by

Alan David Fowless

B.Sc.(Hons.), University of Adelaide, 1969.

Thesis presented for the degree of

Doctor of Philosophy

Department of Physical and Inorganic Chemistry

UNIVERSITY OF ADELAIDE

September, 1973

STATEMENT

This thesis contains no material previously submitted for a degree or diploma in any University, and to the best of my knowledge and belief, contains no material previously published or written by another person, except where due reference is made in the text.

Alan D. Fowless

September, 1973

ACKNOWLEDGEMENTS

I wish to sincerely thank my supervisor, Prof. D.R. Stranks, for his encouragement and assistance throughout this project. Thanks are also due to Professor D.O. Jordan, Head of the Department of Physical and Inorganic Chemistry, for granting me the facilities to carry out this work.

I would also like to thank other members of staff and research students who have assisted me in this work; in particular Mr. Ray Middleton who constructed the stopped-flow apparatus and drew the diagrams for it, and Mr. Andrew Thornton for his advice on certain aspects of experimental and computing techniques.

I acknowledge the financial assistance of a Commonwealth Postgraduate Award.

I express sincere thanks to Miss Kathy Whittall for typing the manuscript, and Miss M. Roberts for preparing the diagrams.

Finally, I wish to thank my parents for their help and sacrifices over the years.

ABBREVIATIONS

The following abbreviations will be used throughout this thesis.

en	ethylenediamine(1,2-diaminoethane), $NH_2CH_2CH_2NH_2$
tn	trimethylenediamine(1,3-diaminopropane), $NH_2CH_2CH_2CH_2NH_2$
tren	2, 2',2''-triaminotriethylamine
Me_6tren	2, 2',2''-tri(N,N-dimethylamino)triethylamine
triol	1,1,1-trimethylolethane
diamol	1,1-dimethylamino-1-methylolethane
QAS	tris-(o-diphenylarsinophenyl)arsine
Qas	tris-(o-dimethylarsinophenyl)arsine
T-B	Trizma Base (tris(hydroxymethyl)amino methane)
CBM-OH_2	Aquocobalamin

All temperature measurements are in degrees Celsius unless otherwise specified.

Summary

The substitution reactions of $[Co(NH_3)_5OH_2]^{3+}$, $[Rh(NH_3)_5OH_2]^{3+}$, *cis*- and *trans*-$[Co(en)_2(OH_2)_2]^{3+}$, and *cis*- and *trans*-$[Co(tn)_2(OH_2)_2]^{3+}$ with selenite have been studied over the pH range 1-10. In addition, preliminary investigations have been made into the substitution reactions of $[Ni(Me_6tren)OH_2]^{2+}$ with Cl^-, Br^-, N_3^-, and $HSeO_3^-$, and also the reaction of aquocobalamin (Vitamin B12a) with selenite.

In the case of aquo-complexes of cobalt(III) (and also $[Rh(NH_3)_5OH_2]^{3+}$) the reaction half-times at 25° range from several seconds around pH 10 to 30 millisecs around pH 3. These short half-times contrast with the half-times of many hours for water-exchange with the aquo-ligands, and the half-time of minutes for the oxygen-exchange rate between selenite and water at pH 10.

Infrared and analytical studies of the crystalline selenito products show that selenite is oxygen-bonded to the metal centre as a monodentate ligand, as in $[Co(NH_3)_5OSeO_2]^+$. However, under forcing conditions selenite can also be made to act as a bidentate ligand bonded through two oxygen atoms, as in $[Co(en)_2O_2SeO]^+$.

The monodentate selenito complexes are susceptible to rapid acid- and base-hydrolysis but significant concentrations still persist at pH 1 and pH 10. Selenito-complex formation is virtually complete in the neutral pH region.

The activation enthalpies for substitution and hydrolysis are generally in the range 46-60 kJ mol^{-1} but fall to around

35 kJ mol^{-1} between pH 6 and pH 8.5. These low values are indicative of Se-O bond formation and rupture and compare favourably with the activation enthalpies for the oxygen-exchange reaction between selenite and water, $\Delta H^{\ddagger}_{ex}$=58.6 kJ mol^{-1}, and the base-hydrolysis of $[Co(NH_3)_5OSeO_2]^+$, $\Delta H^{\ddagger}_{hyd}$ = 48.1 kJ mol^{-1}, both of which proceed through Se-O bond rupture in the rate determining step. Since the metal-oxygen bond remains intact, the substitution process can be conceived as nucleophilic attack of an aquo-ligand at the Se(IV) centre.

Around pH 3 substitution proceeds through a precursor ion-pair, e.g. *cis*-$Co(tn)_2(OH_2)_2^{3+}.HSeO_3^-$. At 30.3° and 1 M ionic strength,

$$k_{an} = 37 \pm 2 \text{ sec}^{-1}; \quad K_{IP} = 11.4 \pm 0.6 \text{ M}^{-1} ;$$

for the substitution of *cis*-$Co(tn)_2(OH_2)_2^{3+}$ with $HSeO_3^-$. In the neutral pH region the observed kinetics are consistent with the rate law

$$k_{obs} = k_1[HSeO_3^-] + k_2[HSeO_3^-]^2.$$

A limiting rate was observed around pH 7 but not at pH 8.

When *cis*- and *trans*-diaquo complexes substitute with selenite there is a two-step reaction sequence:

$$\underset{(cis)}{trans[Co(NN)_2(OH_2)_2]^{3+}} + HSeO_3^- \underset{\rightleftarrows}{\overset{I}{\rightleftarrows}} \underset{(cis)}{trans[Co(NN)_2(OH)OSeO_2H]^{2+}} \overset{II}{\rightleftarrows}$$

$$\underset{(trans)}{cis\ [Co(NN)_2(OH_2)OSeO_2H]^{2+}}$$

Step I, substitution by selenite, proceeds up to 10^5 times faster than step II, isomerization of the selenito product, when NN=en and up to 10^2 times faster when NN = tn. Whereas step I is virtually independent of amine ring size, step II is markedly accelerated with

6-membered tn rings. The activation enthalpies for step II are of the order of 110 kJ mol^{-1}, indicative of Co-O bond cleavage. At 25° and 1 M ionic strength, K *trans* → *cis* = 13.5 ± 1 at pH 3.3, and 70 ± 20 at pH 7.0.

In the case of $[Ni(Me_6tren)OH_2]^{2+}$, the reaction half-times at 25° range from several seconds for $HSeO_3^-$ to 100 millisecs for N_3^-. The kinetics are consistent with the rate law

$$k_{obs} = k_1 + k_2[Y^-],$$

where k_1 and k_2 are both dependent on the nature of Y.

No discernible reaction was found between selenite and aquocobalamin.

CONTENTS

Chapter 1. Introduction

1.1 Inorganic Substitution Reactions

The class of inorganic reactions involving the replacement of one ligand in a metal complex by another, commonly called substitution, has been the subject of extensive investigation and review in recent years.[1-3]

The advent of fast reaction techniques[4] such as stopped-flow, line-broadening (N.M.R. and E.S.R.), temperature-jump and pressure-jump, ultrasonic absorption, and flash photolysis has progressively extended the time range available to the kineticist by a factor of roughly 10^{10}. As a direct result, the available data on inorganic substitution reactions have increased enormously over the past twenty years. Together with a better understanding of the role of the solvent in these reactions and the significance of ion-ion interactions in solution, this has led to a reappraisal of conventional mechanistic ideas.

A good example of this is the apparently simple reaction

$$[Co(NH_3)_5Cl]^{2+} + NO_2^- \xrightarrow{H_2O} [Co(NH_3)_5NO_2]^{2+} + Cl^- \qquad 1.1$$

which was originally thought to proceed by direct substitution of Cl by NO_2^- and subsequently found in 1954 to follow a complex 5-step reaction pathway.[5]

1.2 Assignment of Reaction Mechanism: Activation Modes

Since any substitution reaction inherently involves bond-

rupture and bond-formation, a fundamental question arises as to whether the formation of a new bond between the metal and the incoming ligand is concurrent with, or subsequent to, dissociation of the outgoing ligand from the complex. These alternative modes of activation are termed dissociative, and associative, respectively.

A substitution reaction proceeding by a purely dissociative mechanism is commonly classified as D[6] or $S_N1(lim)$,[1] whereas a purely associative pathway is designated A[6] or $S_N2(lim)$.[1] The D-type mechanism leads to an intermediate of reduced coordination number in a rate determining dissociative step, followed by rapid association of the new ligand. In the A-type mechanism, rapid dissociation of the old ligand from an intermediate of increased coordination number follows the rate-determining associative step.

Most substitution reactions have mechanisms which are somewhere between these two extreme cases. Such reactions can be classified as S_N1 and S_N2,[1] or better, Id and Ia,[6] which are representative of the interchange mechanism in which emphasis is placed on the interchange of ligands between the first and second coordination spheres of a metal.

1.3 Anation Reactions

The replacement of an aquo-ligand by an anion comprises a particular class of substitution known as anation which can be written in the general form

$$ROH_2^{3+} + X^- \underset{k_{H_2O}}{\overset{kx}{\rightleftharpoons}} RX^{2+} + H_2O \qquad 1.2$$

where kx and kH_2O are the rate constants for the forward anation and reverse aquation reactions, respectively.

In the past, particular emphasis has been placed on studying anation reactions in non-aqueous solvents, where ion-association plays an important role.

In aqueous solution, however, the effect of ion-association is more subtle and generally only indirect evidence of ion-pair formation based on kinetic data is available, rather than the direct detection of ion-pairs in solution. Ion-association constants which are derived purely from kinetic measurements are subject to doubt if the ion-associated state resembles more closely the reactant state than the transition state and wherever possible an independent determination should be made from conductance, charge-transfer or ultrasonic absorption data. An added difficulty in aqueous solution is that most ion-association constants have rather low values in water.

1.4 Ion-Association in Aqueous Solution

It was not until the early 1950s that a sudden revival of interest in inorganic substitution reactions, coinciding with the introduction of such techniques as N.M.R. and ultrasonic absorption, focussed attention on the importance of ion-association in reaction kinetics.

1.4.1 The Solvated Ion

The classic continuum solvent model of Debye[7] and Onsager,[8] which has been utilized by Bjerrum[9] and Fuoss[10] for associated

electrolytes, considers the solvent as structureless and completely characterized by its bulk properties such as viscosity and dielectric constant. This model, which disregards any specific ion-solvent interactions, is only adequate for ions separated by two or more solvent molecules.

The limitations of the continuum model prompted Frank and Wen[11] to introduce the concept of "structure-making" and "structure-breaking" by ions in solution. Their model considers the ion in solution as surrounded by three concentric regions:

1. region A, containing a definite number of solvent molecules in a regular orientation, is the structure-making region;
2. region B, where the solvent is randomly oriented, is the structure-breaking region;
3. region C is the bulk solvent.

Regions A and B are commonly referred to as the primary and secondary coordination spheres, respectively, of the solvated ion. Measurement of the exact composition of the first coordination sphere (i.e. the coordination number) has been made for various ions using the N.M.R. method.[12]

1.4.2 Ion-Association Mechanism: The Relaxation Method.

The occurrence of two distinct maxima whose shapes are characteristic of a single relaxation process, in the ultrasonic absorption curves of a number of 2:2 electrolytes in aqueous solution, particularly the sulphates of divalent cations, led to Eigen's[13] proposal of a 3-step reaction sequence for ion-association in

solution. This is shown in the reaction scheme below:

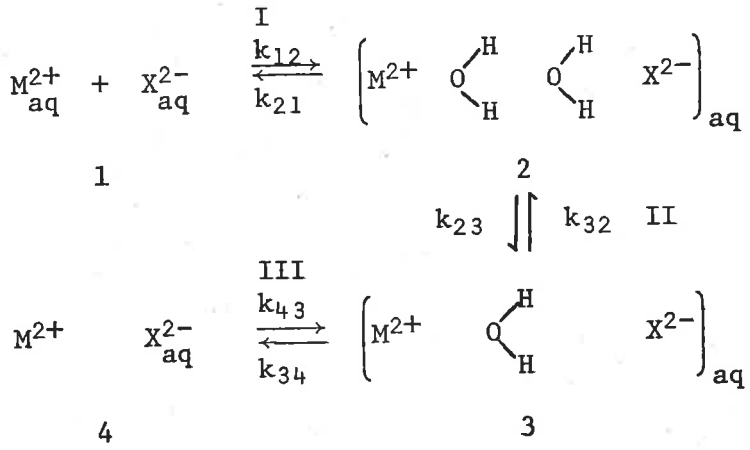

Step I was identified as the diffusion-controlled approach of the solvated metal and ligand ions, M^{2+}_{aq} and X^{2-}_{aq}, to form the solvent separated ion-pair, 2.

Step II corresponds with the removal of a water molecule from the first coordination sphere of the anion to form the intimate or outer-sphere ion-pair, 3.

Step III, which is the rate-determining step for ion-association, corresponds with the removal of a water molecule from the first coordination sphere of the cation and its subsequent replacement by the X^{2-} ion to form the contact, or inner-sphere ion-pair, 4.

This multistep ion-association process has been confirmed by Atkinson and Kor[14] who observed three relaxation peaks at $\sim$ 3, 30, and 200 MHz during an investigation into the ion-association of $MnSO_4$ in aqueous solution. Only the 3 and 200 MHz peaks had been originally found by Eigen[13] who assumed the existence of a third peak.

For $MnSO_4$ in aqueous solution, step I in the above reaction scheme can now be identified with the 200 MHz peak, step II with the 30 MHz peak, and step III with the 3MHz peak.

The existence of three relaxation peaks at $\sim$ 0.13, 11, and 170 MHz has also been reported for $MgSO_4$ in aqueous solution,[15] which is responsible for the large excess absorption at ultrasound in sea water.

The outstanding features which emerge from the Eigen treatment of ion-association are:

1. the forward rate constant, k_{12}, for step I is in good agreement with that predicted for a diffusion-controlled rate;
2. the forward rate constant, k_{23}, for step II is virtually independent of the cation, M^{2+};
3. the forward rate constant, k_{34}, for step III is very similar to k_{ex}, the rate constant for the solvent exchange on M^{2+} - in the case of M = Mn, $k_{34} \simeq k_{ex}$.

Although the importance of ion-pair formation and solvent exchange in relation to the mechanistic interpretation of ligand substitution has been recognized qualitatively for some time,[16] the Eigen model provides a sound basis for a quantitative treatment of the processes involved in the region of the solvated ion. In addition, application of the relaxation method has proved to be particularly valuable in the study of labile metal complexes which undergo very rapid reactions.[17]

1.5 *Activation Parameters for Substitution Reactions*

The rate law for a reaction is determined from a concentration study which leads to an evaluation of the rate constant. The activation parameters, $\Delta H^{\ddagger}$ and $\Delta S^{\ddagger}$, are determined from a temperature dependence study of the rate, and $\Delta V^{\ddagger}$, from a pressure dependence study.

Dissociative reactions, in the absence of solvent interaction and charge alteration in the transition state, are characterized by relatively high $\Delta H^{\ddagger}$ values, indicative of the large amount of energy required for bond-rupture, and positive $\Delta S^{\ddagger}$ values, arising from the increased disorder in dissociating a ligand from the metal complex. In addition, the rates of dissociative substitution reactions are independent of the nature of the nucleophile.

By contrast, associative substitution reactions have lower $\Delta H^{\ddagger}$ values, negative $\Delta S^{\ddagger}$ values, and reaction rates which vary according to the nucleophile.

Consider the substitution reaction involving the replacement of a neutral ligand from an uncharged metal complex by another neutral ligand in a non-aqueous solvent of low interaction:

$$[Mo(CO)_6] + PnBu_3 \xrightarrow{MeOH} [Mo(CO)_5PnBu_3] + CO \qquad 1.3$$

This reaction[18] is described by a two-term rate law

$$R = k_1[Mo(CO)_6] + k_2[Mo(CO)_6][PnBu_3] \qquad 1.4$$

indicating that substitution is proceeding through two alternative pathways. The activation parameters for the dissociative and

associative pathways described by the k_1 and k_2 terms are

$$\Delta H_1^{\ddagger} = 132.6 \text{ kJ mol}^{-1}, \qquad \Delta S_1^{\ddagger} = 28.0 \text{ J K}^{-1} \text{ mol}^{-1};$$

$$\Delta H_2^{\ddagger} = 90.8 \text{ kJ mol}^{-1}, \qquad \Delta S_2^{\ddagger} = -62.3 \text{ J K}^{-1} \text{ mol}^{-1}.$$

Since most substitution reactions involve solvent participation, especially if carried out in aqueous solution, and also involve a change in charge leading to formation of the transition state, the assignment of reaction mechanism is generally not as facile as in the above case.

Bennetto and Caldin[19] have shown that there is a linear relation between $\Delta H^{\ddagger}$ and $\Delta S^{\ddagger}$ for ligand substitution reactions, including the specific case of solvent-exchange, of divalent metal ions in various solvents, after ligand-field stabilization effects have been taken into account. Using the structural model of Frank and Wen[12] they have interpreted this linear relation as arising from a "solvent-modified dissociative process" with the solvent playing an active role in controlling the overall ligand substitution reaction.

The activation term, $\Delta V^{\ddagger}$, is also strongly dependent on solvent and electrostrictive charge effects and no simple comparison can be made between the sign of this term and the mechanism of the reaction.

An example of this is the aquation of $[Co(NH_3)_5X]^{(3-n)+}$, where X = SO_4^{2-}, Cl^-, Br^-, and NO_3^-, which has been shown[20] to proceed by a dissociative mechanism and yet the activation parameters,

$\Delta V^{\ddagger}$ and $\Delta S^{\ddagger}$, are negative because of electrostrictive interaction. For the particular case where X = H_2O, $\Delta V^{\ddagger}$ is positive since there is no electrostrictive component for water.

1.6 Anation Reactions of Octahedral Cobalt (III)-Amine Complexes.

Many of the anation studies at octahedral centres have been made on cobalt(III)-amine complexes because of their suitability for kinetic investigation with regard to stability, ease of preparation, and relative inertness to substitution. Some of these reactions have been recently reviewed.[2]

Most anation reactions of these complexes in aqueous solution are found to have a non-linear dependence on anion concentration, $[L^{m-}]$. A plot of k_{an} vs. $[L^{m-}]$, where k_{an} is the observed first order rate constant, generally shows an initial linear dependence at low $[L^{m-}]$ tending towards a limiting value, $k_{an}(lim)$, at high $[L^{m-}]$. In some cases, however, the linear dependence is maintained up to the highest anion concentrations used.

The observed rate law, which can be expressed in its reciprocal form as

$$1/k_{obs} = b/a + 1/a\ [L^{m-}] \qquad 1.5$$

where a and b are experimental parameters, is consistent with either of two closely related mechanisms.

In the dissociative competition mechanism (D or $S_N1(lim)$), dissociation of an aquo-ligand from the metal complex leading to a 5-coordinate intermediate in the rate-determining step, is

followed by competitive attack between solvent water and the incoming nucleophile on the newly formed species. The limiting rate of anation in the case of the D-mechanism is reached when the concentration of the anion is such that it reacts with the intermediate as soon as it is formed, leading to a steady-state situation where the rate of formation of the intermediate is equal to its rate of removal. The anation rate is then independent of the anion concentration.

The ion-pair mechanism (S_N IP) involves the rapid pre-equilibrium formation of an ion-pair between the charged reactants, followed by rate-determining interchange within the ion-pair. For relatively inert aquo-complexes the Eigen mechanism can be simplified:

$$RH_2O^{n+} + L^{m-} \underset{\text{fast}}{\overset{K}{\rightleftharpoons}} \{RH_2O^{n+}, L^{m-}\} \qquad 1.6$$

$$\{RH_2O^{n+}, L^{m-}\} \xrightarrow[\text{slow}]{k_L} RL^{(n-m)+} + H_2O \qquad 1.7$$

The emergence of a limiting rate in the case of the S_NIP mechanism occurs when all the substrate cations are completely ion-paired and each act of dissociation within the ion-pair leads to substitution. The one-step interchange process can proceed through either mode of activation and is therefore classified as Id or Ia.

The D-mechanism has recently been demonstrated for the anation of *trans*$[Co(en)_2\ SO_3(OH_2)]^+$ by SO_3^{2-},[21] where the rate data are consistent with the 2-step reaction scheme

$$trans\text{-}[Co(en)_2SO_3(OH_2)]^+ \rightleftharpoons Co(en)_2SO_3^+ + H_2O \qquad 1.8$$

$$Co(en)_2SO_3^+ + SO_3^{2-} \rightleftarrows \textit{trans}\text{-}[Co(en)_2(SO_3)_2]^- \qquad 1.9$$

where the 5-coordinate intermediate, $Co(en)_2SO_3^+$, is sufficiently stable to be selective towards different nucleophiles. This is shown by the competition ratio of

$$k_s/k_w = (9 \pm 5) \times 10^3 \text{ at } 25°C$$

between SO_3^{2-} and H_2O for the $Co(en)_2SO_3^+$ intermediate. The alternative S_NIP mechanism has been ruled out because of the improbably high ion-association constants required at the ionic strengths employed.

Another instance where this type of mechanism is thought to be operative is the anation of *cis* and *trans*-$[Co(cyclam)Cl(OH_2)]^{2+}$ by Cl^- and NCS^-,[22] where the reaction proceeds through a 5-coordinate square pyramidal intermediate leading to a competition ratio between NCS^- and H_2O of

$$k_{NCS}/k_{H_2O} = 4.9 \times 10^4 \text{ at } 59° \text{ for the } \textit{trans}\text{-substrate;}$$
$$k_{NCS}/k_{H_2O} = 4.3 \times 10^2 \text{ at } 25° \text{ for the } \textit{cis}\text{-substrate.}$$

This difference in ratios has been taken as excluding the possibility of a trigonal-bipyramidal intermediate. Again the high value required for the ion-association constant in the case of the *trans*-substrate has been cited as evidence against an S_NIP mechanism.

Finally, it is worth mentioning an anation reaction which does not involve an amine complex, namely the anation of $[RhCl(OH_2)_5]^{2+}$ by Cl^-,[23] where it has been possible to mechanistically discriminate

between the D and S_NIP pathways by comparing the observed rate law with that derived for each of these two alternative mechanisms. This unusual source of evidence comes as a result of the acid and conjugate-base forms of the complex simultaneously undergoing chloride anation at different rates.

An investigation into the formation of $[Co(NH_3)_5X]^{2+}$ complexes, where X = Cl^-, Br^-, NO_3^-, SCN^-, and $H_2PO_4^-$, by the reaction of $[Co(NH_3)_5N_3]^{2+}$ with HNO_2 in the presence of the above anions led to the original proposal by Haim and Taube[24] that a D-mechanism, leading to formation of the 5-coordinate intermediate, $Co(NH_3)_5^{3+}$, was operative for this reaction and also for the direct anation of $Co(NH_3)_5OH_2^{3+}$ by X^-, viz.,

$$[Co(NH_3)_5OH_2]^{3+} \underset{k+H_2O}{\overset{k-H_2O}{\rightleftharpoons}} Co(NH_3)_5^{3+} + H_2O \qquad 1.10$$

$$Co(NH_3)_5^{3+} + X^- \underset{k-x}{\overset{k+x}{\rightleftharpoons}} [Co(NH_3)_5X]^{2+} \qquad 1.11$$

This mechanistic proposal, which necessarily requires competition between X^- and H_2O for the $Co(NH_3)_5^{3+}$ intermediate, has been refuted by Pearson and Moore,[25] however, who found no evidence for any direct formation of $[Co(NH_3)_5NCS]^{2+}$ during an investigation into the acid hydrolysis of $[Co(NH_3)_5NO_3]^{2+}$ in the presence of excess NCS^-.

In order to account for this discrepancy, and also for the observation that the rates of anation of the $[Co(NH_3)_5OH_2^{3+}]$ species by SO_4^{2-}, Cl^-, SCN^-, and $H_2PO_4^-$ are nearly a constant factor of 5 less

than the rate of water exchange, Langford and Stengle[6] put forward the proposal of a dissociative interchange, Id, mechanism. Partial dissociation of an aquo-ligand from the metal complex results in an unstable intermediate which immediately reacts with any available ligand in the secondary coordination sphere. Thus for a 1:1 ion-pair in an octahedral system the Id mechanism predicts a $k_{an}(lim)/k_{H_2O}$ ratio of 1:5 based on the statistical population of the secondary coordination sphere.

An exception to the above prediction occurs for the anation of $[Co(NH_3)_5OH_2]^{3+}$ by N_3^-,[26] where $k_{an}(lim)/k_{H_2O} = 1$. This has been attributed to specific association of the incoming azide group with the dissociating aquo-ligand through hydrogen bonding so that each act of aquo dissociation results in azide entry.

The similarity of the rates of entry of the incoming nucleophiles, with the exception of N_3^-, is consistent with a dissociative mode of activation.

Conversely, the anation of the $[Rh(NH_3)_5OH_2]^{3+}$ species by Cl^- and Br^- is considered to proceed through an Ia mechanism,[27] with the incoming ligand providing a greater degree of nucleophilic assistance than water. The ratio $k_{an}(lim)/k_{H_2O}$, is approximately 2:1, which is 10 times as large as for the dissociative interchange in the analogous cobalt(III) system and is presented as evidence for an associative mode of activation.

Although the Langford model is experimentally supported in a number of cases, it should be remembered that it is based on the

assumption that the rate of water-exchange within the ion-pair, coincident with a limiting rate of anation, is the same as the water-exchange rate in the absence of any competetive anation. This implies that there is no marked change in the nature of the transition-state arising from ion-pairing. For a truly valid comparison the rate of water-exchange within the ion-pair should be measured simultaneously with the rate of ligand substitution.

It now seems quite likely that aquation reactions and, by inference from the principle of microscopic reversibility, anation reactions involving octahedral cobalt(III) complexes are dissociative in character. Initial studies on the aquation of *cis* and *trans*-$[Co(en)_2ACl]^{n+}$ complexes,[28] where A = OH^-, Cl^-, NCS^-, NH_3, and NO_2^-, gave rise to the dual reaction mechanism postulate, whereby S_N1 or S_N2 kinetics were assigned on the basis of the steric course of the reaction. However, subsequent investigations into structure variation, leading to the Langford[29] linear free-energy relation between rate and equilibrium constants for different leaving groups, have shown that there is very little nucleophilic assistance from the incoming ligand in the transition state for these reactions, which effectively rules out the possibility of bimolecular or A-type substitution.

1.7 Anation Reactions Involving Group V and VI Oxyanions.

The anation reactions of the $[Co(en)_2(OH_2)_2]^{3+}$ species with SO_4^{2-}, SeO_4^{2-},[30] and PO_4^{3-},[31] have been found to proceed by the rapid pre-equilibrium formation of an ion-pair species followed by rate determining interchange within the ion-pair. For the

oxygen-exchange reaction of the *cis* and *trans*-diaquo species, $t_{\frac{1}{2}} \sim 23$ hrs. at 25°, and for a 50:50 mixture of diaquo and hydroxo-aquo ions, $t_{\frac{1}{2}} \sim 25$ mins., at 25°.[32] The ratio, $k_{an}(lim)/k_{H_2O}$, is approximately 1:7 for SO_4^{2-} and SeO_4^{2-}, and 1:15 for PO_4^{3-}, which, according to the Langford classification, is consistent with a d-mode of activation.

The high $\Delta H^{\ddagger}$ values,

$\Delta H^{\ddagger}$ = 146.4 kJ mol^{-1} for SO_4^{2-} anation,

and $\Delta H^{\ddagger}$ = 125.5 kJ mol^{-1} for PO_4^{3-} anation,

are consistent with Co-O bond rupture in the rate-determining step.

For the anation reaction of $[Co(NH_3)_5OH_2]^{3+}$ with SO_4^{2-},[16] $k_{an}(lim)/k_{H_2O} \sim 1:5$ and $\Delta H^{\ddagger} = 99.2 \pm 2.1$ kJ mol^{-1}, which is again consistent with an S_NIP mechanism with Co-O bond cleavage in the rate-determining step.

In contrast to the phosphate anation of $[Co(en)_2(OH_2)_2]^{3+}$, substitution by arsenate of the $[Co(NH_3)_5OH_2]^{3+}$ ion is thought to proceed through an associative mechanism involving nucleophilic attack by the aquo-ligand of the complex on the As(v) centre in $HAsO_4^{2-}$.[33] For the oxygen exchange reaction of $HAsO_4^{2-}$,

$t_{\frac{1}{2}} \sim 25$ mins. at pH 6 and 25°.[34]

The $HAsO_4^{2-}$ ion was found to be approximately 10 times more susceptible to nucleophilic attack than the $H_2AsO_4^-$ ion. In contrast to the analogous phosphate reaction, the rate-determining step in the arsenate anation is formation of an As-O bond, not cleavage of a Co-O bond.

The greater facility of reactions involving arsenate compared with analogous reactions involving phosphate can be attributed to the relative ease with which As(v) can expand its coordination number to 5.

As previously described in section 1.6, anation of *trans*-$[Co(en)_2SO_3(OH_2)]^+$ by SO_3^{2-} is considered to proceed through a D-mechanism. The sulphito ligand is responsible for a marked acceleration in the rate of substitution compared with similar reactions for other diamagnetic cobalt(III) complexes and also exhibits a very strong *trans*-effect.

The low enthalpy of activation term, $\Delta H^{\ddagger}$ = 66.5 kJ mol^{-1}, can be compared with the usual range of $\Delta H^{\ddagger}$ values between 104.6 - 125.5 kJ mol^{-1} for analogous cobalt(III) substitution reactions. Since the sulphito ligand can potentially bond through either O or S, a possible explanation for the low $\Delta H^{\ddagger}$ value is that anation proceeds through a pseudo tetragonal intermediate, $Co(en)_2SO_3^+$, utilizing the empty Eg cobalt(III) orbital to form a 3-centre π-π bond.

The anation reactions of $[Co(NH_3)_5OH_2]^{3+}$ and *cis*-$[Co(en)_2NO_2(OH_2)]^{2+}$ by NO_2^- have been found to involve the initial formation of the unstable nitrito isomer, followed by intramolecular rearrangement to the stable nitro product which is the rate-determining step at moderately high concentrations of NO_2^-.[5,35]

The fact that the key step in the reaction sequence involves rapid nitrosation of the complex by N_2O_3 ($2HNO_2 \rightarrow N_2O_3 + H_2O$)

and not Co-O bond cleavage has been confirmed by ^{18}O studies.[36] The rate of anation is much greater than the rate of water-exchange, which proceeds by the normal dissociative pathway.

1.8 Plan of the Present Investigation.

Preliminary investigations in these laboratories indicated that substitution of the aquo ligand of $[Co(NH_3)_5OH_2]^{3+}$ by $HSeO_3^-$ and the reverse aquation of the selenito product occurred at very fast rates ($t_{\frac{1}{2}}$ of the order of seconds or less) compared with typical cobalt(III) substitution rates which have half-times of minutes or hours at 25°. For the particular case of aquo-ligand exchange on $[Co(NH_3)_5OH_2]^{3+}$, $t_{\frac{1}{2}} \sim 32$ hrs. at 25°.[37] The rate of exchange of oxygen between selenite and solvent water, however, is considerably faster than the aquo-ligand exchange rate for $[Co(NH_3)_5OH_2]^{3+}$. At 0°, $t_{\frac{1}{2}} \sim 60$ mins. at pH $\gtrsim$ 10 and $\sim$ 12 mins. at pH $\sim$ 8.7.[38]

It was therefore decided to launch a detailed kinetic and thermodynamic investigation into the anation reactions of a series of octahedral aquo-amine cobalt(III) complexes with selenite, in aqueous solution, and to extend this study to other transition metals such as Rh(III) and Ni(II).

The base hydrolysis of $[Co(NH_3)_5OSeO_2]^+$ has been studied in these laboratories[39] and found to proceed by cleavage of a Se-O bond in the rate-determining step. A pressure-dependence study, also carried out in these laboratories,[40] has confirmed the associative

nature of the rate-determining step. The activation parameters for the hydrolysis of $[Co(NH_3)_5OSeO_2]^+$ are,

$$\Delta H^{\ddagger} = 48.1 \pm 1.4 \text{ kJ mol}^{-1} ;$$

$$\Delta S^{\ddagger} = -121 \pm 4 \text{ J K}^{-1} \text{ mol}^{-1};$$

$$\Delta V^{\ddagger} = -20.8 \pm 1.0 \text{ cm}^3 \text{ mol}^{-1} ;$$

where the low $\Delta H^{\ddagger}$ value is indicative of Se-O bond rupture.

The cobalt(III) complexes chosen for the anation study were $[Co(NH_3)_5OH_2]^{3+}$, *cis* and *trans*-$[Co(en)_2(OH_2)_2]^{3+}$, and *cis*- and *trans*-$[Co(tn)_2(OH_2)_2]^{3+}$. A later addition was the macrocyclic cobalt(III) compound, Vitamin B 12a (aquo-cobalamin).

Of particular interest was the effect of ring size on the rate of anation. The inclusion of an extra CH_2 group into the amine ring has been found to have a considerable effect on the rates of reactions involving octahedral cobalt(III) *tn* complexes as compared with those involving the analogous cobalt(III) *en* complexes. For instance, the base-hydrolysis of the $[Co(tn)_3]^{3+}$ complex proceeds by a factor of $\sim 10^4$ faster than the base-hydrolysis of the $[Co(en)_3]^{3+}$ complex, and the isomerisation rate for *trans*-$[Co(tn)_2(OH_2)_2]^{3+}$ is 10^3 greater[41] than that for the analogous *trans*-$[Co(en)_2(OH_2)_2]^{3+}$ complex.[42] Table 1.1 compares the relevant kinetic data for the *tn* and *en* base-hydrolysis reactions.

Table 1.1

Effect of Ring Size on Reaction Rate

Reaction	$k_{40°}$ ($M^{-1}sec^{-1}$)	$\Delta H^{\ddagger}$ (kJ mol^{-1})	$\Delta S^{\ddagger}$ (J $K^{-1}mol^{-1}$)	ref.
$[Co(tn)_3]^{3+} + OH^-$	$(7.30 \pm 0.38)x10^{-3}$	138 ± 5	155 ± 18	43
$[Co(en)_3]^{3+} + OH^-$	2.2×10^{-7}	156	126	44

By extending this a step further to include a macrocyclic compound such as aquocobalamin, which has a very labile aquo-ligand,[45] it was hoped to gain a greater appreciation of the nature of the "steric effects" which give rise to these dramatic increases in substitution rates. The aquocobalamin species is particularly suitable for kinetic study because of its water solubility and monomeric form in solution, and as a comparison with the kinetically inert model cobalamin complexes, iodo- and nitroaquobis(dimethylglyoximato)cobalt(III), and the similar cobalt(III) complexes usually investigated.

In order to test the influence of the nature of the metal ion on aquo lability, the $[Rh(NH_3)_5OH_2]^{3+}$ and $[Ni(Me_6tren)OH_2]^{2+}$ complexes were also included in the investigation.

Preliminary studies into the substitution reactions of $[Ni(Me_6tren)OH_2]^{2+}$, and the analogous Co(II) and Cu(II) complexes, with nucleophiles such as Cl^-, Br^-, and SCN^-,[46] have indicated half-times of seconds in striking contrast to the very much faster rates generally observed for complexes of these metal ions. An extension of this work

to include selenite substitution would seem valuable in the interpretation of the reaction mechanism, with particular emphasis on whether 5-coordinate complexes, such as $[Ni(Me_6tren)OH_2]^{2+}$, undergo substitution in a manner similar to that of either 4- or 6- coordinate complexes.

Since there are very little data available on inorganic selenito complexes, a detailed preparative and analytical investigation was also deemed necessary, especially considering the biological importance of naturally occurring selenium compounds.[47-54]

References to Chapter 1.

1. F. Basolo and R.G. Pearson, *"Mechanisms of Inorganic Reactions"*, 2nd. edn., *John Wiley and Sons Inc., New York*, 1967.
2. C.K. Poon, *Inorg. Chim. Acta Revs.*, 1970, 4, 123.
3. C.H. Langford and H.B. Gray, *"Ligand Substitution Processes"*, *W.A. Benjamin Inc., New York*, 1966.
4. E.F. Caldin, *"Fast Reactions in Solution"*, *Blackwell Scientific Publications, Oxford*, 1964.
5. R.G. Pearson, P.M. Henry, J.G. Bergmann, and F. Basolo, *J. Am. Chem. Soc.*, 1954, 76, 5920.
6. C.H. Langford and T.R. Stengle, *Ann. Rev. Phys. Chem.*, 1968, 19, 193.
7. P. Debye, *Phys Z.*, 1912, 13, 97.
8. L. Onsager, *J. Am. Chem. Soc.*, 1936, 58, 1486.
9. N. Bjerrum, *Kgl. dans. Videnskab, Mat. fys. Medd.*, 1926, 7.
10. R.M. Fuoss, *J. Am. Chem. Soc.*, 1958, 80, 5059.
11. H.S. Frank and W.Y. Wen, *Discuss. Faraday Soc.*, 1957, 24, 133.
12. R.E. Connick, *"Advances in the Chemistry of the Coordination Compounds"*, *S. Kirschner ed., Macmillan and Co. New York*, 1961, 15.
13. a) M. Eigen, G. Kurtze, and K. Tamm, *Z. Elektrochem*, 1953, 57, 103.
    b) M. Eigen and K. Tamm, ibid., 1962, 66, 93.
14. G. Atkinson and S.K. Kor, *J. Phys. Chem.*, 1965, 69, 128.
15. G. Atkinson and S. Petrucci, ibid., 1966, 70, 3122.

16. a) H. Taube and F.A. Posey, *J. Am. Chem. Soc.*, 1953, 75, 1463.

b) J.P. Hunt and H. Taube, *J. Chem. Phys.*, 1951, 19, 602.

17. M. Eigen and R.G. Wilkins, *"Mechanisms of Inorganic Reactions", Advan. Chem. Ser.*, 1965, 49, 55.

18. R.J.Angelici and J.R. Graham, *J. Am. Chem. Soc.*, 1966, 88, 3657.

19. H.P. Bennetto and E.F. Caldin, *J. Chem. Soc.*, 1971, 2198.

20. W.E. Jones, L.R. Carey, and T.W. Swaddle, *Can. J. Chem.*, 1972, 50, 2739.

21. D.R. Stranks and J.K. Yandell, *J. Phys. Chem.*, 1969, 73, 840.

22. a) C.K. Poon and M.L. Tobe, *J. Chem. Soc.*, 1967, 2069.

b) C.K. Poon and M.L. Tobe, ibid., 1968, 1549.

23. M.J. Pavelich and G.M. Harris, *Inorg. Chem.*, 1973, 12, 2.

24. A. Haim and H. Taube, ibid, 1963, 2, 1199.

25. R.G. Pearson and J.W. Moore, ibid., 1964, 3, 1334.

26. T.W. Swaddle and G. Guastalla, ibid., 1969, 8, 1604.

27. H.L. Bott, A.J. Poe and K. Shaw., *J. Chem. Soc.*, 1970, 1745.

28. S. Asperger and C.K. Ingold, ibid, 1956, 2862.

29. C.H. Langford, *Inorg. Chem.*, 1965, 4, 265.

30. R.S. Murray, *Ph.D. Thesis, University of Adelaide*, 1967.

31. S.F. Lincoln and D.R. Stranks, *Aust. J. Chem.*, 1968, 21, 1745.

32. W. Kruse and H. Taube., *J. Am. Chem. Soc.*, 1961, 83, 1280.

33. T.A. Beech, N.C. Lawrence, and S.F. Lincoln, in press.

34. R.F. Kouba and J.E. Varner, *Biochem. Biophys. Res. Comm*, 1959, 1, 129.

35. F. Basolo, B.D. Stone, J.G. Bergmann, and R.G. Pearson, *J. Am. Chem. Soc.*, 1954, 76, 3079,

36. R.K. Murmann and H. Taube, ibid., 1956, 78, 4886.

37. H.R. Hunt and H. Taube, ibid, 1958, 80, 2642.

38. A. Okumura and N. Okazaki, *Bull. Chem. Soc. Jap.*, 1973, 46, 1084.

39. N. Vanderhoek, *Honours Report, University of Adelaide*, 1969.

40. J.V. Dubrawski, *Honours Report, University of Adelaide*, 1972.

41. I.R. Jonasson, *unpublished data.*

42. J. Bjerrum and S.E. Rasmussen, *Acta. Chem. Scand.*, 1952, 6, 1265.

43. A.D. Fowless, *Honours Report, University of Adelaide*, 1969.

44. J.A. Friend and E.K. Nunn, *J. Chem. Soc.*, 1958, 1567.

45. D. Thusius, *J. Am. Chem. Soc.*, 1971, 93, 2629.

46. D. Weatherburn, *unpublished data.*

47. C.J. Asher, C.S. Evan, and C.M. Johnson, *Aust. J. Biol. Sci.*, 1967, 20, 737.

48. B.G. Lewis, C.M. Johnson, and C.C. Delwiche, *Agric. Food Chem.*, 1966, 14, 638.

49. A. Schrift, *Ann. Rev. Plant Physiol*, 1969, 20, 475.

50. C.W.R. McCray and I.S. Hurwood, *Qld. J. Agric. Sci.*, 1964, 20, 475.

51. S.G. Knott and C.W.R. McCray, *Aust. Vet. J.*, 1959, 35, 161.

52. S.G. Knott, C.W.R. McCray, and W.T.K. Hall, *Qld. J. Agric. Sci.*, 1958, 15, 43.

53. I. Rosenfeld and O.A. Beath, *"Selenium", Academic Press, New York*, 1964.

54. S.F. Trelease and H.M. Trelease, *Am. J. Bot.*, 1939, 26, 530.

Chapter 2. Preparation and Characterization of Selenito Complexes

2.1 Introduction

To date, the only inorganic metal selenito complexes reported, with selenite directly coordinated to the metal centre, are the series of red hygroscopic solids, $[Co(en)_2(OH_2)SeO_3]X.nH_2O$, where X = Cl^-, NO_3^-, Br^-, and SO_4^{2-}.[1] However no indication was given as to whether the selenite ligand is coordinated through selenium or oxygen.

Recently, Vanderhoek[2] has prepared and characterized the new selenito complexes, $[Co(NH_3)_5 . OSeO_2]X.H_2O$, where X = ClO_4^- and Br^-, in these laboratories. The selenite ligand was found from infrared spectral evidence to be coordinated to cobalt(III) through oxygen.

Other oxyanions, such as SO_4^{2-}, SeO_4^{2-},[3] and $HAsO_4^{2-}$,[4] are also coordinated to the metal centre through oxygen. The NO_2^- ion can coordinate through either oxygen or nitrogen, although the ~~oxygen~~ nitrogen-bonded nitrite complex is more stable than the ~~nitrogen~~ oxygen-bonded nitrito complex which readily undergoes linkage isomerization to form the stable nitrite complex.[5] In the case of SO_3^{2-}, coordination occurs predominantly through sulphur. There is, however, some evidence for the existence of the unstable oxygen-bonded species in solution.[6]

Our investigations into the substitution reactions of octahedral cobalt(III) amine-aquo complexes with selenite necessitated the preparation and characterization of the resultant selenito complexes.

It was found that the syntheses of these compounds are complicated by their extreme solubility in water, resulting in an inherent tendency to form an oil rather than a solid product. Also, the use of excess selenite results either in contamination of the product or substitution of the supporting anion by selenite. By careful control of the reaction conditions, however, it was possible to obtain a number of air-stable, crystalline compounds with selenite coordinated to the metal centre both as a monodentate and a bidentate ligand.

2.2 *Experimental*

2.2.1 *Spectra*

All infrared spectra were run as solid KBr discs on a Perkin-Elmer 457 grating infrared spectrophotometer with either bromide (where possible) or perchlorate as the supporting anion of the metal complex.

All U.V. - visible spectra were recorded on a Unicam SP800 spectrophotometer. Optical absorbance values required for the determination of molar absorptivities were measured on a manual Shimadzu QR 50 spectrophotometer to an accuracy of ± 0.001.

2.2.2 *pKa Determinations*

All pKa measurements were made on a Radiometer pH meter 28 to an accuracy of ± 0.05. This instrument was also used for measuring the pH of the various complex solutions.

Anhydrous sodium selenite in perchloric acid was potentiometrically titrated against sodium hydroxide of known molarity. The ionic strength was adjusted to 1.0 M with sodium perchlorate.

Cis and *trans*-$[Co(en)_2(OH_2)OSeO_2H](ClO_4)_2$ in water were similarly titrated against sodium hydroxide.

2.2.3 *Preparations*

The complexes, $[Co(NH_3)_5OH_2](ClO_4)_3$,[7] *cis*-$[Co(en)_2OH\ (OH_2)](ClO_4)_2$ and *trans*-$[Co(en)_2OH(OH_2)](ClO_4)_2.2H_2O$,[8] were prepared by the methods reported in the literature. The preparation[9] of *trans*-$[Co(tn)_2OH(OH_2)](ClO_4)_2 2H_2O$ was modified, as reported below, resulting in a significant

increase in the product yield.

Analyses for C, N, H,and Cl were performed by the Australian Microanalytical Service; analyses for Se, Co, H_2O,and NH_3 were performed in these laboratories.

trans-$[Co(tn)_2OH.(OH_2)](ClO_4)_2.2H_2O$

A. *trans*-$[Co(tn)_2Cl_2]Cl.\ 3.5\ H_2O$

Anhydrous $CoCl_2$ (6.9 g) and LiCl (2.3 g) were dissolved in methanol (300 ml.) and the solution filtered (if necessary) to remove cobalt oxide. To this solution was added a slight excess of 1,3 diaminopropane (9.2 ml), and concentrated HCl (7 ml.) was then added to make the solution slightly acidic. Oxygen was bubbled through this solution for 1-2 hours and the resultant green needle crystals were collected, washed with ethanol, then acetone, and air-dried. A second batch was obtained by adding more 1,3 diaminopropane (2 ml.) and concentrated HCl (1.5 ml.) to this filtrate and bubbling oxygen through the solution for a further ½ hour. The resultant green crystals were collected and dried as before. Yield 75%.

B. $[Co(tn)_2CO_3]ClO_4$

trans-$[Co(tn)_2Cl_2]Cl.3.5\ H_2O$ (6.8 g.) and Li_2CO_3(5.0 g.) were dissolved together in water (50 ml.) at 75° to give a deep red-purple solution. After 15 minutes at 75° the solution was allowed to cool and the product crystallized from solution by the addition of ethanol. The fine red crystals were collected, washed with a small amount of

cold water, then ethanol, and air-dried. A second batch was obtained by reducing the volume of the filtrate and crystallizing by addition of ethanol. The red crystals were collected and dried as before. Yield of chloride salt 80%.

The perchlorate salt was then prepared by dissolving $[Co(tn)_2CO_3]Cl.H_2O$ (5.0 g.) and $LiClO_4$(1.7 g.) together in the minimum volume of water at 75°. On cooling, the resultant dark red crystals were collected, washed with ethanol, then ether, and air-dried. Yield of perchlorate salt 95%.

C. *trans*-$[Co(tn)_2OH.(OH_2)](ClO_4)_2.2H_2O$

This complex was then prepared from $[Co(tn)_2CO_3]ClO_4$ by the method of Jonasson et. al.[9] Yield 95%.

$[Co(NH_3)_5OSeO_2]ClO_4.H_2O$; $[Co(NH_3)_5OSeO_2]Br.H_2O$

These complexes were prepared by the method of Vanderhoek.[2]

A. $[Co(NH_3)_5OSeO_2]ClO_4.H_2O$

$[Co(NH_3)_5OH_2](ClO_4)_3$ (10 g.) and Na_2SeO_3(4 g.) were dissolved together in a minimum volume of warm water and the resultant red-purple solution heated to 70°C for several minutes. The red-purple crystals which formed on cooling the solution were collected and washed with ethanol. The product was recrystallized from a minimum volume of hot water to give red crystals which were washed with ethanol, then ether and air-dried. Yield 60%.

$[Co(NH_3)_5OSeO_2](ClO_4).H_2O$ requires Co, 15.20; NH_3, 22.02; Se, 20.40%

Found: Co, 14.80; NH_3, 21.94; Se, 20.00%.

B. $[Co(NH_3)_5OSeO_2]Br.H_2O$

$[Co(NH_3)_5OH_2](ClO_4)_3$(6 g.) was suspended in acetone and then water was added to just dissolve the complex. The addition of excess LiBr resulted in the formation of a red precipitate which was collected and washed with acetone.

The red $[Co(NH_3)_5OH_2]Br_3$ complex (5.0 g.) was then treated with Na_2SeO_3 (2.1 g.) dissolved in a minimum volume of warm water and the procedure used above in the preparation of the perchlorate salt was repeated to yield bright pink crystals of the selenito bromide complex. The pure product was collected, washed with ethanol, then ether, and air-dried. Yield 60%.

$[Co(NH_3)_5OSeO_2]Br.H_2O$ requires Co, 16.00; Se 21.40; NH_3, 23.10%.

Found: Co, 15.80; Se, 21.10; NH_3, 22.90%.

cis-$[Co(en)_2(OH_2)OSeO_2H](ClO_4)_2$

cis-$[Co(en)_2OH(OH_2)](ClO_4)_2$(5 g.) was added to selenious acid (2 g.) dissolved in a minimum volume of warm water to give a deep red-purple solution. Cooling yielded a red-purple oil which was crystallized out as a pink-purple solid by successive additions of ethanol. The crude product was collected, washed with ethanol, then ether, and air-dried. There was a tendency for the solid product to revert to an oil when left on the pump for even a short period of time. Recrystallization from a minimum volume of hot water yielded a mauve solid on addition of ethanol. The pure product, which was washed and dried as above, showed no tendency to revert to an oil even on prolonged exposure to air. Yield 40%.

cis-$[Co(en)_2OSeO_2H(OH_2)](ClO_4)_2$ requires C, 9.16; N, 10.69; H, 3.63; Cl, 13.54; Se, 15.07%.

Found: C, 9.45; N, 10.73; H, 3.50; Cl, 14.40; Se, 15.42%.

trans-$[Co(en)_2OH.(OH_2).OSeO_2H](ClO_4)_2$

trans-$[Co(en)_2OH.(OH_2)](ClO_4)_2$(5 g.) was added to selenious acid (2 g.) dissolved in a minimum volume of cold water. The red *trans* hydroxo-aquo complex dissolved to give a dark green-grey solution from which a grey precipitate rapidly formed. The crude product was collected, washed with ethanol and air-dried.

Recrystallization was carried out in dilute acid solution to prevent the rapid isomerization to the more stable *cis*-isomer which occurs at neutral pH. The pure *trans* product was collected as blue-green needles which were washed with ethanol, then ether, and air-dried. Yield 20%.

trans-$[Co(en)_2OSeO_2H.(OH_2)](ClO_4)_2$ requires C, 9.16; N, 10.69; H, 3.63; Cl, 13.54; Se, 15.07%.

Found: C, 8.83; N, 10.23; H, 3.57; Cl, 13.40; Se, 15.32%.

trans-$[Co(en)_2OSeO_2H(OH_2)]Br_2$

trans-$[Co(en)_2OH(OH_2)]Br_2$ was prepared by adding excess LiBr to a concentrated solution of *trans*-$[Co(en)_2OH(OH_2)](ClO_4)_2$ in water. The red precipitate formed was collected, washed with acetone and air-dried.

A solution of the red complex bromide salt in water was then treated with an equimolar amount of selenious acid to give a blue

solution which was reduced in volume on a rotary evaporator at low temperature. Addition of acetone to the concentrated solution caused the rapid formation of a purple-blue precipitate which was collected, washed with acetone and air-dried. Yield 30%.

trans-$[Co(en)_2OSeO_2H.(OH_2)]Br_2$ requires C, 9.90; N, 11.55; H, 3.92; Br, 32.97; Se, 16.29%.

Found: C, 9.51; N, 11.26; H, 3.83; Br, 31.83; Se, 15.46%.

cis-$[Co(en)_2(OH_2)OSeO_2]Br$

cis-$[Co(en)_2OH.(OH_2)](ClO_4)_2$ (5.0 g.) was suspended in acetone and enough water was then added to just dissolve the complex. The addition of excess LiBr produced a red precipitate which was collected, washed with acetone and air-dried. Yield 90%.

cis-$[Co(en)_2OH.(OH_2)]Br_2$ (4.0 g.) and Na_2SeO_3 (1.9 g.) were dissolved together in a minimum volume of cold water. Addition of excess LiBr and acetone resulted in the formation of a pale pink precipitate which was filtered off. The red filtrate was treated with further acetone to yield a dark-red oil which was allowed to stand overnight under acetone. The resultant wine-red solid was collected, washed with acetone and air-dried. Yield 40%.

cis-$[Co(en)_2(OH_2)OSeO_2]Br$ requires C, 11.89; N, 13.87; H, 4.46; Br, 19.79; Se, 19.55%.

Found: C, 12.03; N, 13.50; H, 4.14; Br, 20.10; Se, 18.83%.

$[Co(en)_2O_2SeO]ClO_4$

cis-$[Co(en)_2OH.(OH_2)](ClO_4)_2$ (6 g.) was added to Na_2SeO_3

(2.5 g.) dissolved in a minimum volume of warm water and the resultant deep red-purple solution heated to 60° for several minutes. Cooling yielded a deep red-purple oil which was precipitated out as a mauve solid by successive additions of ethanol. The crude product was collected, washed with ethanol, then ether and briefly air-dried. The purple ethanolic filtrate was concentrated to yield more product and this was then combined with the original batch for recrystallization from a minimum volume of hot water. Slow cooling produced crimson crystalline plates which were collected, then washed and dried as above. Yield 25%.

$[Co(en)_2O_2SeO]ClO_4$ requires C, 11.84; N, 13.82; H, 3.95; Cl, 8.75; Se, 19.48%.

Found: C, 11.26; N, 13.57; H, 3.94; Cl, 8.82; Se, 18.85%.

$[Co(tn)_2O_2SeO]ClO_4$

trans-$[Co(tn)_2OH.(OH_2)](ClO_4)_2.2H_2O$ (3 g.) and Na_2SeO_3(1.4 g.) were dissolved together in a minimum volume of warm water. The resultant deep red-purple solution was heated to 60° for several minutes. Slow cooling yielded pink needle crystals which were collected, washed with ethanol, then ether and air-dried. Rapid cooling resulted in formation of a thick red oil which was crystallized out as a pink solid by successive additions of ethanol. The pure product was collected, then washed and dried as before. Yield 30%.

$[Co(tn)_2O_2SeO]ClO_4$ requires C, 16.62; N, 12.92; H, 4.62; Cl, 8.18; Se, 18.22%.

Found: C, 17.32; N, 12.36; H, 4.73; Cl, 7.87; Se, 17.66%.

2.3 *Results and Discussion*

2.3.1 *Infrared Data*

Evidence for coordinated selenite is based primarily on infrared spectral data. For a non-linear molecule such as the pyramidal SeO_3^{2-} ion, there are 3N-6 fundamental modes of vibration,[10] where N is the number of atoms in the molecule. Thus there are 6 fundamental vibrations for SeO_3^{2-} of which two pairs are degenerate. This gives rise to 4 fundamental frequencies, ν_1, ν_2, ν_3, and ν_4, all of which are infrared active, for the free selenite anion which has C_{3v} symmetry.

The frequencies, ν_1 and ν_2, correspond to symmetric Se-O bond stretching and deformation modes, and ν_3 and ν_4, to degenerate symmetric and asymmetric Se-O bond stretching and deformation modes, respectively. These frequencies are listed in Table 2.1, for free selenite, as in anhydrous Na_2SeO_3, and for selenite as a supporting anion, as in $[Co(NH_3)_6]_2(SeO_3)_3$.

Table 2.1

Fundamental Vibration	Na_2SeO_3 cm^{-1}	$[Co(NH_3)_6]_2(SeO_3)_3$ cm^{-1}
ν_1	790	788
ν_2	460	450
ν_3	742	740
ν_4	400	395

Coordination of the selenite anion to a metal centre through Se would mean retention of C_{3v} symmetry. However, coordination of selenite through O, either as a monodentate or bidentate ligand, would cause a reduction in symmetry from C_{3v} to Cs. On the basis of group theory there is expected to be an increase in the number of absorption bands from 4 to 6 on lowering the symmetry, coinciding with splitting of the degenerate vibrations. All 6 fundamental frequencies for coordinated selenite are infrared active. The relationship between the C_{3v} and Cs symmetry groups is shown in Table 2.2.

Table 2.2[11]

Symmetry	Vibrational Frequencies					
$C_{3v}(SeO_3^{2-})$	$\nu_1(A_1)$	$\nu_2(A_2)$	$\nu_3(E)$		$\nu_4(E)$	
	νs ↓	δs ↓	νd ↙	↘	δd ↙	↘
$Cs(ROSeO_2^{+})$	$\nu_1(A^1)$	$\nu_3(A^1)$	$\nu_2(A^1)$	$\nu_5(A^{11})$	$\nu_4(A^1)$	$\nu_6(A^{11})$
	νs	δs	νs	νas	δs	δas

ν : stretching
δ : deformation
s : symmetric
as : asymmetric
d : degenerate

Selenite absorbs in the region from 900 - 250 cm^{-1}. Fig. 2.1 compares the infrared spectra of $[Co(NH_3)_5OSeO_2]Br.H_2O$ and $[Co(NH_3)_6]_2(SeO_3)_3$ in this region. The spectrum of the pentaammine-selenito complex is in agreement with the original spectrum obtained by Vanderhoek.[2]

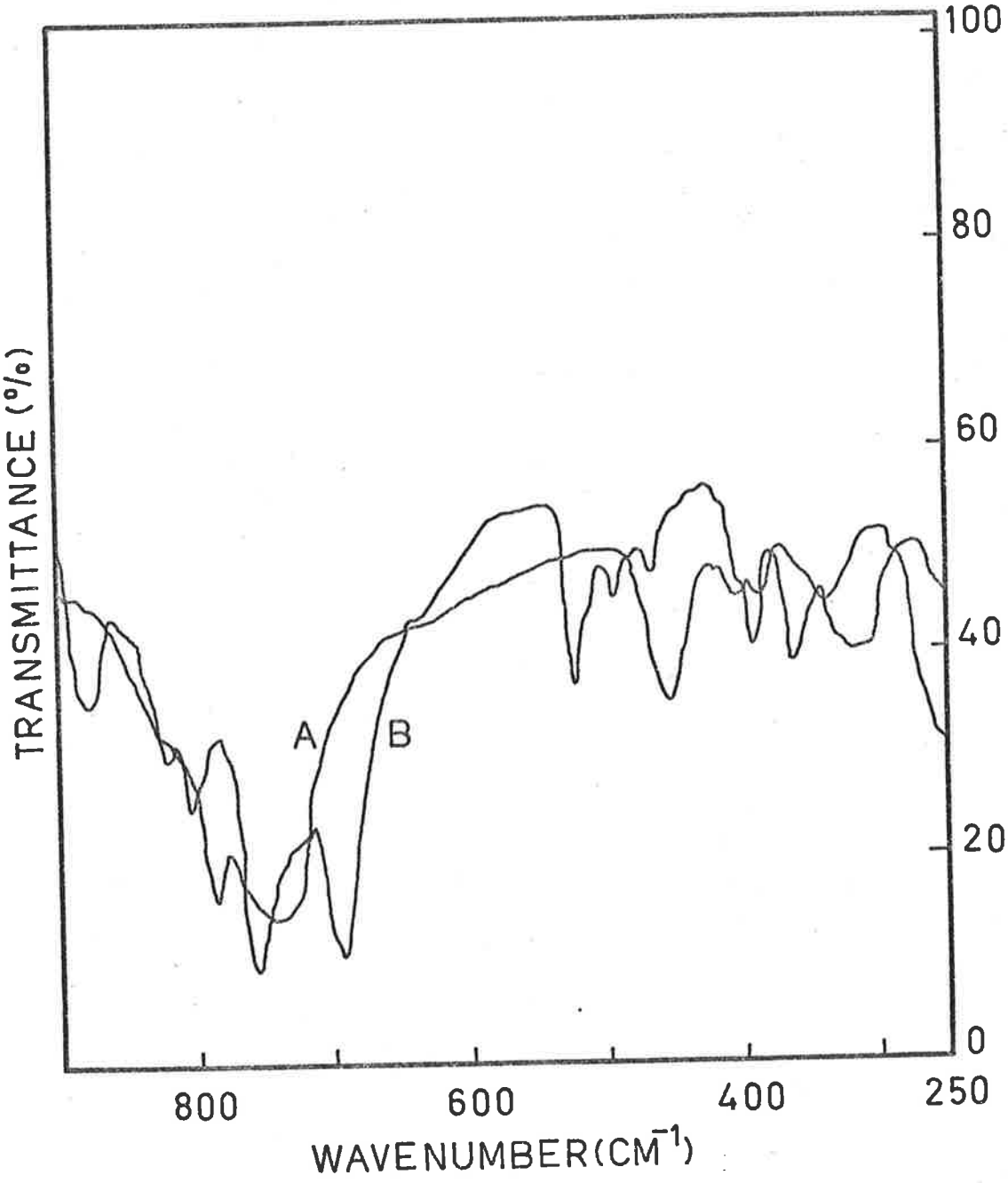

Fig. 2.1 Infrared Spectra of $[Co(NH_3)_6]_2(SeO_3)_3$ (A) and $[Co(NH_3)_5OSeO_2]Br.H_2O$ (B)

The spectra are complicated by the presence, in the region of interest, of a number of absorption bands due to N-H bending modes. Deuteration of the coordinated ammine groups shifts these N-H bending frequencies downfield and enables identification of the selenite absorption bands.

An analysis of the infrared spectra for the following selenito complexes: $[Co(NH_3)_5OSeO_2]Br.H_2O$, *cis*-$[Co(en)_2OSeO_2H.(OH_2)](ClO_4)_2$, *trans*-$[Co(en)_2OSeO_2H.(OH_2)]Br_2$, *cis*-$[Co(en)_2OSeO_2.(OH_2)]Br$, $[Co(en)_2O_2SeO]ClO_4$, and $[Co(tn)_2O_2SeO]ClO_4$; has shown in each case the presence of 6 distinct absorption bands which are clearly attributable to coordinated selenite. A list of the principal absorption frequencies in the region 900 - 250 cm^{-1} before, and where possible, after deuteration for each of the above complexes, is shown in Table 2.3.

On the basis of the available infrared data, therefore, it can be confidently assumed that bonding of selenite to a metal centre occurs through oxygen and not selenium. Since 6 absorption bands are observed for both monodentate and bidentate selenito complexes, no unequivocal distinction between these two forms is possible on this basis. However, from a qualitative assessment of the various I.R. spectra, two distinguishing features emerge which enable tentative identification of the alternate forms, viz.,

1. the absorption bands of the bidentate selenito complexes are much sharper compared to those of the monodentate selenito complexes and,
2. the degenerate ν_3 vibration of the free selenite anion

Table 2.3

Principal Absorption Frequencies for Selenito Complexes in the Region 900 - 250 cm^{-1}.

$[Co(NH_3)_5OSeO_2]Br.H_2O$		*cis*$[Co(en)_2OH_2.OSeO_2H](ClO_4)_2$		*trans*-$[Co(en)_2(OH_2)OSeO_2H](ClO_4)_2$	
$\lambda(cm^{-1})$	Assignment	$\lambda(cm^{-1})$	Assignment	$\lambda(cm^{-1})$	Assignment
880(-)	N-H	850	N-H	850	N-H
820(-)	N-H	830?	ν_1	830	ν_1
805(809)	ν_1	770	ν_2	800	N-H
755(758)	ν_2	580	ν_5	760	ν_2
695(706)	ν_5	530	ν_3	600	ν_5
520(508)	ν_3	470	N-H	520	ν_3
495(-)	N-H	400	ν_4	425	N-H
465(-)	N-H	350	ν_6	380	ν_4
390(386)	ν_4			360	ν_6
360(356)	ν_6				
320(-)	N-H				

Table 2.3 Contd.

cis-$[Co(en)_2(OH_2)OSeO_2]ClO_4$		$[Co(en)_2O_2SeO]ClO_4$		$[Co(tn)_2O_2SeO]ClO_4$	
$\lambda(cm^{-1})$	Assignment	$\lambda(cm^{-1})$	Assignment	$\lambda(cm^{-1})$	Assignment
848(-)	N-H	880(-)	N-H	890(-)	N-H
835(830)	ν_1	830(822)	ν_1	832(832)	ν_1
795(-)	N-H	803(-)	N-H	778(-)	N-H
760(758)	ν_2	762(760)	ν_2	762(760)	ν_2
678(682)	ν_5	678(682)	ν_5	749(-)	N-H
590(-)	N-H	590(-)	N-H	712(-)	N-H
550(-)	N-H	575(563)	ν_3	673(675)	ν_5
510(-)	N-H	515(-)	N-H	541(520)	ν_3
480(465)	ν_3	480(451)	ν_4	500(-)	N-H
400(383)	ν_4	405(388)	ν_6	469(-)	N-H
378(367)	ν_6	360(-)	N-H	448(-)	N-H
355(-)	N-H	303(-)	N-H	401(390)	ν_4
325(-)	N-H			382(363)	ν_6
300(-)	N-H				

( ) after deuteration.

is split into a doublet for the monodentate species but is split into two separate bands in the case of the bidentate species.

2.3.2 pKa Determinations

The potentiometric titration curve for Na_2SeO_3 is shown in Fig. 2.2. From this curve the pKa values determined for Na_2SeO_3 (= 0.1 M) are:

$pK_1 = 2.36 \pm 0.05$;

$pK_2 = 8.06 \pm 0.05$;

at 20° and 1 M ionic strength.

These values are in good agreement with the commonly quoted values of $pK_1 \sim 2.5$ and $pK_2 \sim 8.0$ in "dilute solution" at 20 - 25°.[12]

The potentiometric titration curves for *cis*-$[Co(en)_2OSeO_2H(OH_2)](ClO_4)_2$ and *trans*-$[Co(en)_2OSeO_2H(OH_2)](ClO_4)_2$ are shown in Figs. 2.3 and 2.4, respectively.

For *cis*-$[Co(en)_2OSeO_2H(OH_2)](ClO_4)_2$ the determined pKa values are:

$pK_1 = 4.35 \pm 0.05$;

$pK_2 = 8.30 \pm 0.05$;

and for *trans*-$[Co(en)_2OSeO_2H(OH_2)](ClO_4)_2$ the pKa values are:

$pK_1 = 4.55 \pm 0.05$;

$pK_2 = 7.70 \pm 0.05$;

at 20° and 1 M ionic strength.

The problem now is to assign the pKa values of the selenito complexes, *cis* and *trans*-$[Co(en)_2(OH_2)OSeO_2H](ClO_4)_2$, to the two

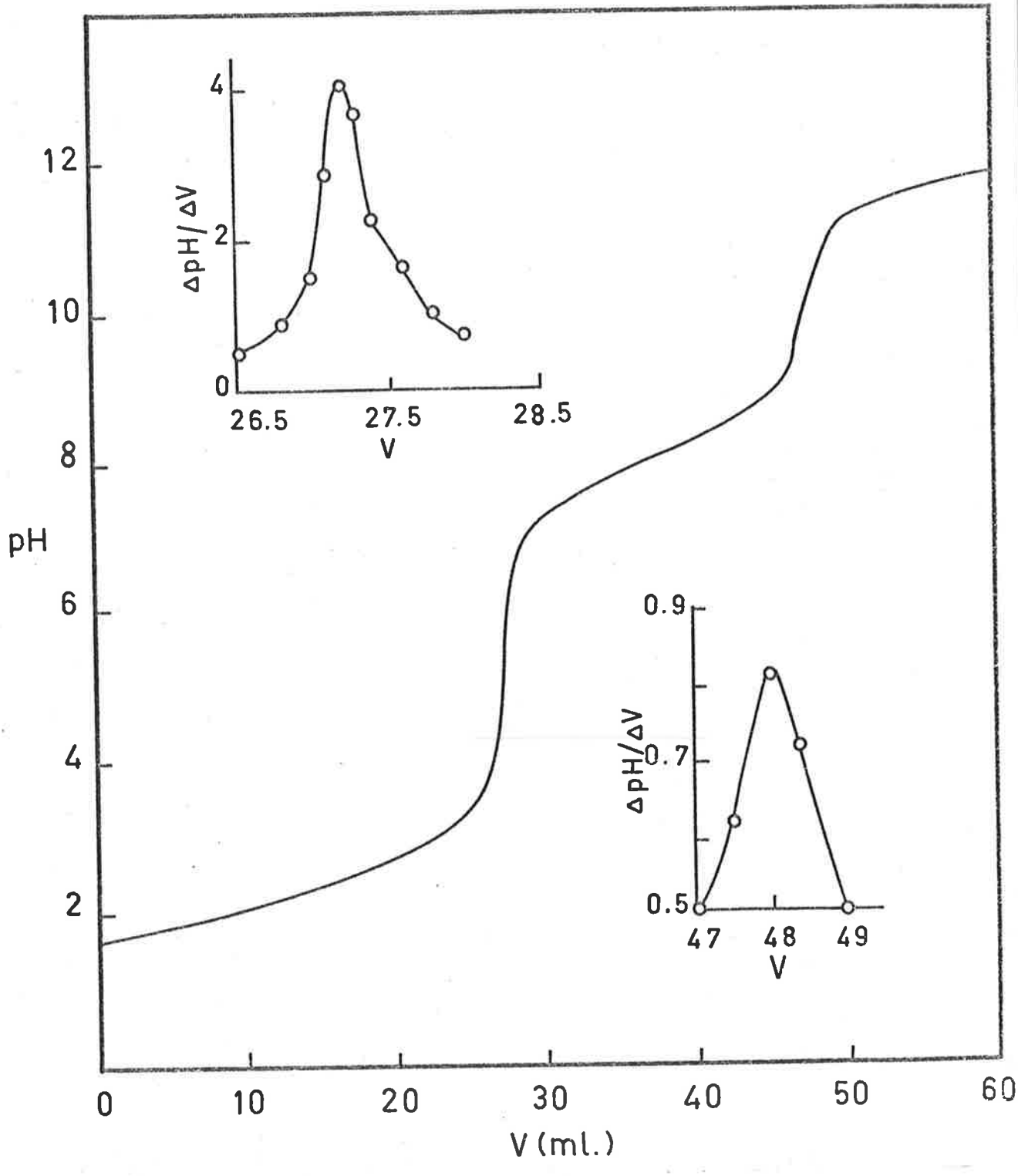

Fig. 2.2 Potentiometric and Differential Curves for Na_2SeO_3

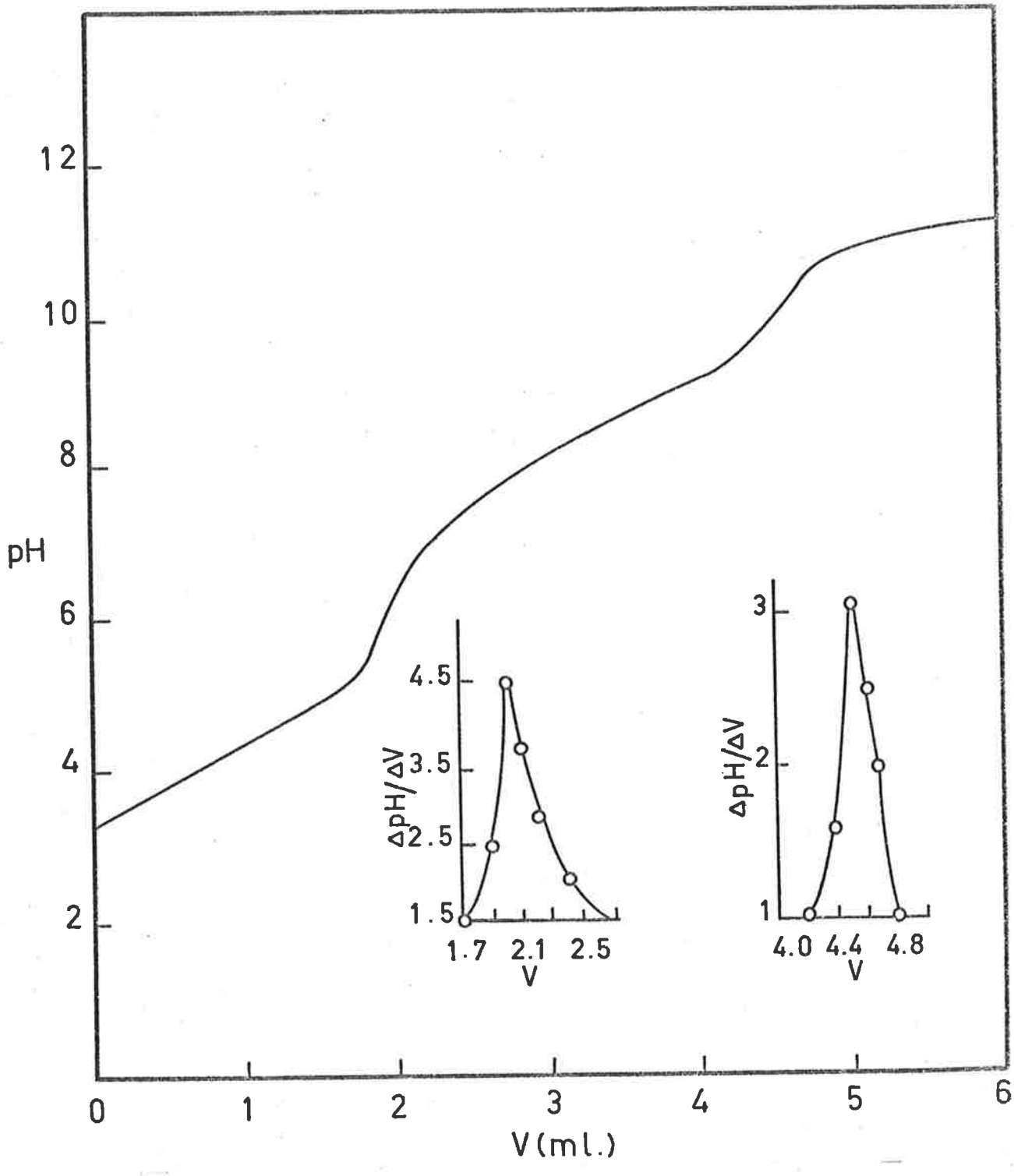

Fig. 2.3 Potentiometric and Differential Curves for *cis*-$[Co(en)_2(OH_2)OSeO_2H](ClO_4)_2$

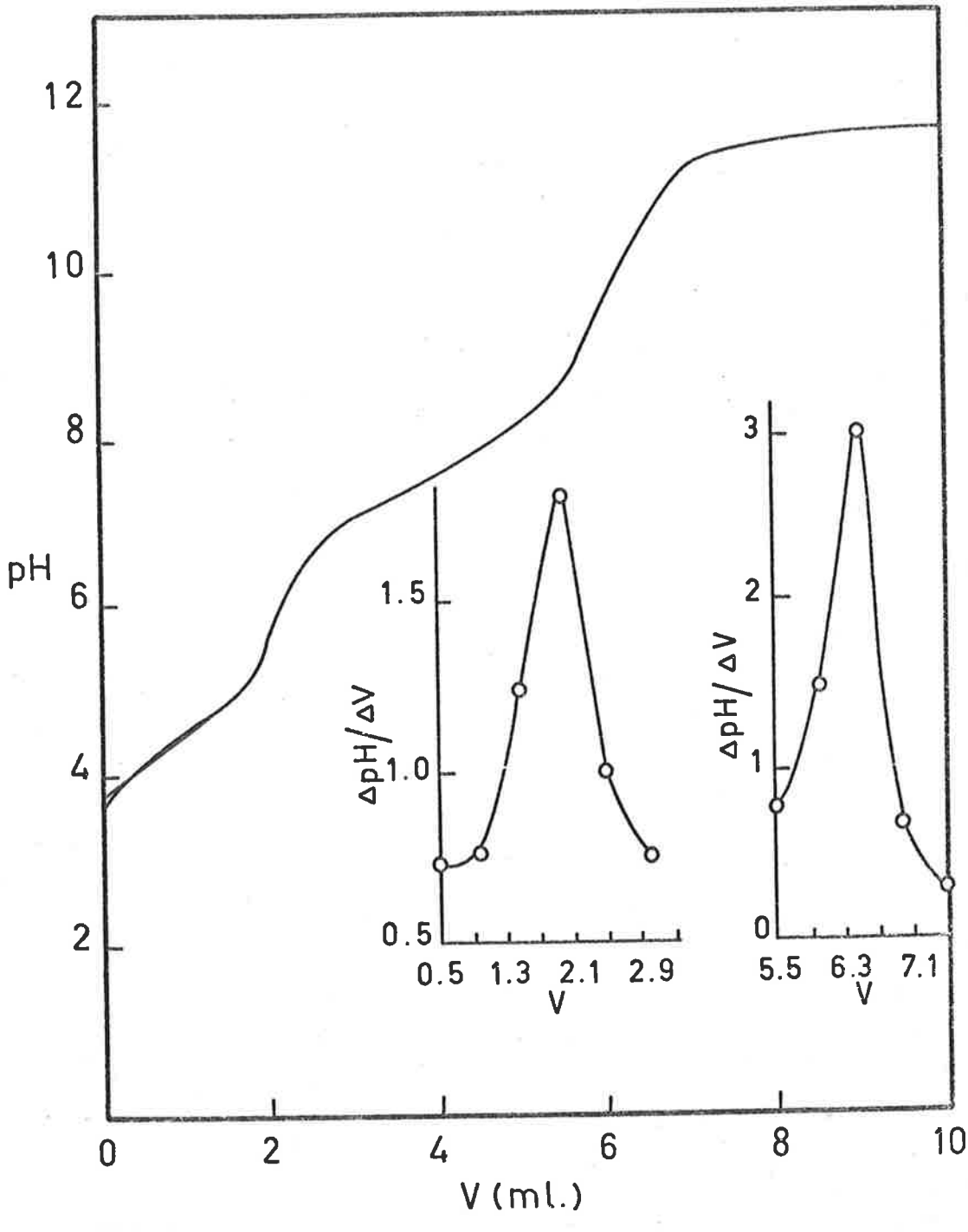

Fig. 2.4 Potentiometric and Differential Curves for *trans*-$[Co(en)_2(OH_2)OSeO_2H](ClO_4)_2$

proton donors.

Coordination of selenite would be expected to lead to a lowering of the two selenite pKa values relative to the values for free selenite, corresponding with the increased acidity of coordinated selenite compared with free selenite. This has been observed in the case of the analogous phosphate complexes.[13] On the basis of this assumption, therefore, the lower of the two pKa values measured for both *cis*- and *trans*-$[Co(en)_2(OH_2)OSeO_2H](ClO_4)_2$ can be tentatively assigned to the second pKa value, pK_2 sel., of the coordinated selenite ligand. By analogy, the first pKa value of the coordinated selenite ligand, pK_1 sel., is expected to be of the order of -2.

The significant increase in optical absorbance accompanied by the shift of λ_{max} to shorter wavelengths in the visible spectrum of the hydroxo-selenito species compared with the aquo-selenito species, as described in section 2.3.3, provides the basis for assigning the higher of the measured pKa values to the aquo-ligand. The observed spectral change can be related to a similar change in the visible spectrum of the hydroxo-aquo species with respect to the diaquo species.

2.3.3 U.V. - Visible Spectral Data

1. $[Co(NH_3)_5OSeO_2]^+$

The U.V. - visible spectrum of the cobalt(III) pentaammine-selenito complex at neutral pH exhibits a maximum at 519 nm (ε = 61.9 M^{-1} cm^{-1}) and a charge transfer band towards the shorter wavelengths.

In acid solution (pH < 4) the selenito-complex undergoes rapid acid-hydrolysis ($t_{\frac{1}{2}}$ < 1 sec at 25°). The shift in λ_{max} towards the shorter wavelengths and the appearance of a shoulder around 360 nm in the charge transfer band with decreasing pH is consistent with the reversible formation of the aquo species. At pH 1, the U.V. - visible spectrum exhibits two maxima:

$\lambda_{max\ 1}$ = 492 nm, ε = 50.0 M^{-1} cm^{-1} ;

$\lambda_{max\ 2}$ = 356 nm, ε = 48.5 M^{-1} cm^{-1} ;

which are characteristic of the aquopentaammminecobalt(III) complex.[14]

In basic solution, the selenito-complex undergoes slow base-hydrolysis to the hydroxo species ($t_{\frac{1}{2}}$ > 1 hr. at 25°).

The various spectra are shown in Fig. 2.5.

2. *cis* and *trans*-$[Co(en)_2(OH_2)\ OSeO_2]^+$

The U.V. - visible spectrum of the *cis*-selenito complex at neutral pH exhibits a maximum at 530 nm (ε = 110 M^{-1} cm^{-1}), a minimum at 450 nm (ε = 29 M^{-1} cm^{-1}), and a shoulder in the charge transfer band at 360 nm (ε = 107 $M^{-1}cm^{-1}$).

The corresponding *trans*-selenito complex spectrum exhibits two maxima at 590 nm (ε = 50.0 M^{-1} cm^{-1}) and 450 nm (ε = 31.0 M^{-1} cm^{-1}) and a minimum at 500 nm (ε = 21.0 M^{-1} cm^{-1}).

These spectra are shown in Fig. 2.6 together with the spectrum of the equilibrium mixture resulting from the slow isomerization of the *cis* and *trans*-isomers (see section 4.8).

Both isomers undergo rapid acid-hydrolysis, as is evidenced by the shift in λ_{max} to shorter wavelengths and the gradual

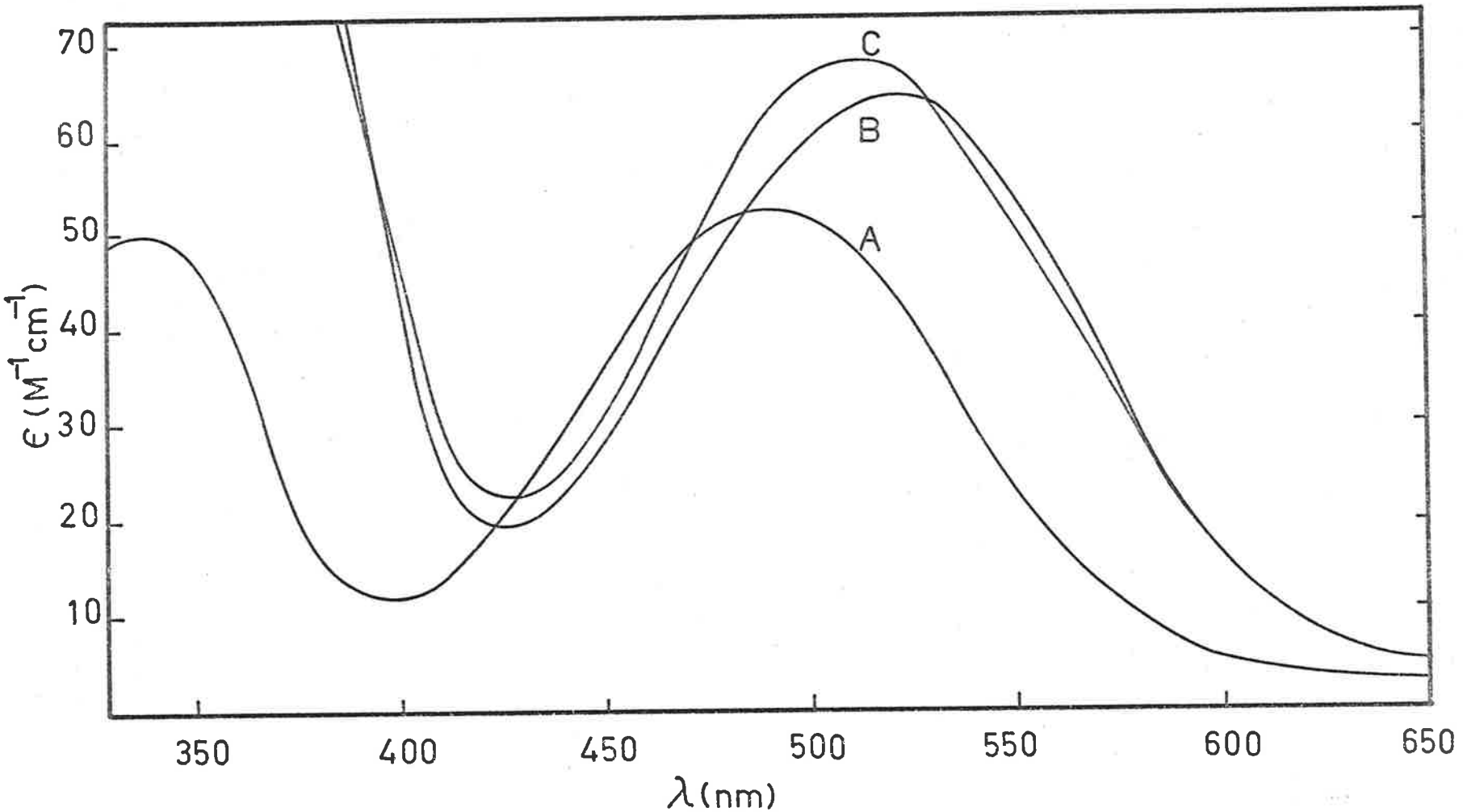

Fig. 2.5 U.V. - Visible Spectra of $[Co(NH_3)_5OSeO_2]^+$ in (A) Acidic Solution (pH ∿ 1), (B) Neutral Solution (pH ∿ 7), (C) Basic Solution (pH ∿ 12).

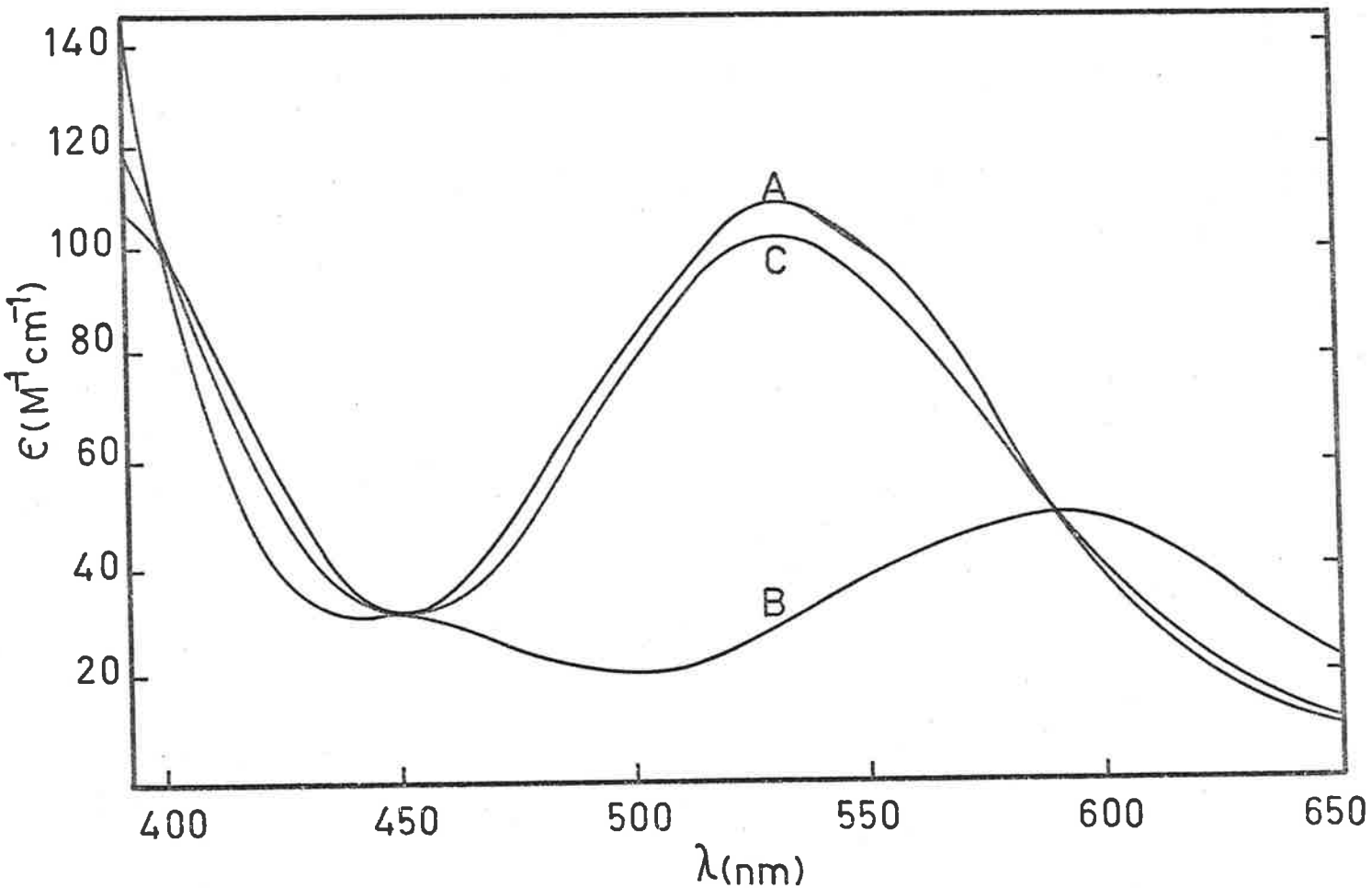

Fig. 2.6 U.V. - Visible Spectra of (A) *cis*-$[Co(en)_2(OH_2)OSeO_2]^+$, (B) *trans*-$[Co(en)_2(OH_2)OSeO_2]^+$, (C) Isomerization Mixture at pH ∿ 7.

emergence of another maximum in place of the charge transfer band with decreasing pH, coinciding with the formation of the diaquo species.[8] However, even at pH 1, there is still a significant concentration of the selenito species remaining after hydrolysis equilibration is complete.

The spectra of the *cis* and *trans*-selenito complexes at pH 1 and pH 3 are shown in Figs. 2.7 and 2.8, respectively, together with the spectra of the equilibrium mixtures obtained on isomerization.

In basic solution both selenito isomers undergo slow base-hydrolysis and there is a resultant shift in the spectra towards the respective dihydroxo species.[8] Basic decomposition to yield cobalt oxides becomes important over a relatively short time period around pH 12 and over a somewhat longer time period in the range pH 10-12. The spectra of the *cis* and *trans*-selenito complexes at pH 10 are shown in Fig. 2.9 together with the isomerization mixture.

3. $[Co(en)_2O_2SeO]^+$, $[Co(tn)_2O_2SeO]^+$

The U.V. - visible spectrum of the $[Co(en)_2O_2SeO]^+$ species at neutral pH, shown in Fig. 2.10, exhibits two maxima at 510 nm and 360 nm, a minimum at 425 nm, and a charge transfer band in the region of 300 nm. A similar spectrum is obtained for the $[Co(tn)_2O_2SeO]^+$ species.

Table 2.4 shows a comparison of the relevant spectral data for the bidentate selenito complex, $[Co(en)_2O_2SeO]^+$, and the monodentate selenito complex, *cis*-$[Co(en)_2(OH_2)OSeO_2]^+$, at pH 1 and pH 7.

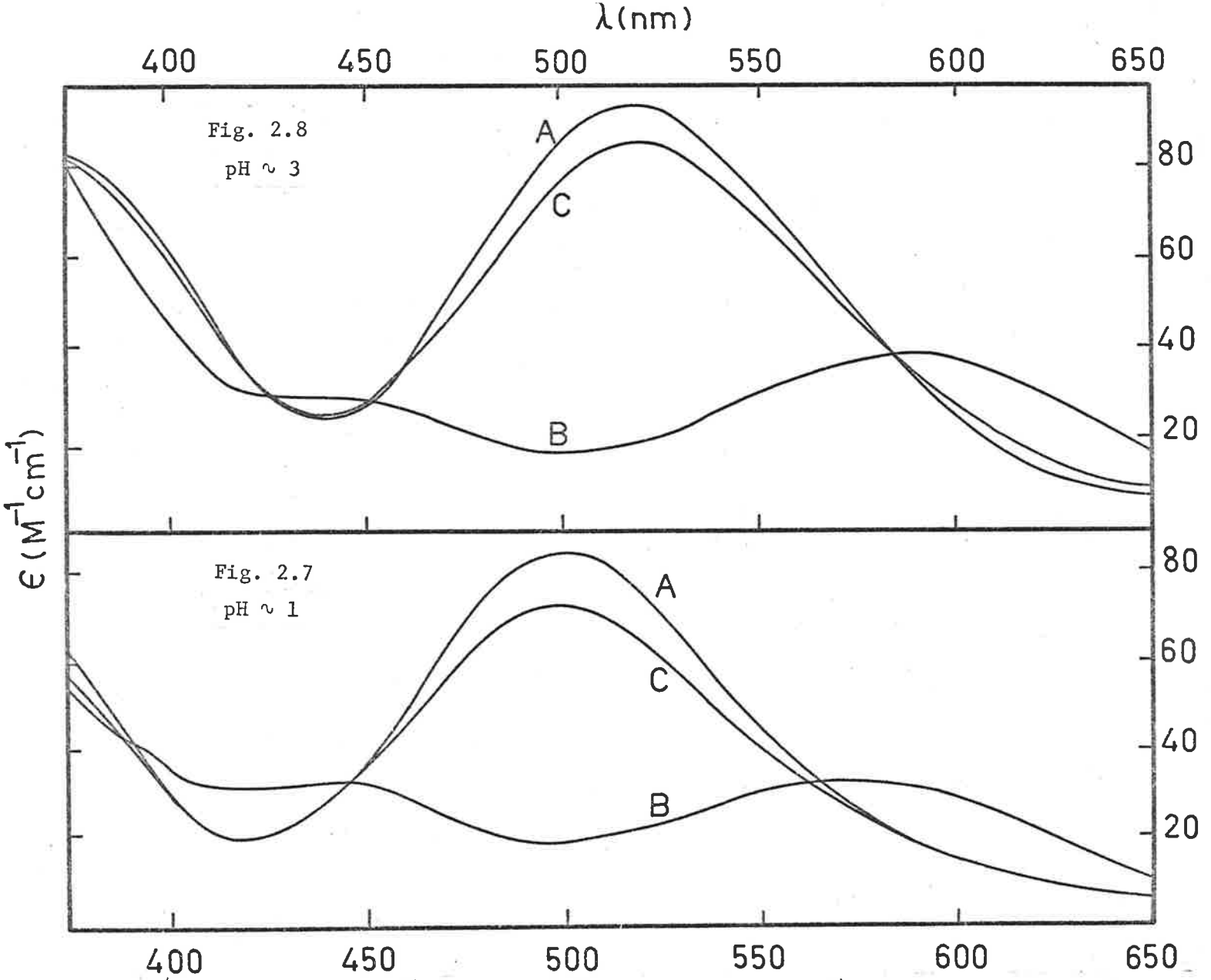

(A) *cis*-$[Co(en)_2(OH_2)OSeO_2H]^{2+}$, (B) *trans*-$[Co(en)_2(OH_2)OSeO_2H]^{2+}$, (C) Isomerization Mixture

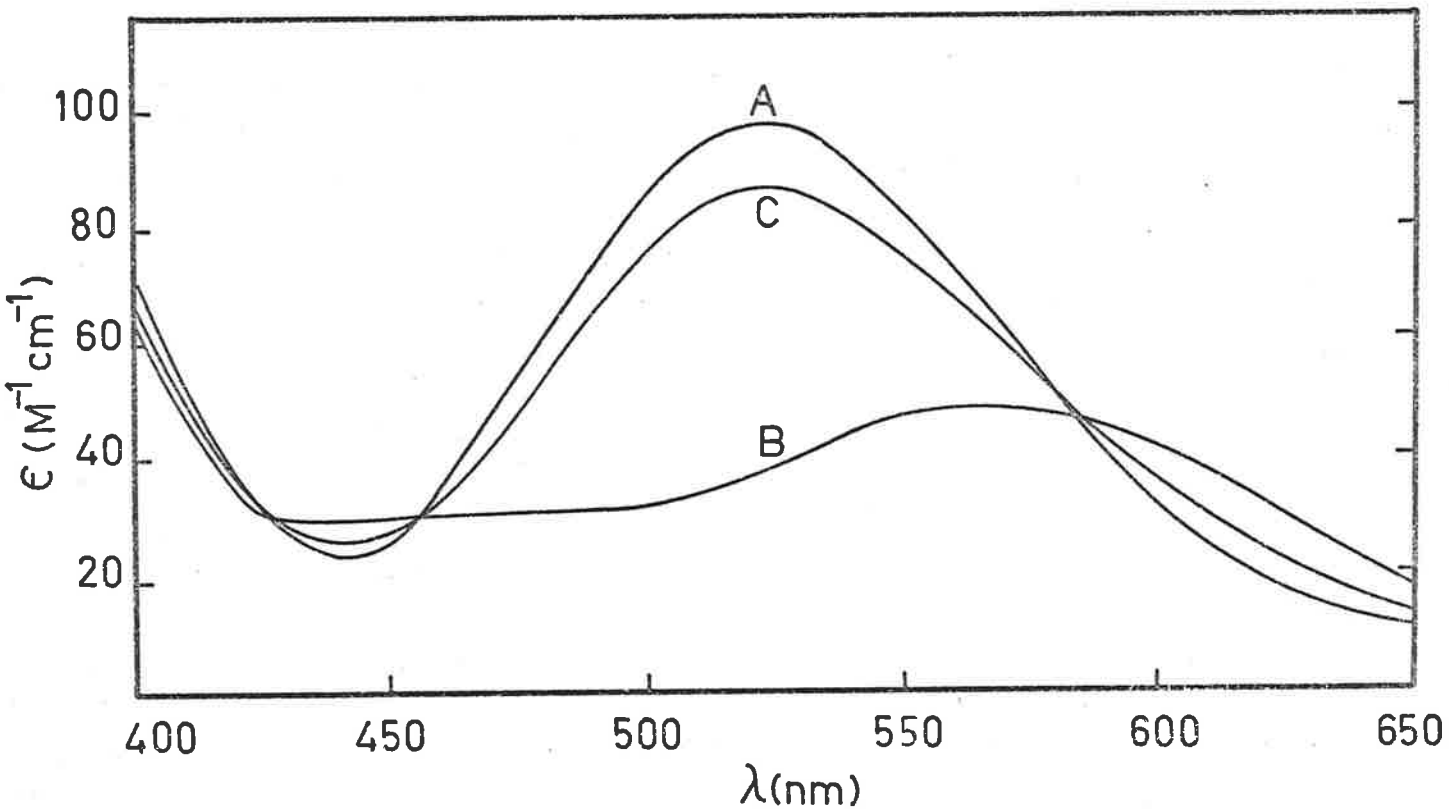

Fig. 2.9 U.V. - Visible Spectra of (A) *cis*-$[Co(en)_2(OH)OSeO_2]$, (B) *trans*-$[Co(en)_2(OH)OSeO_2]$, (C) Isomerization Mixture at pH ∿ 10.

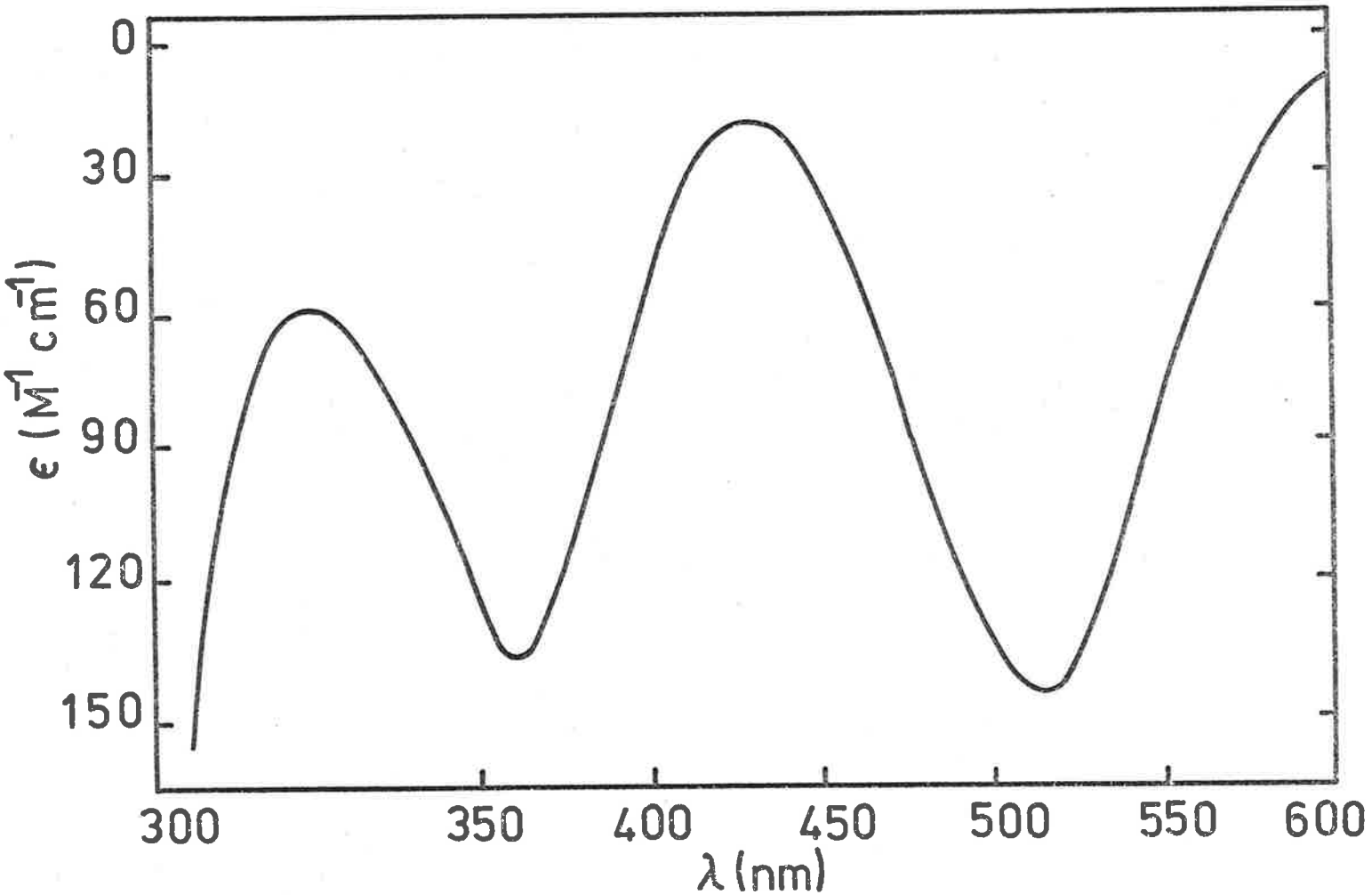

Fig. 2.10 U.V. - Visible Spectrum of $[Co(en)_2OSeO_2]^+$ at pH ∿ 7.

Table 2.4

Molar Absorptivities of Monodentate and Bidentate Selenito Complexes at Selected Wavelengths

$[Co(en)_2O_2SeO]^+$		*cis*-$[Co(en)_2(OH_2)OSeO_2]^+$	
A. pH 7.			
λ(nm)	ε(M^{-1} cm^{-1})	λ(nm)	ε(M^{-1} cm^{-1})
510	155	532	100
425	21.4	450	28.7
360	142	360	107
B. pH 1.			
λ(nm)	ε(M^{-1} cm^{-1})	λ(nm)	ε(M^{-1} cm^{-1})
495	93.7	492	71.6
415	16.1	415	17.1
360	71.4	360	61.5

2.4 *Summary*

The preparative and analytical studies have shown that there are two types of selenito products formed when selenite is reacted with octahedral aquo-amine cobalt(III) complexes in aqueous solution.

Under forcing conditions involving comparatively high temperatures and long time periods, bidentate selenito complexes such as $Co(en)_2O_2SeO^+$, where the selenite ligand is coordinated to the cobalt centre through two oxygen atoms, can be prepared in low yield at neutral pH. Apart from microanalytical evidence, these complexes can be identified by the following physical characteristics:

1. the presence of 6 sharp bands in the I.R. region due to Se-O absorptions with the ν_3 vibration being split into two separate bands;
2. the presence of 2 absorption bands in the visible region which have unusually high molar absorptivities for octahedral complexes;
3. the absence of any pKa value;
4. their slow solubility in water (c.f. the analogous $Co(en)_2PO_4$ complex).[13]

Under normal conditions, however, monodentate selenito complexes, such as *cis* and *trans*-$Co(en)_2(OH_2)OSeO_2H^{2+}$, where the selenite ligand is coordinated to the metal centre through one oxygen atom, are formed in reasonable yield over a fairly wide range of pH. These complexes are characterized by:

1. 6 well-defined bands in the I.R. region due to Se-O absorptions, with the ν_3 vibration being split into a doublet;
2. 1 absorption band in the visible region with a much lower molar absorptivity than for the analogous bidentate species;
3. two pKa values;
4. ready solubility in water.

References to Chapter 2.

1. P. Ray and A.N. Ghosh, *Ind. Chem. Soc.*, 1936, 13, 494.
2. N. Vanderhoek, *Honours Report, University of Adelaide*, 1969.
3. R.S. Murray, *Ph.D. Thesis, University of Adelaide*, 1967.
4. T.A. Beech and S.F. Lincoln, *Aust. J. Chem.*, 1971, 24, 1065.
5. a) F. Basolo and G.S. Hammaker, *Inorg. Chem.*, 1962, 1, 1.
   b) R.G. Pearson, P.M. Henry, J.G. Bergmann, and F. Basolo, *J. Am. Chem. Soc.*, 1954, 76, 5920.
6. a) R.S. Murray and D.R. Stranks, *Inorg. Chem.*, 1970, 9, 1472.
   b) D.R. Stranks and J.K. Yandell, *J. Phys. Chem.*, 1969, 73, 840.
7. F. Basolo and R.K. Murmann, *Inorg. Synthesis*, 4, 171.
8. W. Kruse and H. Taube, *J. Am. Chem. Soc.*, 1961, 83, 1280.
9. I.R. Jonasson, S.F. Lincoln, and D.R. Stranks, *Aust. J. Chem.*, 1970, 23, 2267.
10. C.N. Banwell, *"Fundamentals of Molecular Spectroscopy", McGraw-Hill, London*, 1966, 81.
11. K. Nakamoto, *"Infrared Spectra of Inorganic and Coordination Compounds", John Wiley and Sons Inc., New York*, 1963, 87.
12. a) A. Treinin and J. Wilf, *J. Phys. Chem.*, 1970, 74, 4131.
    b) L. Barcza and L.G. Sillén, *Acta. Chem. Scand.*, 1971, 25, 1250.
13. a) S.F. Lincoln and D.R. Stranks, *Aust. J. Chem.*, 1968, 21, 57.
    b) S.F. Lincoln and D.R. Stranks, ibid., 1968, 21, 1745.
14. C.H. Langford and W.R. Muir, *J. Am. Chem. Soc.*, 1967, 89, 3141.

Chapter 3. Equilibrium Studies On Selenito Complexes.

3.1 Introduction

It will be shown in this chapter, and also in chapter 4, that only monodentate selenito-complex formation is significant under the relatively mild reaction conditions used throughout the equilibrium and kinetic studies of selenito substitution with aquo-complexes. Spectral evidence in this chapter also points to the absence of any appreciable formation of bis-selenito products even up to selenite concentrations 50 times in excess of the diaquo-complex concentration.

Although the monodentate selenito complexes undergo rapid acid-hydrolysis, significant concentrations still persist even at pH 1 especially in the presence of excess selenite. This has enabled a detailed quantitative analysis of the equilibrium properties of several octahedral cobalt(III) amine-selenito complexes to be made at low pH using spectrophotometry. Isomerization of the *cis* and *trans*-$[Co(en)_2(OH_2)_2]^{3+}$ and *cis*-$[Co(tn)_2(OH_2)_2]^{3+}$ complexes (see 4.3.3) and their selenito products (see 4.8) is sufficiently slow in the low pH region to enable an unambiguous interpretation of the equilibrium data in each case. However, it was not possible to perform an equilibrium study on the *trans*-$[Co(tn)_2(OH_2)OSeO_2H]^{2+}$ species because of its rapid isomerization to the corresponding *cis*-isomer even at low temperature (see 4.8).

Only a qualitative equilibrium analysis could be made at neutral pH because of the small optical absorbance changes involved (selenito-complex formation is virtually complete in this region),

and the problems associated with isomerization of the reactant and product species.

A qualitative analysis was also made at high pH ($\geq$ 10).

3.2 *Experimental*

3.2.1 *Materials*

"Anhydrous" sodium selenite (B.D.H.; selenium content analysed as 95%) was recrystallized from concentrated aqueous solution by addition of acetonitrile. The pure hydrated form was then dried *in vacuo* over P_2O_5 at 60 - 80°. Analysis of the anhydrous sodium selenite as selenium by back titration of iodine with sodium thiosulphate[1] gave a selenium content of 99.9%.

Solutions of perchloric acid were prepared by dilution of the concentrated reagent (Baker Analysed, 70.9%) and standardised with red mercuric oxide.[2]

Solutions of sodium hydroxide were prepared by dilution of concentrated volumetric solutions (B.D.H., 0.1 and 1.0 M) and standardised with perchloric acid of known molarity.

Doubly distilled water was used for all dilutions.

Sodium perchlorate ($NaClO_4.H_2O$, Fluka) was used without further purification.

3.2.2 *Optical Absorbance Measurements*

All optical absorbance measurements were made with a manual Shimadzu spectrophotometer, model QR 50, to an accuracy of ± 0.001. The cell housing inside the spectrophotometer was maintained at the desired temperature by rapidly pumping water from an external thermostat through the metal block containing the quartz cells. All solutions were suitably equilibrated prior to recording measurements.

Because the mono-selenito complexes undergo rapid acid-hydrolysis, it was not possible to obtain the product molar absorptivity at low pH by direct measurement of the pure product in acid solution. This value was therefore estimated by plotting the apparent molar absorptivity, ε app, obtained for a number of different ratios of [Se(IV)]/[aquo-complex] at a given pH, against 1/[Se(IV)], and extrapolating back to 1/[Se(IV)] = 0, in order to determine the product molar absorptivity, ε sel, at infinite Se(IV) concentration.

At neutral pH, ε sel could be measured directly from the pure complex in solution. This value was in good agreement with that obtained by reacting the aquo-complex with excess selenite *in situ*.

In all cases the wavelength chosen for the investigation was that corresponding to an optimum difference in optical absorbance between reactant and product.

3.2.3 pH Measurements

All pH measurements were made using a Radiometer pH meter 28 to an accuracy of ± 0.05. A preliminary study was made at each particular selenite concentration used in the equilibrium investigation to determine the exact concentration of acid or base required for each reactant solution which would give the required pH value on mixing.

3.2.4 Experimental Conditions

In all cases the aquo-complex concentration was maintained at a constant value of $\sim 1 \times 10^{-2}$ M. The selenite concentration was varied over the range 1×10^{-2} - 1 M.

The pH was varied over the range pH 1 - pH 10, with actual determinations of equilibrium constants at pH 1 and pH 3, and estimates at pH 7 and pH 10. A minimum of 4 different [Se(IV)]/[aquo-complex] ratios was used for each quantitative determination.

The equilibrium study was carried out over a temperature range of 15 - 40°.

Ionic strength was adjusted to 1 M with sodium perchlorate.

3.3 *Polyselenite Equilibria in Aqueous Solution*

An emf titration study on the reaction between the selenite ion, SeO_3^{2-} ($=L^{2-}$), and H^+, in various aqueous ionic media has been made by Barcza and Sillèn.[3] The results are consistent with the formation of the binuclear selenite species, HL_2^{3-}, $H_2L_2^{2-}$, $H_3L_2^-$, and H_4L_2 in addition to the mononuclear products, HL^- and H_2L, over the concentration range used, viz., L = 0.02 - 3.0 M. The general form of the reaction can be written

$$pL^{2-} + qH^+ \rightleftharpoons H_q L_p^{(2p-q)-} \qquad 3.1$$

The thermodynamics of the polyselenite equilibria have been studied calorimetrically by Arnek and Barcza[4] who found that the stability of the binuclear species increases with dilution of the medium, as a result of the large positive increase in $\Delta S°$ accompanying the decrease in ionic strength.

Prior to these investigations, only qualitative evidence existed for the presence of polynuclear selenite species. In the case of the analogous sulphite ion, however, quantitative evidence for dimerization has been available for some time.[5]

Whereas sulphite dimerization is readily recognizable by the deviation from Beer's law at relatively high anion concentration, this characteristic appears to be less evident in the case of selenite. Treinin and Wilf,[6] while studying the environmental effects on the U.V. spectra of selenites in solution, found no deviation from Beer's law even up to 1 M concentration of $HSeO_3^-$ ion. These results are in

direct contrast to those of Ley and König[7] who ascribed the deviations from Beer's law, which they observed in the U.V. spectra of concentrated solutions of H_2SeO_3, to the formation of the polymeric species, $(H_2SeO_3)n$. The disparity between these two sets of data could conceivably be attributed to the different pH conditions at which the investigations were performed.

It should be clearly stated, however, that although deviation from Beer's law does provide evidence for dimerization or polymerization in certain cases, the absence of any such deviation does not exclude the possibility of their existence. The spectral characteristics of the mononuclear and binuclear species could be so similar as to prevent the detection of any deviation outside the range of experimental error.

The normal solid selenites, such as Na_2SeO_3, are presumed to contain pyramidal SeO_3^{2-} units on the basis of I.R. spectral data.[8] Evidence available from crystal structure analyses of solid acid selenites, such as H_2SeO_3,[9] and Na $H_3(SeO_3)_2$,[10] has indicated no separate polynuclear groups but rather infinite chains or sheets of SeO_3 units connected through hydrogen bonds, as shown below.

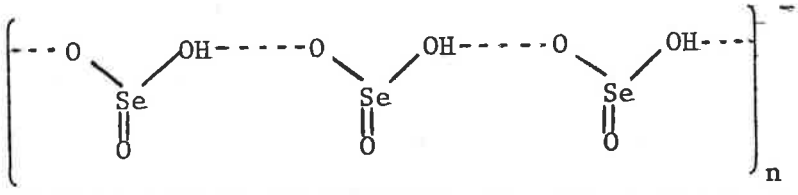

Simon and Paetzold[11] concluded from their observation of identical Raman spectra for concentrated solutions of the acid selenites, $MHSeO_3$ and $M_2Se_2O_5$, that the rapid equilibrium

$$2HSeO_3^- \rightleftarrows Se_2O_5^{2-} + H_2O \qquad 3.2$$

is established between the two species.

As will be described in chapter 4, however, it is more convenient, especially from a kinetic viewpoint, to use the alternative formulation for selenite dimerization

$$2HSeO_3^- \rightleftarrows H_2(SeO_3)_2^{2-} \text{ etc.} \qquad 3.3$$

proposed by Barcza and Sillén.[3] The dimeric species, $H_2(SeO_3)_2^{2-}$, is shown below.

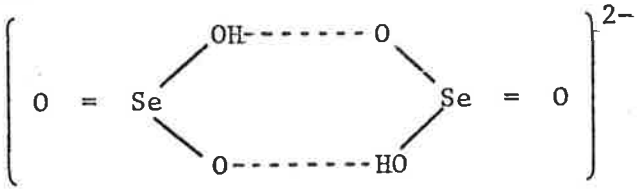

Fig. 3.1 shows the distribution between the various selenite species for (a) L = 0.1 M, (b) L = 1.0 M in 1 M $NaClO_4$ medium at 25°.

The features of general importance which should be noted are:

1. In dilute solution ($L \lesssim 0.1$ M), the predominant selenite species are the mononuclear forms SeO_3^{2-} (= L^{2-}), $HSeO_3^-$ (= HL^-), and H_2SeO_3 (= H_2L), related by the equilibria

$$H^+ + L^{2-} \overset{K_1}{\rightleftharpoons} HL^- \qquad 3.4$$

$$HL^- + H^+ \overset{K_2}{\rightleftharpoons} H_2L \qquad 3.5$$

where $pK_1 = 8.06$ and $pK_2 = 2.36$. (see 2.3.3).

2. The extent of dimerization is negligible at $pH \gtrsim 10$ over the entire selenite concentration range, i.e. the pure SeO_3^{2-} species is completely monomeric.

Fig. 3.1 Distribution of Se(IV) Between Species in 1 M $NaClO_4$ for (A) L = 0.1 M, (B) L = 1.0 M.

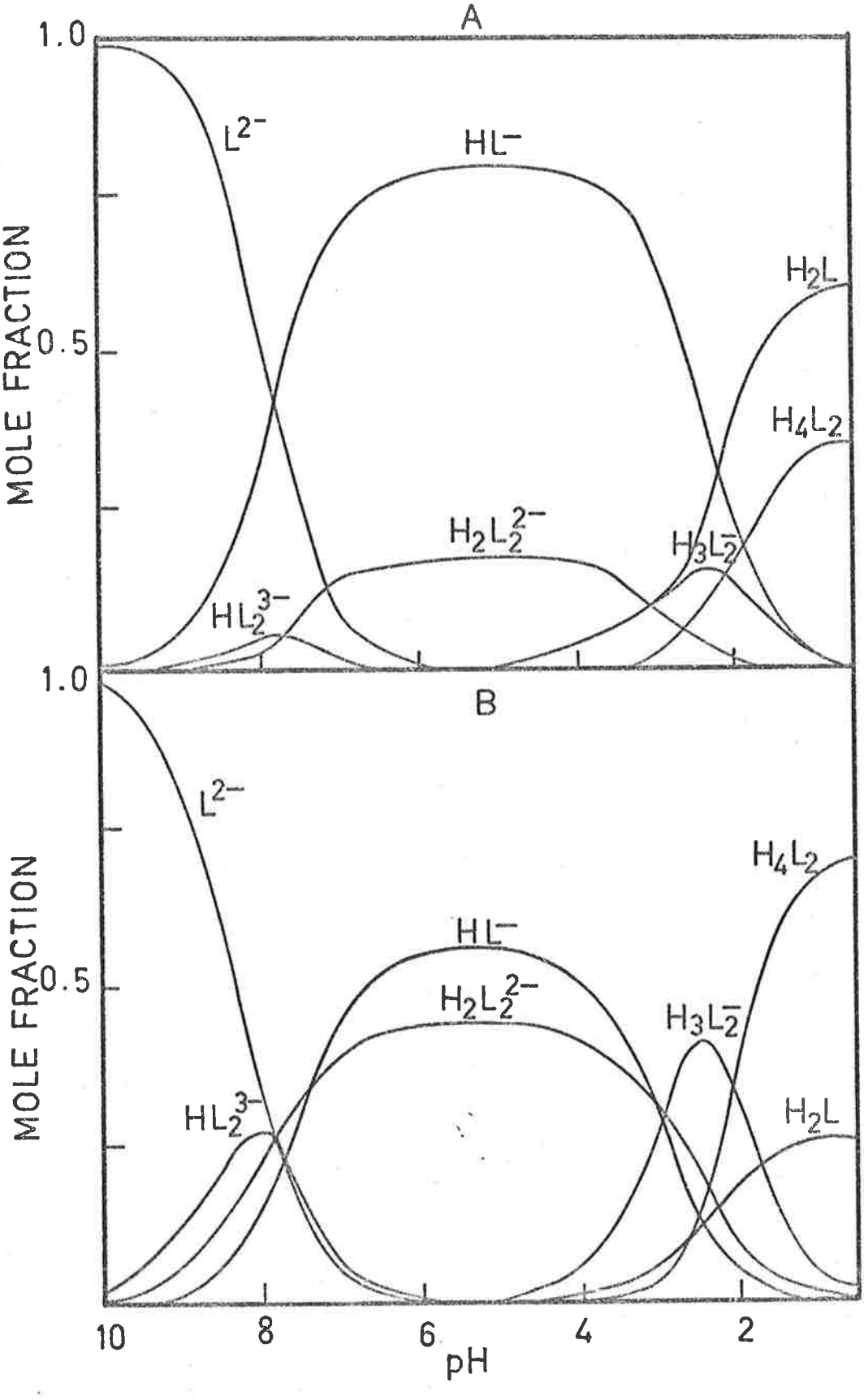

3. Although the existence of trimeric and higher selenite species cannot be entirely discounted, it seems likely that the predominant polynuclear species are dimeric, especially for $L \lesssim 1$ M.

3.4 *Distribution of Aquo Species*

The distribution curves for the *cis*-$[Co(en)_2(OH_2)_2]^{3+}$, *trans*-$[Co(en)_2(OH_2)_2]^{3+}$, and a mixture of *cis* and *trans*-$[Co(tn)_2(OH_2)_2]^{3+}$ ions are shown in Figs. 3.2, 3.3, and 3.4, respectively. These are based on the known pKa values for these complexes which are summarized below:

cis-$[Co(en)_2(OH_2)_2]^{3+}$: $pK_1 = 6.06$, $pK_2 = 8.19$ at 25°;[12]

trans-$[Co(en)_2(OH_2)_2]^{3+}$: $pK_1 = 4.45$, $pK_2 = 7.94$ at 25°;[12]

$[Co(tn)_2(OH_2)_2]^{3+}$: $pK_1 = 4.75$, $pK_2 = 7.45$ at 22°.[13]

No distribution curve has been drawn for the trivial case of the $[Co(NH_3)_5OH_2]^{3+}$ species since the distribution between aquo and hydroxo ions is readily derived from the known pKa value,

$pK_a = 6.6$ at 25°.[14]

Three outstanding features emerge from these data:

1. the predominant complex form at pH < 4 is the aquo or diaquo ion;
2. at neutral pH, the hydroxo or hydroxo-aquo form predominates;
3. at pH > 9, the major complex form is the hydroxo or dihydroxo ion.

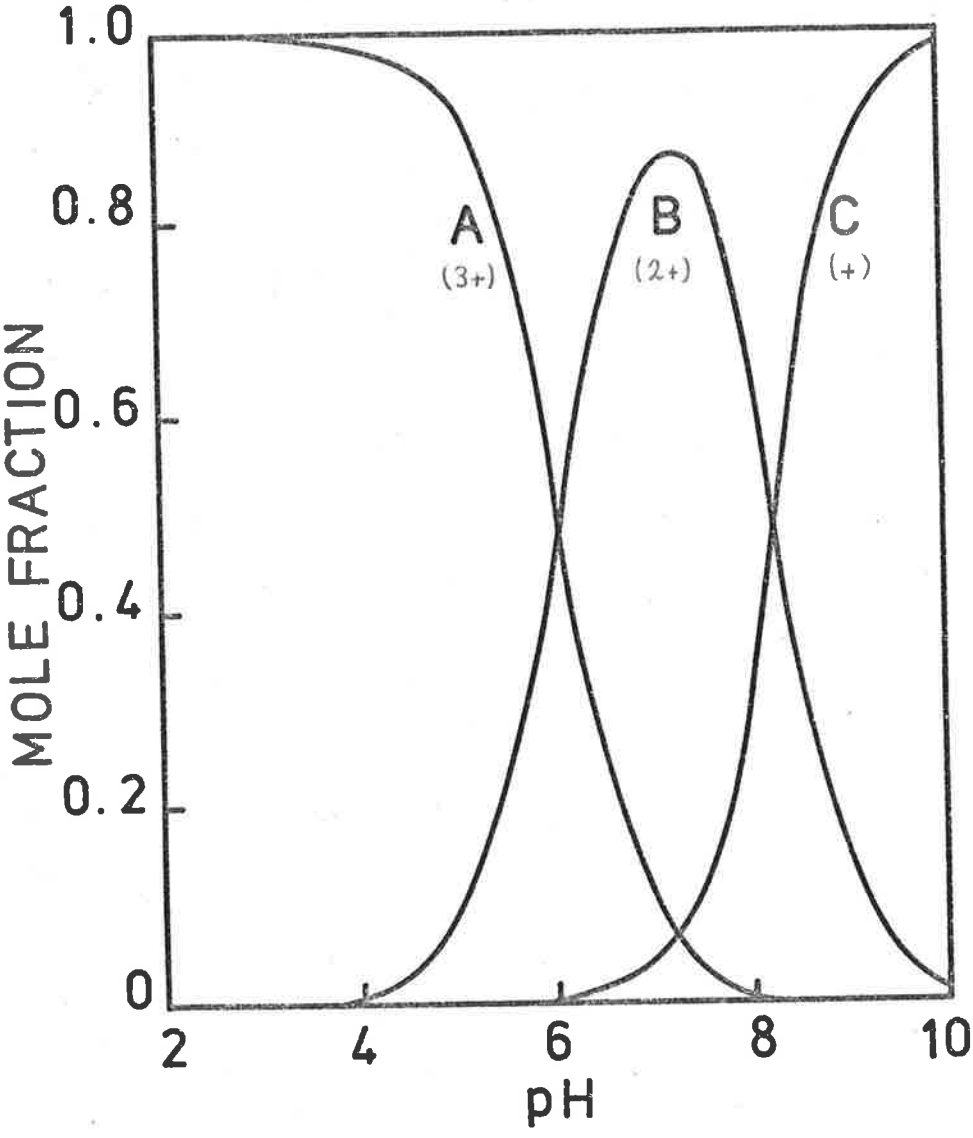

Fig. 3.2 Distribution of Protonated Species for *cis*-$[Co(en)_2(OH_2)_2]^{3+}$.

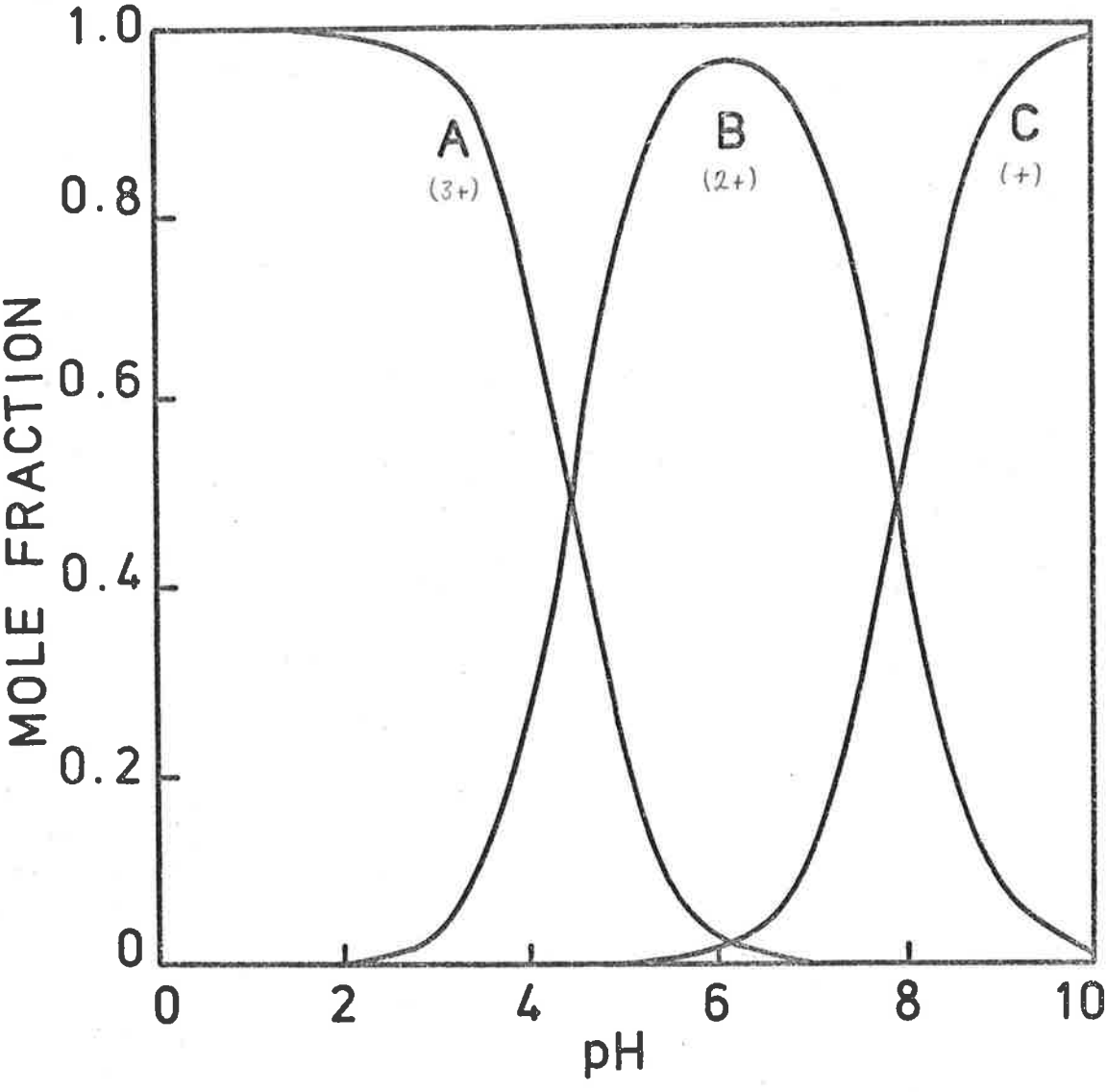

Fig. 3.3 Distribution of Protonated Species for *trans*-$[Co(en)_2(OH_2)_2]^{3+}$.

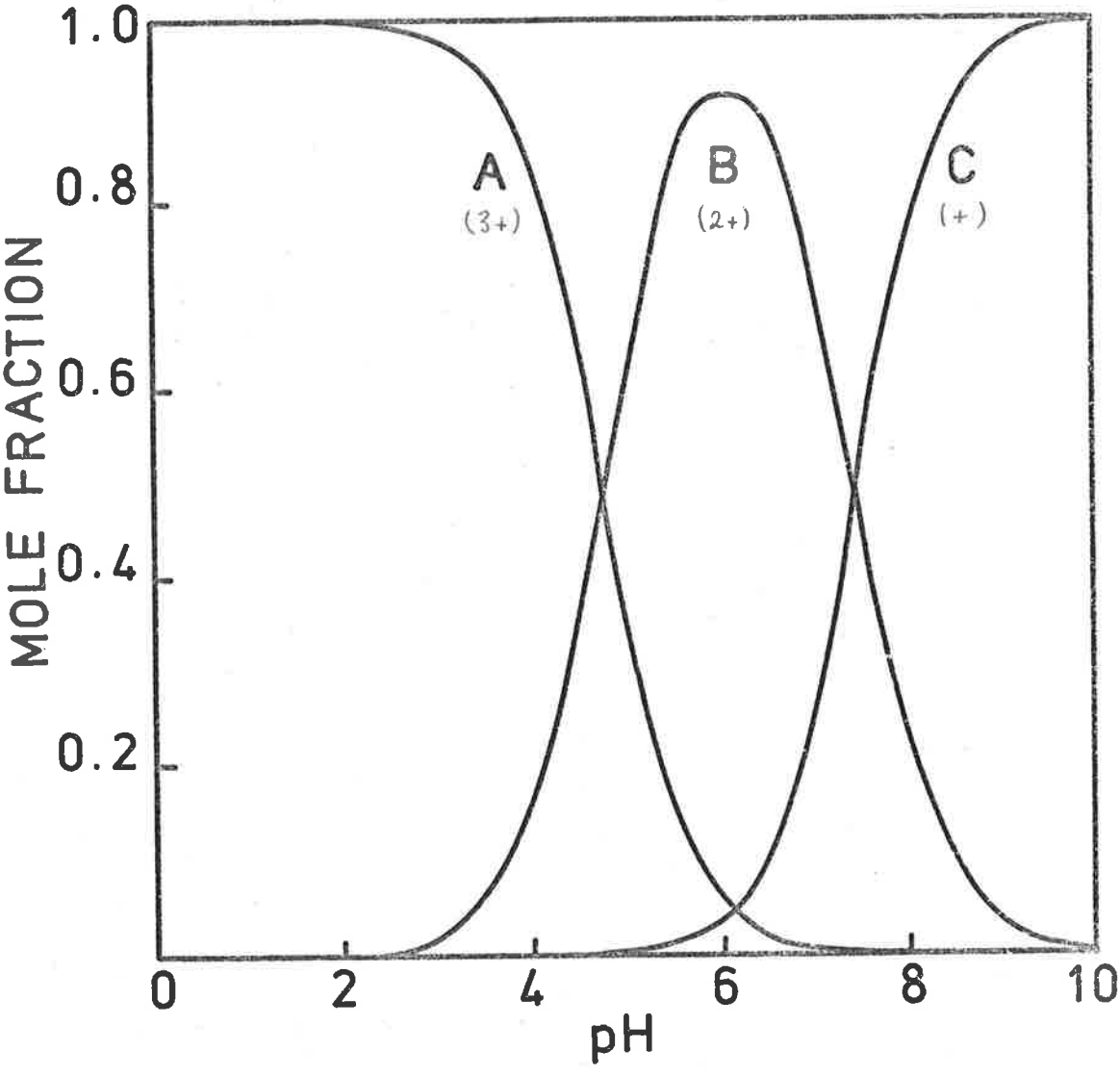

Fig. 3.4 Distribution of Protonated Species for a Mixture of *cis* and *trans*-$[Co(tn)_2(OH_2)_2]^{3+}$.

3.5 Definition of Terms

The term "Se(IV)" will be taken to include all protonated and dimeric forms of SeO_3^{2-}.

The term "selenite" will be used generally as a systematic reference to the oxyanion group itself, and more specifically as a direct reference to the SeO_3^{2-} ion.

The term "biselenite" will be taken to include HL_2^{3-}, $H_2L_2^{2-}$, and $H_3L_2^{-}$, as well as HL^{-}.

The term "selenious acid" will be taken to include H_4L_2 as well as H_2L_2.

The term "aquo-complex" will be used in the general sense to include all the protonated and isomeric forms of $[Co(en)_2(OH_2)_2]^{3+}$ and $[Co(tn)_2(OH_2)_2]^{3+}$, and the protonated forms of $[Co(NH_3)_5OH_2]^{3+}$.

3.6 Results and Discussion

When selenites (SeO_3^{2-} or its protonated forms) are mixed with octahedral aquo-amine cobalt(III) complexes in aqueous solution the degree of complex-selenito formation rises to a maximum at neutral pH and progressively decreases with any pH change away from this region.

A general relation for the equilibrium reaction

$$ROH_2^{3+} + L^{n-} \underset{\leftarrow}{\overset{K}{\rightleftharpoons}} RL^{(3-n)+} + H_2O \qquad 3.6$$

can be written as

$$K = \frac{[\text{selenito complex}]}{[\text{aquo complex}][\text{Se(IV)}]} \qquad 3.7$$

where [Se(IV)] = [Se(IV)] initial - [selenito complex]

3.6.1 Region of Low pH : pH 1 - 4.

At low pH, acid-hydrolysis is competitive with selenite substitution. Excess selenite forces eq. 3.6 to the right, allowing K to be evaluated spectrophotometrically for several different ratios of selenite/aquo-complex, the concentration of the latter being held at a constant value of $\sim 1 \times 10^{-2}$ M. The anion concentration was varied up to 1 M.

Equilibrium data at pH 1 and pH 3 are shown in Tables 3.1, 3.2, 3.3, and 3.4, for the $[Co(NH_3)_5OH_2]^{3+}$, *cis* and *trans*-$[Co(en)_2(OH_2)_2]^{3+}$, and *cis*-$[Co(tn)_2(OH_2)_2]^{3+}$ ions, respectively. The rapid isomerization of the *trans*-$[Co(tn)_2(OH_2)_2]^{3+}$ species[13] precludes any equilibrium study on this isomer.

A comparison of the K values at pH 1 and pH 3 for a particular aquo-ion shows that there is a 10 - 30 times increase in K at the

Table 3.1 Stability Constants for the System $[Co(NH_3)_5OH_2]^{3+}$ + [Se(IV)] at 25.0 ± 0.1°

A. pH ∿ 1.2, μ = 550 nm.

10^2[Se(IV)](M)	pH(± 0.05)	% selenito complex	K	β biselenite(±5)
5	1.25	7	1.5 ± 0.2	26
10	1.15	11	1.2 ± 0.1	25
15	1.10	16	1.3 ± 0.1	27
25	1.25	29	1.6 ± 0.2	27
50	1.30	40	1.3 ± 0.1	20
100	1.20	47	1.8 ± 0.2	29

B. pH ∿ 3.2, μ = 550 nm.

10^2[Se(IV)] (M)	pH(± 0.05)	% selenito-complex	K	β biselenite (±3)
5	2.85	37	13 ± 2	17
7.5	3.25	55	18 ± 2	20
10	2.95	59	15 ± 1	19
15	3.30	71	17 ± 2	19
25	3.15	82	18 ± 2	22
50	3.15	88	14 ± 1	17

($[Co(NH_3)_5OH_2^{3+}]$ = 1.01 x 10^{-2} M; μ = 1.0 M, ClO_4^- medium; ε_{aquo} = 21.6, $\varepsilon_{selenito}$ = 44.3 M^{-1} cm^{-1} at 550 nm.).

Table 3.2 Stability Constants for the System cis-$[Co(en)_2(OH_2)_2]^{3+}$ + [Se(IV)] at 25.0 ± 0.1°

A. pH ∿ 1.2, μ = 550 nm.

10^2[Se(IV)](M)	pH(± 0.05)	% selenito-complex	K	β biselenite(±10)
5	1.30	11	2.6 ± 0.4	50
10	1.20	16	1.9 ± 0.3	50
15	1.15	19	1.6 ± 0.2	59
25	1.25	33	2.0 ± 0.2	58
50	1.35	53	2.2 ± 0.3	51
100	1.20	62	3.3 ± 0.4	55

B. pH ~ 3.2, λ = 510 nm.

10^2[Se(IV)] (M)	pH(± 0.05)	% selenito-complex	K	β biselenite(±5)
1	3.25	28	56 ± 4	67
2.5	3.25	50	50 ± 4	58
5	3.25	65	43 ± 3	52
10	3.15	81	46 ± 3	54
25	3.25	93	57 ± 4	64
50	3.25	95	56 ± 4	63

([*cis*-$Co(en)_2(OH_2)_2^{3+}$] = 0.98 x 10^{-2} M; μ = 1.0 M, ClO_4^- medium; ε_{aquo} = 31.2, $\varepsilon_{selenito}$ = 70.0 M^{-1} cm^{-1} at 550 nm; ε_{aquo} = 67.5, $\varepsilon_{selenito}$ = 93.5 M^{-1} cm^{-1} at 510 nm.)

Table 3.3 Stability Constants for the System trans-$[Co(en)_2(OH_2)_2]^{3+}$ + [Se(IV)] at 15.0 ± 0.1°.

A. pH ∿ 1.2, λ = 600 nm.

10^2[Se(IV)] (M)	pH(± 0.05)	% selenito-complex	K	β biselenite(±20)
10	1.20	39	6.5 ± 0.7	117
15	1.10	45	5.7 ± 0.6	110
25	1.25	58	5.8 ± 0.6	97
50	1.25	65	3.8 ± 0.4	72
100	1.20	72	5.1 ± 0.5	87

B. pH ∿ 3.3, λ = 600 nm.

10^2[Se(IV)](M)	pH(± 0.05)	% selenito-complex	K	β biselenite(±10)
5	3.50	68	53 ± 6	58
10	3.20	77	36 ± 4	42
25	3.25	88	44 ± 5	52
50	3.25	92	44 ± 5	50

([*trans*-$Co(en)_2(OH_2)_2^{3+}$] = 0.98 x 10^{-2} M; μ = 1.0 M, ClO_4^- medium; ε_{aquo} = 17.3, $\varepsilon_{selenito}$ = 42.2 M^{-1} cm^{-1} at 600 nm.)

Table 3.4 Stability Constants for the System cis-$[Co(tn)_2(OH_2)_2]^{3+}$ + [Se(IV)] at 25.0 ± 0.1°.

A. pH ∿ 1.2, λ = 560 nm.

10^2[Se(IV)](M)	pH(± 0.05)	% selenito-complex	K	β biselenite(±10)
5	1.25	17	4.1 ± 0.4	70
10	1.25	22	2.9 ± 0.3	56
15	1.10	25	2.2 ± 0.2	61
25	1.15	36	2.3 ± 0.2	60
50	1.15	60	3.0 ± 0.4	63
100	1.15	73	2.9 ± 0.3	55

B. pH ∿ 3.3, λ = 560 nm.

10^2[Se(IV)](M)	pH(± 0.05)	% selenito-complex	K	β biselenite(±5)
7.5	3.50	80	62 ± 5	67
10	3.30	81	47 ± 4	53
15	3.35	86	45 ± 4	50
25	3.10	90	39 ± 3	46
50	3.10	95	37 ± 3	54

([*cis*-$Co(tn)_2(OH_2)_2^{3+}$] = 0.99 x 10^{-2} M; μ = 1.0 M, ClO_4^- medium; ε_{aquo} = 29.9, $\varepsilon_{selenito}$ = 75.5 M^{-1} cm^{-1} at 560 nm.)

higher pH value. Although this could be simply attributed to the relative effects of acid-hydrolysis at the two pH values, it seems more pertinent to examine the alternative viewpoint that the size of K is dependent on the nature of the reactant species.

From Figs. 3.2, 3.3, and 3.4, it can be seen that the aquo/diaquo ion is the predominant complex form in the pH range 1 - 4. This is true for each of the complex ions studied. Reference to Fig. 3.1 shows, however, that there is a large decrease in the proportion of biselenite present in going from pH 3 to pH 1. At pH 3, biselenite constitutes approximately 90% of the total selenite concentration for L = 0.1 M in 1 M $NaClO_4$ medium, and this falls to only 5% at pH 1. It can therefore be proposed that this decrease in biselenite concentration is responsible for the corresponding decrease in K at low pH.

To test the hypothesis that any contribution to complex formation from the selenious acid fraction is negligible, it is necessary to define the formation constant, β biselenite, which can be written as

$$\beta \text{ biselenite} = \frac{[\text{selenito complex}]}{[\text{aquo complex}][\text{biselenite}]} \qquad 3.8$$

where [biselenite] = [biselenite]initial - [selenito-complex]. If selenito-complex formation is due to biselenite, then β biselenite should be constant at pH 1 and pH 3 within the experimental error. Also if β biselenite at a given pH is independent of the concentrations of the individual species which make up the biselenite fraction, then both the monomeric $HSeO_3^-$ ion and its dimeric forms have comparable

formation constants.

At low total Se(IV) concentration ($L \lesssim 0.1$ M), the $HSeO_3^-$ ion constitutes almost the entire biselenite fraction and $[HSeO_3^-]$ (and hence [biselenite]) can be determined from the pKa values measured for selenite in dilute solution (see 2.3.2).

However, as the total Se(IV) concentration is increased the concentration of the $HSeO_3^-$ species decreases as dimerization becomes increasingly important. At pH 1, when L = 1.0 M, the entire biselenite fraction is composed of dimeric species.

Although the concentrations of the individual biselenite species vary considerably from L = 0.1 M to L = 1.0 M, the percentage of the total selenite concentration attributable to biselenite remains essentially constant for both values of L. If it is assumed that the percentage contribution of biselenite is constant over the entire range of selenite concentration used in the equilibrium study, viz., L = 0.01 - 1.0 M, then the biselenite concentration can be estimated for those L values which lie between 0.1 and 1.0 M. The absolute biselenite concentration increases with total Se(IV) concentration.

The β biselenite values at pH 1 and pH 3 are shown in Tables 3.1, 3.2, 3.3 and 3.4. There is reasonably good agreement between the two sets of data considering the systematic error which is introduced at the higher selenite concentrations in addition to the actual error involved in measuring the optical absorbance values.

The general conclusion which can be drawn, then, is that the

degree of selenito-complex formation at low pH is entirely dependent on the concentration of the $HSeO_3^-$ ion, at low biselenite concentration, and its associated dimeric forms at high biselenite concentration.

A temperature dependence study at pH 1 for each of the aquo-amine cobalt(III) ions indicated that K is virtually invariant with temperature over the range 20 - 40°.

Substitution in the low pH region can therefore be described by the following stoichiometric equation

$$\underset{(+Hq\ Lp)}{ROH_2^{3+}} + HSeO_3^- \rightleftharpoons \underset{(+Hq_{-1}Lp_{-1})}{ROSeO_2H^{2+}} + H_2O \qquad 3.9$$

3.6.2 Region of Neutral pH : pH 6 - 8.

At neutral pH the optical absorbance value obtained by reacting the aquo complex with excess selenite is identical with that of the pure monodentate selenito compound. In fact, when selenite is present in large excess there is a progressive decrease in the product molar absorptivity below that of the pure complex. This suggests that selenite-catalysed hydrolysis becomes important at high selenite concentration. Bis-selenito complex formation can be ruled out as a possible alternative explanation since this would be expected to lead to an increase in optical absorbance by analogy with the similar increase found for the bidentate selenito species (see 2.3.3).

Because of the very small optical absorbance differences involved when the selenite concentration is held constant and the aquo-complex concentration varied, any quantitative evaluation of K by spectrophotometric means is precluded in the neutral pH region.

However a qualitative analysis indicates K > 100 which means that in the absence of any competitive acid- or base-hydrolysis reactions, substitution of selenite proceeds essentially to completion. The rise in K to a maximum value in this region coincides with an optimum concentration of biselenite. Between pH 4 and pH 6 biselenite constitutes virtually 100% of the total selenite concentration and at pH 7 greater than 90%.

Substitution at neutral pH can be stoichiometrically written as

$$\underset{(+Hq\ Lp)}{ROH^{2+}} + HSeO_3^- \rightarrow \underset{(+Hq_{-1}Lp_{-1})}{ROSeO_2^+} + H_2O \qquad 3.10$$

3.6.3 Region of High pH : pH ≥ 10

The decrease in K at high pH is consistent with the decrease in biselenite concentration and the increasing importance of base-hydrolysis. At pH 11.5, the rate of base-hydrolysis is competitive with the rate of substitution, the value of K being ∿ 5 at 25° and 0.5 M ionic strength for the $Co(NH_3)_5OH^{2+}$ ion.[15] The low value of K at high pH is also indicative of the relatively poorer coordinating ability of selenite compared with biselenite. Substitution in this region can be stoichiometrically written as

$$\underset{(+HSeO_3^-)}{ROH^{2+}} + SeO_3^{2-} \rightleftarrows \underset{(+H_2O)}{ROSeO_2^+} + OH^- \qquad 3.11$$

3.7 Summary

The equilibrium study has shown that substitution by selenite on octahedral aquo-amine cobalt(III) complexes proceeds essentially to completion when there is an optimum concentration of biselenite, viz., in the neutral pH region. Under the reaction conditions employed there is no significant bidentate selenito-complex formation. There is also good evidence to suggest that bis-selenito complex formation is relatively unimportant, at least up to [Se(IV)] = 0.5 M.

Although there is a substantial decrease in the overall equilibrium constant, K, for selenito-complex formation with increasing and decreasing pH away from the neutral region, significant concentrations of the monodentate selenito species still persist at pH 1 and pH 10, especially in the presence of excess selenite. This decrease in the value of K can be ascribed to the relatively poorer coordinating ability of the selenious acid and selenite species compared with the biselenite species which means that acid and base hydrolysis become competitive with selenite substitution at low and high pH respectively.

The following stoichiometric equations can be written for selenite substitution:

$$\underset{(+Hq\ Lp)}{ROH_2^{3+} + HSeO_3^-} \rightleftarrows \underset{(+Hq_{-1}Lp_{-1})}{ROSeO_2H^{2+} + H_2O}$$

in acidic solution (pH 1 - 4);

$$\underset{(+Hq\ Lp)}{ROH^{2+} + HSeO_3^-} \longrightarrow \underset{(+Hq_{-1}Lp_{-1})}{ROSeO_2^+ + H_2O}$$

in neutral solution (pH 6 - 8);

$$ROH^{2+} + SeO_3^{2-} \longrightarrow ROSeO_2^{+} + OH^{-}$$
$$(+HSeO_3^{-}) \qquad\qquad (+H_2O)$$

in basic solution (pH $\gtrsim$ 10).

References to Chapter 3.

1. A.I. Vogel, *"Quantitative Inorganic Analysis", 3rd edn., Longmans, London,* 1961, 303.
2. R.D. Brown and T.A. O'Donnel, *"Manual of Elementary Practical Chemistry", 2nd edn., Melbourne University Press,* 1957, 52.
3. L. Barcza and L.G. Sillén, *Acta. Chem. Scand.,* 1971, 25, 1250.
4. R. Arnek and L. Barcza, ibid., 1972, 26, 1.
5. R.M. Golding, *J. Chem. Soc.,* 1960, 3711.
6. A. Treinin and J. Wilf, *J. Phys. Chem.,* 1970, 74, 4131.
7. H. Ley and E.Z. König, *Physik. Chem. (Leipzig),* 1938, B41, 365.
8. K. Nakamoto, *"Infrared Spectra of Inorganic and Coordination Compounds," John Wiley and Sons Inc., New York.,* 1963, 89.
9. A.F. Wells and M.J. Bailey, *J. Chem. Soc.,* 1949, 1282.
10. K.D. Chou and Y.C. Tang, *Chem. Abstr.,* 1959, 53, 8761.
11. A. Simon and R. Paetzold, *Z. anorg. allgem Chem.,* 1960, 303, 46.
12. J. Bjerrum and S.E. Rasmussen, *Acta. Chem. Scand.,* 1952, 6, 1265.
13. I.R. Jonasson, *unpublished data.*
14. F. Basolo and R.G. Pearson, *"Mechanisms of Inorganic Reactions", 2nd edn., John Wiley and Sons Inc., New York,* 1967, 32.
15. J.V. Dubrawski, *Honours Report, University of Adelaide,* 1972.

Chapter 4. Kinetics of Selenite Substitution With Aquo-Ligands

A Substitution at Selenium (IV): Selenito-Complex Formation.

4.1 Introduction

A number of anation studies have been made on the reactions of octahedral aquo-amine cobalt(III) complexes with group V and VI oxyanions. Table 4.1 summarizes the relevant kinetic and mechanistic data obtained for some of these reactions. In each case a comparison has been made between the rate of anation, k_{an}, and the rate of water-exchange, k_{ex}, with a view to assigning reaction mechanism on the basis of the Langford model.

It can be seen from Table 4.1 that the labile-oxygen containing ligands, such as $HAsO_4^{2-}$ (group V) and SO_3^{2-} (group VI), undergo substitution more readily than the inert-oxygen containing ligands, such as PO_4^{3-} and SO_4^{2-}, respectively. On this basis, therefore, SeO_3^{2-}, which is analogous to SO_3^{2-}, would be expected to be more reactive with regard to substitution than SeO_4^{2-}, which is analogous to SO_4^{2-}.

Previous qualitative studies[6,7] on the oxygen-exchange reaction between selenite and solvent water indicated that the rate of exchange is rapid even in strong alkali solution. Davies[8] found that the rate of exchange for Se(IV) was greater than that for both S(IV) and Se(VI), and also that the reaction was acid-catalysed with exchange occurring rapidly through the monoanion, $HSeO_3^-$. This dependence of the exchange rate on $[H^+]$ for oxyanions is

Table 4.1

Group V and VI Oxyanion Anation Reactions

Reaction	Temp(°C)	pH	k_{an} (sec^{-1})	k_{ex}/k_{an}	Mech.	Ref.
trans-$[Co(en)_2OH(OH_2)]^{2+}$ + PO_4^{3-}	48	7	4.3×10^{-3}	15	Id	1
$[Co(NH_3)_5OH_2]^{3+}$ + $HAsO_4^{2-}$	22	6	4.9×10^{-3}	0.37	Ia	2
$[Co(NH_3)_5OH_2]^{3+}$ + SO_4^{2-}	45		2.4×10^{-5}	5	Id	3
$[Co(en)_2(OH_2)_2]^{3+}$ + SO_4^{2-}	52	3.5	4.0×10^{-4}	7	Id	4
$[Co(en)_2(OH_2)_2]^{3+}$ + SeO_4^{2-}	52	3.5	3.6×10^{-4}	7	Id	4
trans-$[Co(en)_2(OH_2)SO_3]^{+}$ + SO_3^{2-}	25	8.1	13.4		D	5

well known.[9]

Recently, Okumura and Okuzaki[10] have measured the oxygen-exchange rate on selenite at 0° over the pH range 8.7 - 12.5. The kinetics were found to be consistent with the rate law

$$R = k_1[SeO_3^{2-}] + k_2[HSeO_3^-] + k_3[HSeO_3^-]^2 + k_4[HSeO_3^-][SeO_3^{2-}] \quad 4.1$$

The important conclusions arising from this study were

1. at pH > 10, the exchange rate, R, is independent of pH and depends on $[Se(IV)]^{1.0}$, i.e. the exchange proceeds exclusively by the reaction path

$$Se\overset{*}{O}_3^{2-} + H_2O \rightleftarrows SeO_3^{2-} + H_2\overset{*}{O} \; ; \quad 4.2$$

2. at pH ≲ 9, R depends on pH and on $[Se(IV)]^{1.32}$ indicating that exchange by the dimeric pathways

$$HSeO_3^- + HSeO_3^- \rightleftarrows Se_2O_5^{2-} + H_2O \quad 4.3$$

$$HSeO_3^- + SeO_3^{2-} \rightleftarrows Se_2O_5^{2-} + OH^- \quad 4.4$$

is also important;

3. the exchange rate increases rapidly with decreasing pH.

The enthalpy of activation, $\Delta H^{\ddagger}_{ex} = 58.6 \pm 3.8$ kJ mol^{-1}, for exchange at pH 9.1 is similar in magnitude to the enthalpy of activation, $\Delta H^{\ddagger}_{hyd} = 48.1 \pm 1.4$ kJ mol^{-1}, for the base-hydrolysis of $[Co(NH_3)_5OSeO_2]^+$,[11] which is also known to proceed by Se-O bond cleavage in the rate-determining step.

In order to examine the kinetics of selenite substitution for a variety of aquo-ligands with a view to comparing the rates of substitution with those for other group V and VI oxyanions, and also

with the rate of oxygen-exchange on selenite, the complexes, $[Co(NH_3)_5OH_2]^{3+}$, $[Rh(NH_3)_5OH_2]^{3+}$, *cis* and *trans*-$[Co(en)_2(OH_2)_2]^{3+}$, and *cis*- and *trans*-$[Co(tn)_2(OH_2)_2]^{3+}$, were selected for investigation over the pH range 1 - 10.

4.2 STOPPED-FLOW APPARATUS

The stopped-flow apparatus used throughout the kinetic investigation was one based on the design of Tregloan and Laurence[12] and constructed in these laboratories. The apparatus was adapted for spectrophotometric use in the U.V. and visible regions and has a cell path length of 0.2 cm and dead time of about 5 msec. Temperature stability to an accuracy of ± 0.1° was maintained by the rapid circulation of water pumped from an external thermostat tank through chrome-plated panels which enclosed the mechanical section of the apparatus. A detailed layout of this section is contained in Appendix I.

4.2.1 Optics

1. Light Source

A quartz-tungsten lamp with an operating voltage of 11.6 v and operating current of 9.2 a was used for following kinetic runs in the visible region. The lamp was connected to a constant-power supply which had a variation of ± 0.001 v in output-voltage for an input-voltage variation of ± 1 v.

For work in the U.V. region, a 75 watt arc-xenon lamp with an operating voltage of 12.6 v and operating current of 5.5 a was used. The lamp was connected to a stabiliser to minimize noise.

In each case the lamp housing was rigidly mounted and cooling was by convection.

2. Observation Cell

The fused quartz observation cell (Spectrosil) has a path

length of 0.2 cm and approximate volume of 0.1 c.c.

4.2.2 Mechanics

1. Pneumatic Drive

This was based on the design of Tregloan and Laurence.[12] Pressures of 40 - 80 p.s.i. of nitrogen were applied through a quick opening valve to a brass piston mounted in a cylinder behind the syringe driving trolley.

2. Mixing Chamber

The original mixing chamber, made of perspex and fitted with a teflon seal, was found to be unsatisfactory even under moderate gas pressures. This was therefore discarded in favour of a Sturtevant[13] mixing chamber which consists of a series of teflon plates screwed firmly together (see Appendix I) and was found to seal effectively even under prolonged application of nitrogen at 80 p.s.i.

3. Stopping Device

The stopping section of the apparatus was modified from the design of Sibly and Laurence.[14] After passing through the observation cell the reaction solution enters a teflon block with access to a stopping-syringe and outlet tube. The inlet hole of the stopping-block is centrally located but the outlet hole is shifted horizontally and vertically off-centre and linked to the stopping-syringe and outlet tube by means of a 3-way teflon tap. This is shown schematically in Fig. 4.1.

By adjusting the 3-way tap to the required position the reaction solution can be directed straight to the outlet tube, by-passing the

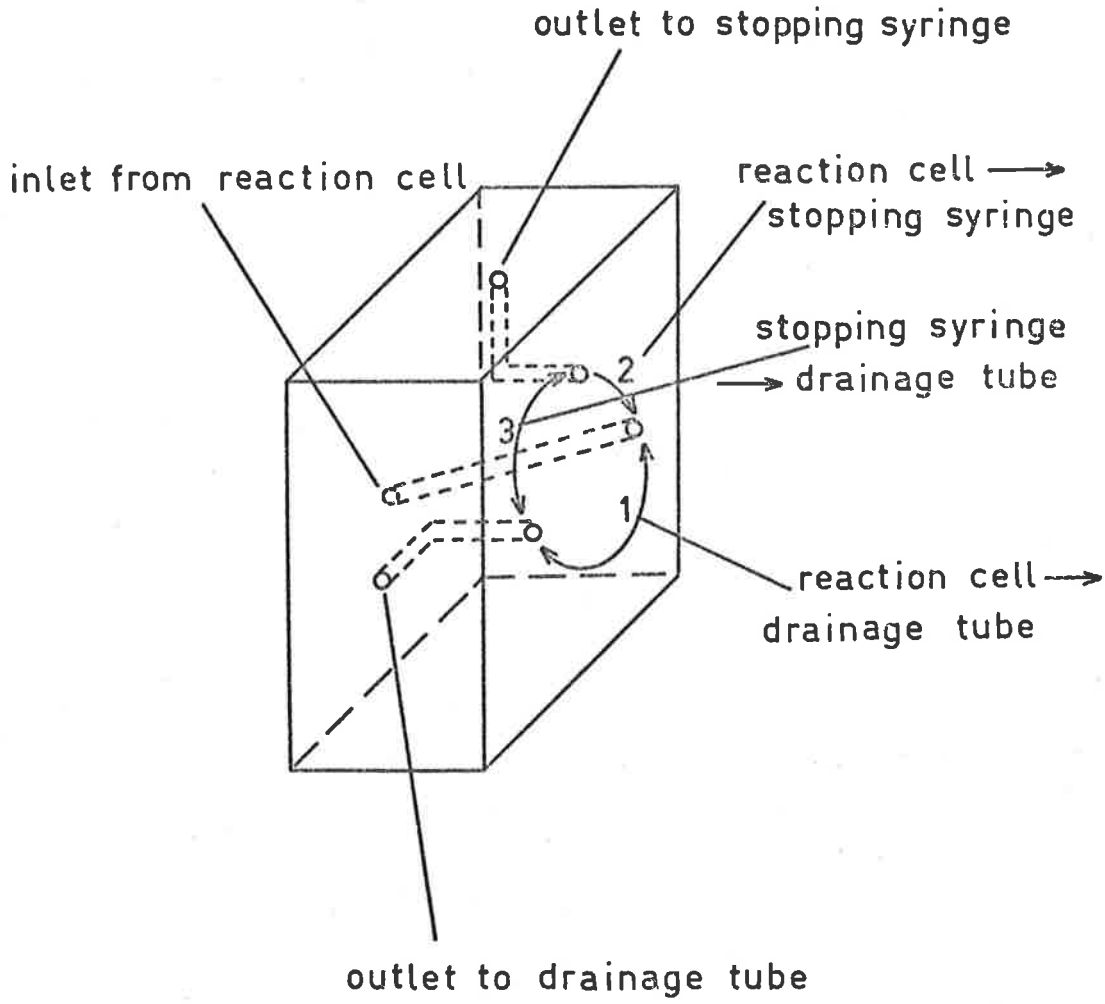

Fig. 4.1 Stopping Device.

the stopping-syringe and thus providing a means for flushing out the observation cell prior to the commencement of a kinetic run.

During the run itself the solution is directed into the barrel of the stopping-syringe after passing through the observation cell and forces the syringe plunger into an overhead metal frame. This provides an efficient means of stopping the solution flow. After completion of the run the solution can be drained from the stopping-syringe by the necessary adjustment of the 3-way tap.

The tap itself was designed so that the brass handle is clamped around the teflon (see Appendix I) rather than passing through it because of the ease with which teflon is distorted. This design allowed ease of movement even though the tap-face was securely held against the teflon stopping-block by means of a brass pressure plate.

The overhead metal frame, which holds the stopping-syringe, was firmly anchored to the assembly support, and the distance between the syringe plunger and the top of the frame could be adjusted by varying the size of the packing pieces between the base of the frame and the assembly.

4.2.3 Electronics

1. Triggering

The cathode ray oscilloscope could be triggered either internally or externally. Internal triggering, which is activated by the change in optical absorbance which occurs when new solution is introduced into the observation cell, has the disadvantage of recording the

actual push as well as any subsequent reaction.

All recorded traces were therefore triggered externally at the precise instant of stopping the flow. Triggering occurred whenever a thin copper strip, which was glued to the plunger of the stopping-syringe and linked through a 15v battery to the external trigger contact of the oscilloscope, came into contact with the overhead metal stopping frame. This meant that apart from the time taken for mixing of the reactant solutions only the reaction itself was recorded during a kinetic run.

2. Photomultiplier

The operating voltage of the photomultiplier was $\sim$ 0.5 kv and the output large enough to couple directly to the d-c amplifier of the oscilloscope. The total amount of light falling on the photomultiplier after passing through the reaction solution in the observation cell was backed off by means of a backing-off potentiometer. Up to 10v of light could be backed off in this way but generally the figure was kept in the region of 4 - 6 v. The amount of light backed-off gives the base-line voltage, V_o, measured in volts.

3. Capacitors

Three different capacitors, viz., 0.001, 0.005, and 0.056 μF, were employed to reduce high frequency noise with a consequent increase in the response-time. The largest capacitor (0.056 μF) was used only for the slowest reactions and then only when necessary. Wherever possible the 0.001 μF capacitor was used in preference to the 0.005 μF capacitor which has a slightly larger time-constant.

4. Storage

Traces were recorded on a Tektronix 564 storage oscilloscope with a 2A63 differential amplifier and 2B67 time base. The stored traces were photographed using Polaroid P/N 55 4 x 5 Land film in a Tektronix Oscilloscope C12 camera.

4.2.4 Data Processing

The Polaroid film negatives were placed in an overhead projector and traced onto graph paper using a magnification factor of 3. A number of data pairs, Vt and t, corresponding to trace height and time, respectively, were read off from the expanded trace and fed into an IBM 6400 computer, using Program Amod (listed in Appendix II) to calculate the observed first-order rate constants (see section 4.3.4).

4.2.5 Performance

Constant flow velocity was reached in 20 - 30 msec using the pneumatic drive and remained constant until the flow was stopped. The time between mixing and observation was measured to be about 3 msec using an acid-base neutralization reaction with added indicator as the test reaction. The stopping time was of the order of 1 - 2 msec, giving a total dead time of about 4 - 5 msec.

The stopping-syringe, which is basically a hydraulic stopping device, was found to be far superior to the alternative mechanical stopping device, the stopping-peg, in that mechanical bounce is virtually eliminated. This enables higher pressures of nitrogen to be used with a consequent reduction in stopping-time

and an increase in the reproducibility of the results.

Tests carried out on degassed and non-degassed reactant solutions indicated that there was no appreciable difference in the reproducibility of the results which means that cavitation effects are unimportant.

4.3 *Experimental*

4.3.1 *Materials*

trans$[Co(tn)_2OH(OH_2)](ClO_4)_2 \cdot 2H_2O$ was prepared as previously described in ch. 2, section 2.2.3.

The *cis* and *trans*-$[Co(en)_2OH(OH_2)](ClO_4)_2$ complexes were prepared according to the method of Kruse and Taube.[15]

$[Co(NH_3)_5OH_2](ClO_4)_3$ was prepared using the method of Basolo and Murmann.[16]

$[Rh(NH_3)_5OH_2](ClO_4)_3$ was prepared by the method of Swaddle and Stranks.[17]

For all other materials used, see ch. 3, section 3.2.1.

4.3.2 *pH Measurements*

All pH measurements were made on a pH-radiometer 25 with expanding scale to an accuracy of ± 0.01.

4.3.3 *Kinetics*

All substitution reactions were followed in the U.V. - visible region using the stopped-flow apparatus previously described. Concentrations of aquo-complexes were usually in the range 0.5 - 1.0 x 10^{-2} M. Selenite concentrations varied from 5 - 50 times excess of aquo-complex concentrations after mixing. The kinetic investigation was carried out over a temperature range of 10 - 40° and a range of pH from 1 - 10. Ionic strength was adjusted to 1 M with perchlorate ion. Where possible, kinetic runs were carried out at two different wavelengths corresponding with an increase, and a decrease in optical

absorbance, respectively, in going from reactants to products. Reactant solutions were equilibrated for up to 1 hr. before mixing, the actual time taken being dependent on the rate of isomerization (where relevant) of the particular aquo-complex involved.

4.3.4 Kinetic Procedure

The overall plan of the kinetic investigation was based on a knowledge of the pKa values of the aquo-complexes involved, the pKa values of selenite in dilute solution, and the rates of isomerization of the *en* and *tn* aquo-complexes. In order to measure the effect of pH on the selenite substitution process, a number of pH values covering the range 1 - 10 were selected, corresponding with an optimum concentration of a particular aquo-complex or selenite species. The pH values used for each system and the percentage distribution of the aquo-complex and selenite species at these values are summarized in Tables 4.2 and 4.3, respectively.

The selenite distribution figures shown in Table 4.3 are derived from the pKa values for selenite in dilute solution (see 2.3.2) and as such are based on the assumption that only the monomeric forms, H_2SeO_3, $HSeO_3^-$, and SeO_3^{2-} are of importance. These figures vary slightly from the data of Barcza and Sillén,[18] shown in Fig. 3.1 for L = 0.1 M, where contributions from dimeric forms are taken into account, but are included here to illustrate the initial basis for the subsequent plan of kinetic investigation. The aquo-complex distribution figures correspond with those shown in Figs. 3.2, 3.3, and 3.4.

Table 4.2 Distribution of Aquo-Complex Protonated Forms

pH	% Distribution of Major Protonated Form				
	cis $Co(en)_2(OH_2)_2^{3+}$	*trans* $Co(en)_2(OH_2)_2^{3+}$	$Co(tn)_2(OH_2)_2^{3+}$	$Co(NH_3)_5OH_2^{3+}$	$Rh(NH_3)_5OH_2^{3+}$
1	100	100	100	100	100
3	100	96.6	98.3	100	100
	cis $Co(en)_2OH.OH_2^{2+}$	*trans* $Co(en)_2OH.OH_2^{2+}$	$Co(tn)_2OH.OH_2^{2+}$	$Co(NH_3)_5OH^{2+}$	$Rh(NH_3)_5OH^{2+}$
6		96.2	91.5		
7	85.2				
8				96.2	99.2
	cis $Co(en)_2(OH)_2^{+}$	*trans* $Co(en)_2(OH)_2^{+}$	$Co(tn)_2(OH)_2^{+}$	$Co(NH_3)_5OH^{2+}$	$Rh(NH_3)_5OH^{2+}$
10	98.5	99.1	99.7	100	100

Table 4.3 Distribution of Se(IV) Between Monomeric Species (based on $K_1 = 4.37 \times 10^{-3}$, $K_2 = 8.71 \times 10^{-9}$ at 25°).

pH	% Distribution		
	H_2SeO_3	$HSeO_3^-$	SeO_3^{2-}
1	95.8	4.2	-
3	18.6	81.4	-
6	-	99.1	0.9
7	-	92.0	8.0
8	-	53.4	46.6
10	-	1.1	98.9

An isomerization study of the bis ethylenediaminediaquo cobalt(III) system has been made by Bjerrum and Rasmussen.[19] The data they obtained are presented in the reaction scheme below.

$$\begin{array}{ccccc} cis\text{-}[Co(en)_2(OH_2)_2]^{3+} & \underset{}{\overset{6.06}{\rightleftharpoons}} & cis\text{-}[Co(en)_2OH(OH_2)]^{2+} & \overset{8.19}{\rightleftharpoons} & cis\text{-}[Co(en)_2(OH)_2]^{+} \\ k_1\ (=kt) \downarrow\uparrow Kc/t = 58 & & k_2 \downarrow\uparrow Kc/t = 1.42 & & k_3\ (=kt) \downarrow\uparrow Kc/t = 0.80 \\ trans\text{-}[Co(en)_2(OH_2)_2]^{3+} & \underset{}{\overset{4.45}{\rightleftharpoons}} & trans\text{-}[Co(en)_2OH(OH_2)]^{2+} & \overset{7.94}{\rightleftharpoons} & trans\text{-}[Co(en)_2(OH)_2]^{+} \end{array}$$

The reaction half-times[15] for isomerization at 25° are:

$t_{\frac{1}{2}} \sim$ 24 hrs. for the diaquo species;

$t_{\frac{1}{2}} \sim$ 14 mins for the hydroxo-aquo species;

$t_{\frac{1}{2}} \sim$ 24 hrs. for the dihydroxo species.

The pH values selected for the kinetic study of selenite substitution in the $[Co(en)_2(OH_2)_2]^{3+}$ system were pHs 1, 3, 7, and 10 (see Table 4.2). In order to circumvent the problem of isomerization during equilibration of the reactant solutions, both the *cis*- and *trans*-isomers were stored as the diaquo species in 0.1 M perchloric acid. The pH of the reaction solution was then adjusted to the desired value at the time of mixing.

Since all of the above pH values fall outside the effective buffering range for selenite, viz., around pH 2.4 and pH 8.1, the selenite reactant solutions were made up in acid or base whose concentration was predetermined to give the required overall pH on mixing with the acidic complex reactant solution. The pH of the mixed solutions could be measured after reaction to ensure that the anticipated pH on mixing had been attained.

An isomerization study of the bis trimethylenediaminediaquo-cobalt(III) system was made by Jonasson.[20] The data he obtained are summarized below.

$$\begin{array}{ccccc} cis\text{-}[Co(tn)_2(OH_2)_2]^{3+} & \rightleftharpoons & cis\text{-}[Co(tn)_2OH(OH_2)]^{2+} & \rightleftharpoons & cis\text{-}[Co(tn)_2(OH)_2]^{+} \\ \Big\Downarrow\Big\Uparrow \text{Kc/t} = 100 \quad 4.75 & & \Big\Downarrow\Big\Uparrow \text{Kc/t} = 0.71 \quad 7.45 & & \Big\Downarrow\Big\Uparrow \text{Kc/t} = 1.56 \\ trans\text{-}[Co(tn)_2(OH_2)_2]^{3+} & \rightleftharpoons & trans[Co(tn)_2OH(OH_2)]^{2+} & \rightleftharpoons & trans[Co(tn)_2(OH)_2]^{+} \end{array}$$

Because of the rapid isomerization processes, only an averaged set of pKa values could be measured although the quoted values are close to those for the *trans-en* complexes.

The reaction half-times for isomerization at 25° are:

$t_{\frac{1}{2}} \sim 70$ secs for the diaquo species;

$t_{\frac{1}{2}} \sim 1$ sec for the hydroxo-aquo species;

$t_{\frac{1}{2}} \sim 130$ mins for the dihydroxo species.

The rapid isomerization of the *trans*-diaquo species to the analogous *cis* species proceeds virtually to completion. This provides a means for following the substitution by selenite on the pure *cis*-diaquo species and its associated protonated forms. The *trans*-$[Co(tn)_2OH(OH_2)](ClO_4)_2.2H_2O$ complex was therefore dissolved in 0.1 M perchloric acid and allowed to isomerize to the *cis*-diaquo complex. As in the case of the analogous *en* system the desired pH of the reaction solution was attained on mixing the reactant solutions. The concentrations of acid or base required for making up the selenite reactant solutions were again predetermined.

The isomerization of the *trans*-dihydroxo species to an equilibrium mixture of *cis*- and *trans*- isomers is sufficiently slow

to enable a kinetic study of selenite substitution on the pure *trans* species and its associated protonated forms. Accordingly, the *trans*-$[Co(tn)_2OH(OH_2)](ClO_4)_2.2H_2O$ complex was dissolved in 0.1 M sodium hydroxide and the pH of the reaction solution adjusted to the desired pH value as above. Isomerization was kept to a minimum in the *trans* system by not exceeding a temperature of 25° throughout the kinetic investigation.

Initial investigations into the substitution on selenite in the $[Co(NH_3)_5OH_2]^{3+}$ and $[Rh(NH_3)_5OH_2]^{3+}$ systems were performed at neutral pH using Trizma Base (pKa = 8.15 at 25°) as a buffer. The pKa values of the complex species at 25° are:

$$pKa = 6.6 \text{ for } [Co(NH_3)_5OH_2]^{3+};^{21}$$

$$pKa = 5.9 \text{ for } [Rh(NH_3)_5OH_2]^{3+}.^{21}$$

However, because of the large variation of pKa with temperature associated with the use of this particular buffer, later runs were carried out by dissolving the complex species in 0.1 M perchloric acid and using the same technique of pH adjustment as for the *en* and *tn* systems.

4.3.5 Treatment of Results

First-order rate constants were derived form computer plots of $\log_{10}$ (Vo - Vt) vs time, using program AMOD (see Appendix II), where V is the intensity of the transmitted light measured in mV, and (Vo - Vt) is proportional to (O.D.o - O.D.t) when (Vo - Vt)/Vo < 0.1. The rate constants obtained for a particular kinetic run, performed in duplicate, were consistent to within ± 5%. At

least two individual sets of data were obtained for each pair of reactant concentrations so that the particular rate constant measured was the average of four or more separate determinations. Any rate constant having a linear correlation coefficient of < 0.995 on the basis of a least squares analysis was rejected.

Activation parameters, $\Delta H^{\ddagger}$ and $\Delta S^{\ddagger}$, were derived from plots of $\log_{10} k_{obs}$ vs1/T using program ACTPAR (see Appendix III), where k_{obs} is the observed first-order rate constant and T is the temperature in °K. The activation enthalpy, $\Delta H^{\ddagger}$, is determined from the slope of the above linear plot, with allowance for the RT contribution, and the activation entropy, $\Delta S^{\ddagger}$, from the intercept.

In order to simplify the kinetic interpretation, the concentrations of the monomeric selenite species were determined from the two pKa values

$pK_1 = 2.36 \pm 0.05$; $pK_2 = 8.06 \pm 0.05$;

at 20° and 1 M ionic strength.

Since most of the kinetic work was carried out in the temperature range 20 - 40° and the variation of pKa over this range is < 0.15,[18] it was decided to use the above values throughout the kinetic analysis, except for a slight adjustment at temperatures < 20°.

Although the non-consideration of dimeric species will naturally lead to a slight error in the absolute values of the monomeric selenite concentrations calculated by this method, nevertheless the relative kinetic trend with increasing selenite

concentration will still be apparent. The maximum absolute concentration of selenite used throughout the kinetic study was 0.25 M, and as most of the concentrations were of the order of 0.1 M or less, this means that the total dimer concentration is relatively low over the entire selenite concentration range.

Since the outstanding feature which emerges from the substitution study is the similarity of kinetic behaviour for all systems within a particular pH region, it is convenient to divide the results into three separate sections, viz., the low pH region 1 - 4, the neutral pH region 6- 8.5, and the high pH region around pH 10.

4.4 Results and Discussion

4.4.1 Low pH Region: pH 1 - 4

A kinetic study of the anation reaction between the *cis*-$[Co(tn)_2(OH_2)_2]^{3+}$ species and selenite was carried out at pH ∿ 3.3. The aquo-complex concentration was held constant at 5×10^{-3} M and the selenite concentration varied from $2.5 - 25 \times 10^{-2}$ M. Table 4.4 shows the final pH values of the reaction solutions for each individual selenite concentration used in the kinetic study. These pH values were measured at four different temperatures, viz., 25, 30, 35 and 40°. Over this range the pH is virtually invariant with temperature.

The U.V. - visible spectra of the *cis*-$[Co(tn)_2(OH_2)_2]^{3+}$ complex and the selenito product are shown in Fig. 4.2. Two wavelengths, λ = 560 nm and λ = 480 nm, corresponding with an increase and decrease in optical absorbance respectively, between reactant and product, were selected for the substitution investigation.

A concentration dependence study was carried out at 30.3°. The observed first-order rate constants obtained are summarized in Table 4.5. These data are also shown in graphical form in Figs 4.3 and 4.4 where k_{obs} is plotted as a function of [Se(IV)] and $[HSeO_3^-]$, respectively. As previously mentioned, $[HSeO_3^-]$ was calculated using the single pKa value, $pK_1 = 2.36$.

The plots of k_{obs} vs [Se(IV)] and k_{obs} vs $[HSeO_3^-]$ increase linearly with anion concentration at first but then tend towards a limiting value. The reciprocal form of the functional dependence,

Table 4.4 pH of Reaction Solutions for Substitution of cis-$[Co(tn)_2(OH_2)_2]^{3+}$ by Se(IV)

10^2[Se(IV)](M)	pH (±0.01)			
	25.2°	30.2°	34.8°	40.0°
2.5	3.00	3.01	3.02	3.03
3.75	3.17	3.18	3.19	3.20
5.0	3.10	3.11	3.11	3.12
7.5	3.46	3.46	3.47	3.48
10	3.21	3.23	3.23	3.25
15	3.48	3.48	3.50	3.51
25	3.35	3.38	3.38	3.40

([aquo complex] = 5×10^{-3} M ; μ = 1.0 M, ClO_4^- medium)

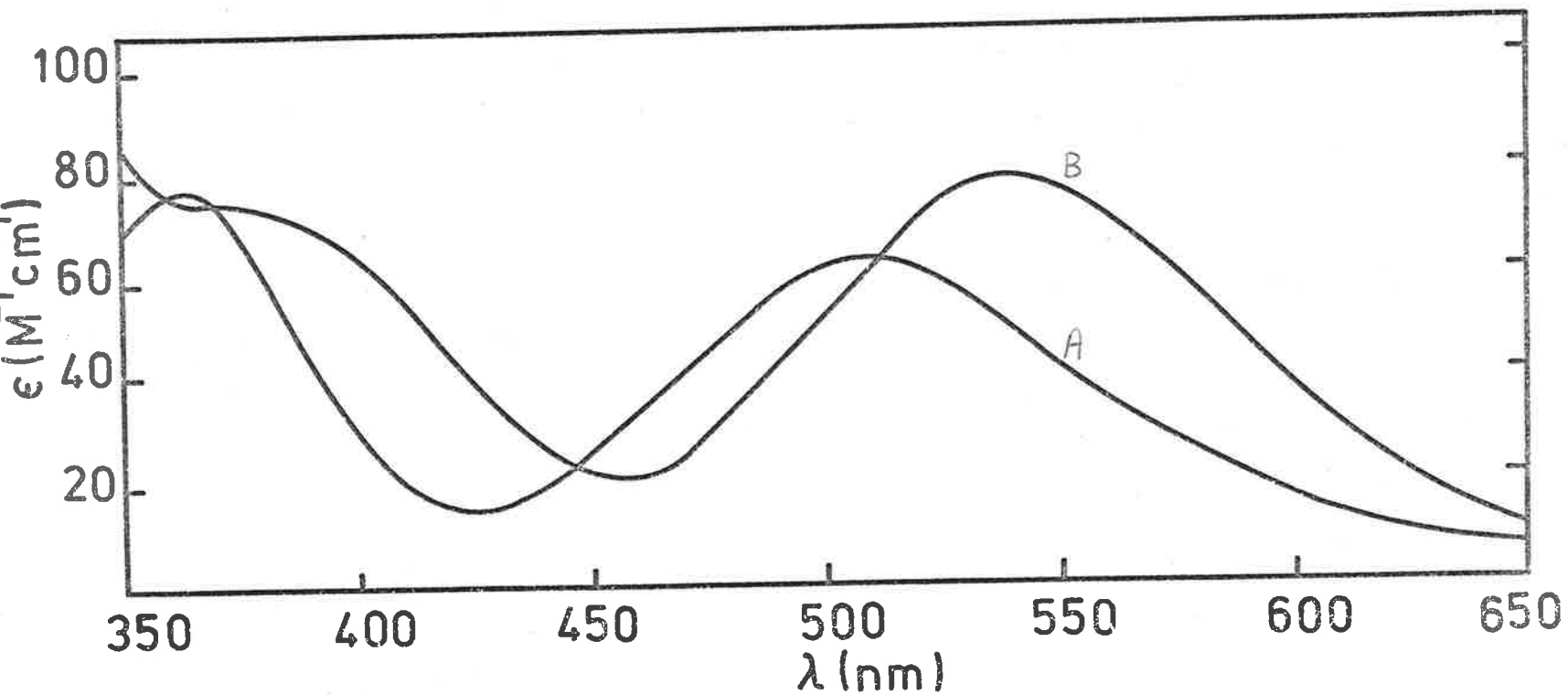

Fig. 4.2 U.V. - Visible Spectra of (A) *cis*-$[Co(tn)_2(OH_2)_2]^{3+}$, (B) *cis*-$[Co(tn)_2(OH_2)OSeO_2H]^{2+}$ at pH 3.3.

Table 4.5 Rate Data for Substitution of *cis*-$[Co(tn)_2(OH_2)_2]^{3+}$ by Se(IV).

10^2[Se(IV)](M)	$k_{obs}(sec^{-1})^{\ddagger}$	$k_{obs}(sec^{-1})^{*}$
2.5	$6.8_6 \pm 0.2_3$	$6.1_0 \pm 0.3_5$
3.75	10.6 ± 0.4	10.1 ± 0.3
5.0	12.3 ± 0.6	12.1 ± 0.5
7.5	15.2 ± 0.3	15.8 ± 0.6
10	18.5 ± 0.3	18.1 ± 0.4
15	21.1 ± 0.6	23.1 ± 1.0
25	-	28.7 ± 1.2

(Temp = 30.3 ± 0.1° ; μ = 1.0 M, ClO_4^- medium; [aquo complex] = 5×10^{-3} M; pH = 3.3 ± 0.3)

‡ measured at 480 nm * measured at 560 nm

Fig. 4.4 Plot of k_{obs} vs. $[HSeO_3^-]$ for Substitution of *cis* -$[Co(tn)_2(OH_2)_2]^{3+}$ with Selenite at pH 3.3.

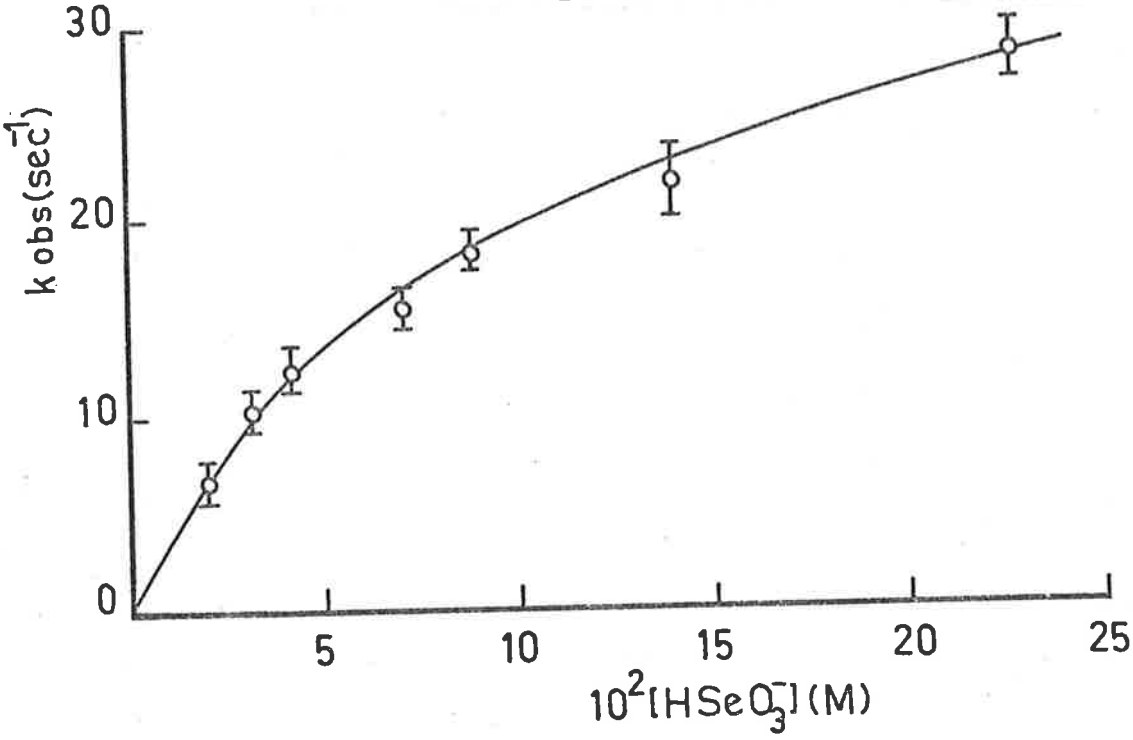

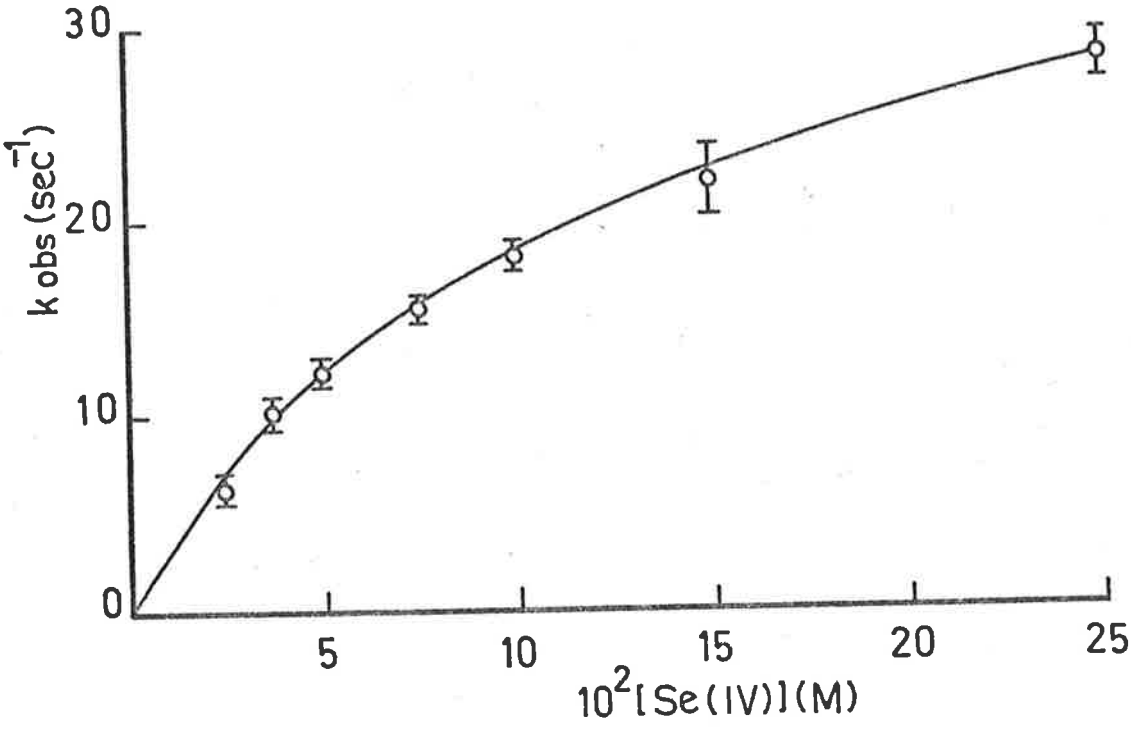

Fig. 4.3 Plot of k_{obs} vs. [Se(IV)] for Substitution of *cis*-$[Co(tn)_2(OH_2)_2]^{3+}$ with Selenite at pH 3.3.

$1/k_{an}$ vs $1/[HSeO_3^-]$, is shown in Fig. 4.5 and is characteristic of a general ion-pair mechanism. From the intercept, $k_{an} = 37 \pm 2\ sec^{-1}$, and from the slope, $K_{IP} = 11.4 \pm 0.6\ M^{-1}$, at 30.3 ± 0.1° and 1 M ionic strength.

The significant features to emerge from an analysis of the rate data for the above species are:

1. the similarity of the reaction rates between the *cis*-$[Co(tn)_2(OH_2)_2]^{3+}$, *cis*-$[Co(en)_2(OH_2)_2]^{3+}$, and $[Co(NH_3)_5OH_2]^{3+}$ ions;
2. the existence of a significant *trans*-effect at pH 1 and pH 3, where the rates of substitution for the *trans*-$[Co(tn)_2(OH_2)_2]^{3+}$ and *trans*-$[Co(en)_2(OH_2)_2]^{3+}$ complexes are approximately 5 times as great as for the analogous *cis* complexes;
3. the k_{obs} values at pH 3 are up to 25 times larger than the values at pH 1 within a particular aquo-system.

A temperature dependence study was carried out at pH 1.1 and pH 3.3 for the *cis*-$[Co(tn)_2(OH_2)_2]^{3+}$ anation reaction over the range 25 - 40° at an aquo-complex concentration of 1×10^{-2} M and a selenite concentration of 10^{-1} M. At this selenite concentration, ion-pairing of the cation is almost complete. Similar studies were also undertaken for the anation by selenite of the *trans*-$[Co(tn)_2(OH_2)_2]^{3+}$ *cis*- and *trans*-$[Co(en)_2(OH_2)_2]^{3+}$, $[Co(NH_3)_5OH_2]^{3+}$, and $[Rh(NH_3)_5OH_2]^{3+}$ complex ions. The rate data obtained are summarized in Table 4.6 and the activation parameters, $\Delta H^{\ddagger}$ and $\Delta S^{\ddagger}$, derived from these data are shown in Table 4.7.

The $\Delta H^{\ddagger}_{obs}$ values shown in Table 4.7 all lie in the range of

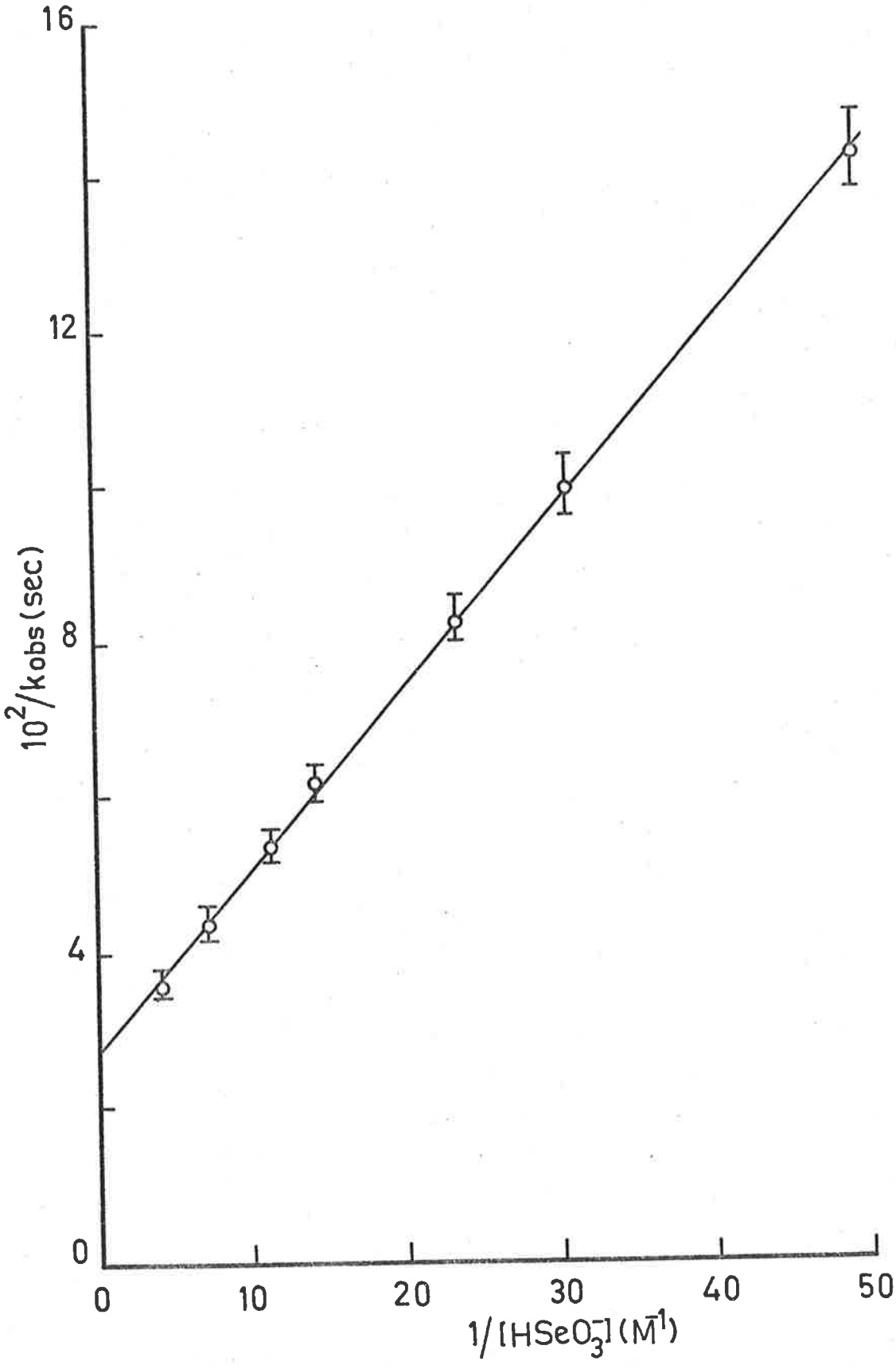

Fig. 4.5 Plot of k_{obs} vs. $1/[HSeO_3^-]$ for Substitution of *cis*-$[Co(tn)_2(OH_2)_2]^{3+}$ with Selenite at pH 3.3.

Table 4.6 Temperature Dependence Studies of Se(IV) Substitution with Various Aquo-Metal Complexes

Aquo-Complex	Temp(°C)	pH 1 $k_{obs}(sec^{-1})$	pH 3 $k_{obs}(sec^{-1})$
cis-$Co(tn)_2(OH_2)_2^{3+}$	25	0.76 ± 0.03	17.4 ± 0.6
	30	1.05 ± 0.02	25.9 ± 0.8
	35	1.50 ± 0.01	37.2 ± 1.1
	40	2.17 ± 0.02	50.5 ± 2.8
trans-$Co(tn)_2(OH_2)_2^{3+}$	10	2.27 ± 0.04	20.2 ± 0.7
	15	3.26 ± 0.10	29.9 ± 1.1
	20	5.05 ± 0.26	44.1 ± 1.4
cis-$Co(en)_2(OH_2)_2^{3+}$	25	0.58 ± 0.01	16.8 ± 0.5
	30	0.83 ± 0.02	25.1 ± 0.7
	35	1.10 ± 0.02	35.2 ± 0.3
	40	1.68 ± 0.06	50.0 ± 0.8
trans $Co(en)_2(OH_2)_2^{3+}$	15	3.47 ± 0.10	22.9 ± 0.6
	20	4.81 ± 0.28	30.6 ± 0.6
	25	7.21 ± 0.17	47.0 ± 1.0
$Co(NH_3)_5(OH_2)^{3+}$	25	0.71 ± 0.02	8.81 ± 0.21
	30	1.00 ± 0.03	13.6 ± 0.4
	35	1.39 ± 0.03	18.8 ± 0.5
	40	1.93 ± 0.04	27.1 ± 0.5

([aquo complex] = 1 x 10^{-2} M; [Se(IV)] = 10^{-1} M; μ = 1.0 M, ClO_4^- medium)

Table 4.7 A. Activation Parameters for Substitution by Se(IV) at pH 1.

Aquo-Complex	$\Delta H^{\ddagger}$ (kJ mol^{-1})	$\Delta S^{\ddagger}_{298}$ (J $K^{-1}mol^{-1}$)	$\Delta G^{\ddagger}_{298}$ (kJ mol^{-1})
cis-$Co(en)_2(OH_2)_2^{3+}$	52.0 ± 2.1	-66.9 ± 2.6	71.9 ± 2.9
trans-$Co(en)_2(OH_2)_2^{3+}$	48.8 ± 1.4	-56.6 ± 1.5	65.7 ± 1.9
cis-$Co(tn)_2(OH_2)_2^{3+}$	52.8 ± 1.5	-62.1 ± 1.8	71.3 ± 2.0
trans-$Co(tn)_2(OH_2)_2^{3+}$	54.3 ± 1.9	-37.8 ± 1.3	65.6 ± 2.3
$Co(NH_3)_5OH_2^{3+}$	49.4 ± 0.6	-73.8 ± 0.9	71.4 ± 0.9

Table 4.7 B. Activation Parameters for Substitution by Se(IV) at pH 3.

Aquo-Complex	$\Delta H^{\ddagger}$ (kJ mol^{-1})	$\Delta S^{\ddagger}_{298}$ (J $K^{-1}mol^{-1}$)	$\Delta G^{\ddagger}_{298}$ (kJ mol^{-1})
cis-$Co(en)_2(OH_2)_2^{3+}$	54.3 ± 1.9	-30.9 ± 0.9	63.5 ± 2.2
trans-$Co(en)_2(OH_2)_2^{3+}$	48.0 ± 2.5	-49.6 ± 2.3	62.8 ± 3.2
cis-$Co(tn)_2(OH_2)_2^{3+}$	53.8 ± 1.3	-26.8 ± 0.5	61.8 ± 1.5
trans-$Co(tn)_2(OH_2)_2^{3+}$	50.5 ± 3.1	-24.0 ± 1.3	57.6 ± 3.5
$Co(NH_3)_5(OH_2)^{3+}$	56.6 ± 2.0	-28.9 ± 0.9	65.2 ± 2.3

46 - 54 kJ mol^{-1}. This is consistent with a common rate-determining step involving the breaking or forming of a Se-O bond. A value of $\Delta H^{\ddagger} = 48.1 \pm 1.4$ kJ mol^{-1} has been measured for the base-hydrolysis of $[Co(NH_3)_5OSeO_2]^+$ which is known to proceed by Se-O bond cleavage.[11] Substitution reactions proceeding by Co-O bond cleavage or formation in the rate-determining step generally have $\Delta H^{\ddagger}$ values in the range 100 - 150 kJ mol^{-1}, as evidenced, for example, by the substitution of *cis*-$[Co(en)_2(OH_2)_2]^{3+}$ by SO_4^{2-},[4] and PO_4^{3-},[1] where $\Delta H^{\ddagger} = 146.4$ kJ mol^{-1}, and 125.5 kJ mol^{-1}, respectively.

Using the known equilibrium data (see 3.6.1), the observed first-order rate constants at pH 1 can be split up into the forward anation and backward aquation rate constants for the general reaction,

$$ROH_2^{3+} + \text{selenite} \underset{k_{aq}}{\overset{k_{an}}{\rightleftharpoons}} ROSeO_2H^{2+} + H_2O \qquad 4.5$$

Since $k_{obs} = k_{an} + k_{aq}$, and $k_{an}/k_{aq} = K$, where k_{obs} and K are both known, the individual anation and aquation rate constants, k_{an} and k_{aq}, can be determined. These values are shown in Table 4.8 for the various aquo-complexes involved. Because of the rapid isomerization of the *trans*-$[Co(tn)_2(OH_2)_2]^{3+}$ species (see 4.3.4) which prevented the determination of K for this ion, a value of 6 was assigned by analogy with the value measured for the *trans*-$[Co(en)_2(OH_2)_2]^{3+}$ ion. This is based on the reasoning that since the K values for the *cis*-$[Co(tn)_2(OH_2)_2]^{3+}$ and *cis*-$[Co(en)_2(OH_2)_2]^{3+}$ ions at pH 1 are similar, the same should be true of the respective *trans*-isomers.

Table 4.8 Experimental and Calculated k_{an} Values at pH 1.

Aquo-Complex	Temp(°C)	$k_{hyd}(sec^{-1})$	$k_{an}(sec^{-1})$ ‡	$k_{an}(calc)(sec^{-1})$ *
cis-$Co(tn)_2(OH_2)_2^{3+}$	25	0.20	0.56	0.5
	30	0.27	0.78	0.8
	35	0.39	1.11	1.0
	40	0.56	1.61	3.0
cis-$Co(en)_2(OH_2)_2^{3+}$	25	0.18	0.40	0.4
	30	0.25	0.58	0.7
	35	0.33	0.67	1.0
	40	0.51	1.17	1.5
trans-$Co(tn)_2(OH_2)_2^{3+}$	10	0.32	1.90	0.6
	15	0.47	2.79	0.9
	20	0.72	4.33	1.1
trans-$Co(en)_2(OH_2)_2^{3+}$	15	0.54	2.93	0.7
	20	0.75	4.06	0.9
	25	1.13	6.08	1.3
$Co(NH_3)_5(OH_2)^{3+}$	25	0.28	0.43	0.3
	30	0.40	0.60	0.4
	35	0.56	0.83	0.5
	40	0.77	1.16	0.8

‡ experimentally determined values at pH 1.

* calculated from data at pH 3.

The size of the K value at pH 3, viz., > 20 for all systems studied, precludes any reliable separation of the observed first-order rate constant into the individual forward and backward rate constants and it can be assumed that $k_{obs} = k_{an}$ at this pH.

Because of the invariance of K with temperature (see 3.6.1), the $\Delta H^{\ddagger}$ values for the anation and aquation reactions are the same within experimental error. Table 4.9 shows the $\Delta H^{\ddagger}$ and $\Delta S^{\ddagger}$ values for the anation and aquation reactions.

The decrease in rate in going from pH 3 to pH 1 must be related to a change in the character of the selenite species present, since from the aquo-complex distribution curves presented in Figs. 3.2 - 3.4, the aquo or diaquo form is the predominant complex species in each case and any contribution from hydroxo or hydroxo-aquo forms can be considered to be negligible.

The Se distribution data of Barcza and Sillén for [Se(IV)] = 0.1 M in 1 M $NaClO_4$ as supporting electrolyte show that the extent of selenite dimerization varies from about 40% at pH 1 to 20% around pH3 (Fig. 3.1). At pH 1 the predominant monomeric selenite form is the neutral H_2SeO_3 species which is present to the extent of about 60%, and at pH 3 it is the $HSeO_3^-$ ion which predominates to the extent of about 65%. Thus the striking difference in the Se distribution between the two pH values is the sharp drop in the percentage of $HSeO_3^-$ which is present to the extent of only about 2.5% at pH 1.

A preliminary analysis of the kinetic data indicated that the fall off in rate with decreasing pH could be correlated with a similar fall off in $HSeO_3^-$ ion concentration. In order to test the proposition

Table 4.9 Activation Parameters For Anation and Aquation Reactions at pH 1 and 25°.

Aquo-Complex	$\Delta H^{\ddagger}$ (kJ mol^{-1})	$\Delta S^{\ddagger}$ (J $K^{-1}mol^{-1}$)	$\Delta G^{\ddagger}$ (kJ mol^{-1})
cis $Co(tn)_2(OH_2)_2^{3+}$	52.7 ± 2.4[a]	-64.3 ± 2.8	71.9 ± 5.2
	52.9 ± 2.6[b]	-74.6 ± 3.8	75.1 ± 6.4
trans $Co(tn)_2(OH_2)_2^{3+}$	54.0 ± 2.6	-40.2 ± 1.8	66.0 ± 4.4
	54.0 ± 2.6	-55.0 ± 2.6	70.4 ± 5.2
cis $Co(en)_2(OH_2)_2^{3+}$	52.2 ± 2.5	-68.7 ± 3.3	72.7 ± 5.8
	52.0 ± 2.9	-78.5 ± 4.6	75.4 ± 7.5
trans $Co(en)_2(OH_2)_2^{3+}$	48.8 ± 2.4	-58.1 ± 2.7	66.1 ± 5.1
	48.8 ± 2.4	-72.2 ± 3.6	70.3 ± 6.0
$Co(NH_3)_5OH_2^{3+}$	49.5 ± 2.0	-77.6 ± 3.1	72.7 ± 5.1
	51.3 ± 3.0	-75.2 ± 4.6	73.7 ± 7.6

([aquo complex] = 1 x 10^{-2} M ; [Se(IV)] = 10^{-1} M ; μ = 1.0 M, ClO_4^- medium)

a = anation b = aquation

that substitution in the low pH region is due only to the $HSeO_3^-$ species, the predicted anation rate constants at pH 1, $k_{an}(calc)$, were calculated from the observed anation rate constants at pH 3 which were normalised to $[HSeO_3^-]/[Se(IV)] = 1$ and multiplied by the concentration of $HSeO_3^-$ ion at pH 1. The measured and calculated values are compared in Table 4.8 for each of the systems studied. In all cases there is good agreement between the two sets of data.

This treatment provides good evidence that the active selenite species in the low pH region, at least in relatively dilute solution, is indeed the monomeric $HSeO_3^-$ ion. Any contribution from H_2SeO_3 and dimeric species towards the overall substitution rate must necessarily be regarded as very small. The non-reactivity of H_2SeO_3 may be related to an unfavourable ion-pair formation constant between the aquo-complex and the neutral selenite species.

The substitution of an aquo-ligand by selenite in acidic solution can now be written in the general forms,

$$[M(NN)_2(OH_2)_2]^{3+} + HSeO_3^- \underset{k_{hyd}}{\overset{k_{an}}{\rightleftharpoons}} [M(NN)_2(OH_2)OSeO_2H]^{2+} + H_2O \qquad 4.6$$

(where M = Co(III) and NN = *en* or *tn*), and

$$[M(N)_5OH_2]^{3+} + HSeO_3^- \underset{k_{hyd}}{\overset{k_{an}}{\rightleftharpoons}} [M(N)_5OSeO_2H]^{2+} + H_2O \qquad 4.7$$

(where M = Co(III) and N = NH_3).

The kinetic data for substitution of *cis*-$[Co(tn)_2(OH_2)_2]^{3+}$ by selenite are consistent with an S_NIP mechanism involving the initial rapid formation of the precursor ion-pair species, *cis*-$[Co(en)_2(OH_2)_2]^{3+}.HSeO_3^-$.

Although the Se distribution data of Barcza and Sillén indicate a significant fall-off in the concentration of the $H_2(SeO_3)_2^{2-}$ species around pH 3, this decrease is not sufficient to account for the absence of the dimeric pathway

$$ROH_2^{3+} + H_2(SeO_3)_2^{2-} \rightleftarrows ROSeO_2H^{2+} + HSeO_3^- + H_2O \qquad 4.8$$

at high [Se(IV)]. It seems likely, therefore, that the actual sharp drop in the $H_2(SeO_3)_2^{2-}$ concentration occurs at slightly higher pH (around pH 4) and that the concentration of this species around pH 3 is low. Barcza and Sillén themselves point out that the use of the same equilibrium constants over the broad range of Se(IV) concentrations used in their distribution study (viz. 0.02 - 3 M) is open to question and this may well explain the discrepancy which arises from our kinetic observations. Arnek and Barcza[22] have also found that the distribution between the various Se(IV) species is markedly affected by medium changes (e.g. in going from 3M to 1 M $NaClO_4$). Whereas the kinetic study was performed on solutions adjusted to 1 M ionic strength with sodium perchlorate, the Sillén equilibrium study was carried out in solutions where the concentration of sodium perchlorate was itself 1 M. This should also be taken into consideration when referring to the Se distribution data in Fig. 3.1.

Although the $H_3(SeO_3)_2^-$ species is also present in low concentration around pH 3, it is presumably not as effective as the smaller $HSeO_3^-$ species with regard to ion-pair formation and appears to have no significant effect on the rate of substitution, even at high [Se(IV)].

4.4.2 Neutral pH Region

A. pH 6 - 7.5

A concentration dependence study was carried out on the anation reaction between the *cis*-$[Co(en)_2OH(OH_2)]^{2+}$ ion and selenite at each of 4 different temperatures viz., 25, 30, 35 and 40°. The hydroxo-aquo complex concentration was maintained at 1×10^{-2} M and the selenite concentration varied from $5 - 25 \times 10^{-2}$ M. Table 4.10 shows the pH of the reaction solutions for each selenite concentration used at 25 and 40°. As for the region around pH 3, there is again only minimal variation of pH with temperature.

The U.V. - visible spectra of the *cis*-$[Co(en)_2(OH)(OH_2)]^{2+}$ ion and the selenito product are shown in Fig. 4.6. Most runs were performed at λ = 530 nm, corresponding with an increase in optical absorbance from reactants to products. Some, however, were followed at λ = 480 nm where there is a decrease in optical absorbance from reactants to products.

The observed first-order rate constants which were obtained from this study are shown in Table 4.11.

Plots of k_{obs} vs [Se(IV)] and k_{obs} vs $[HSeO_3^-]$, where $[HSeO_3^-]$ was calculated from the single pKa value, $pK_2 = 8.06$, were approximately linear with negative intercepts as shown in Figs. 4.7 and 4.8. However, when k_{obs} was plotted as a function of $[Se(IV)]^2$ and $[HSeO_3^-]^2$ as in Figs. 4.9 and 4.10, there was an initial linear dependence on the second power of the anion concentration and then a tend towards a limiting value. The reciprocal plots, $1/k_{an}$ vs

Table 4.10 pH of Reaction Solutions for Substitution of cis-$[Co(en)_2(OH)(OH_2)]^{2+}$ by Se(IV)

10^2[Se(IV)](M)	pH (±0.01) 25.2°	40.0°
5.0	7.21	7.25
7.5	7.05	7.08
10	7.28	7.32
15	7.10	7.13
20	7.06	7.10
25	7.18	7.22

([aquo complex] = 1×10^{-2} M ; μ = 1.0 M, ClO_4^- medium)

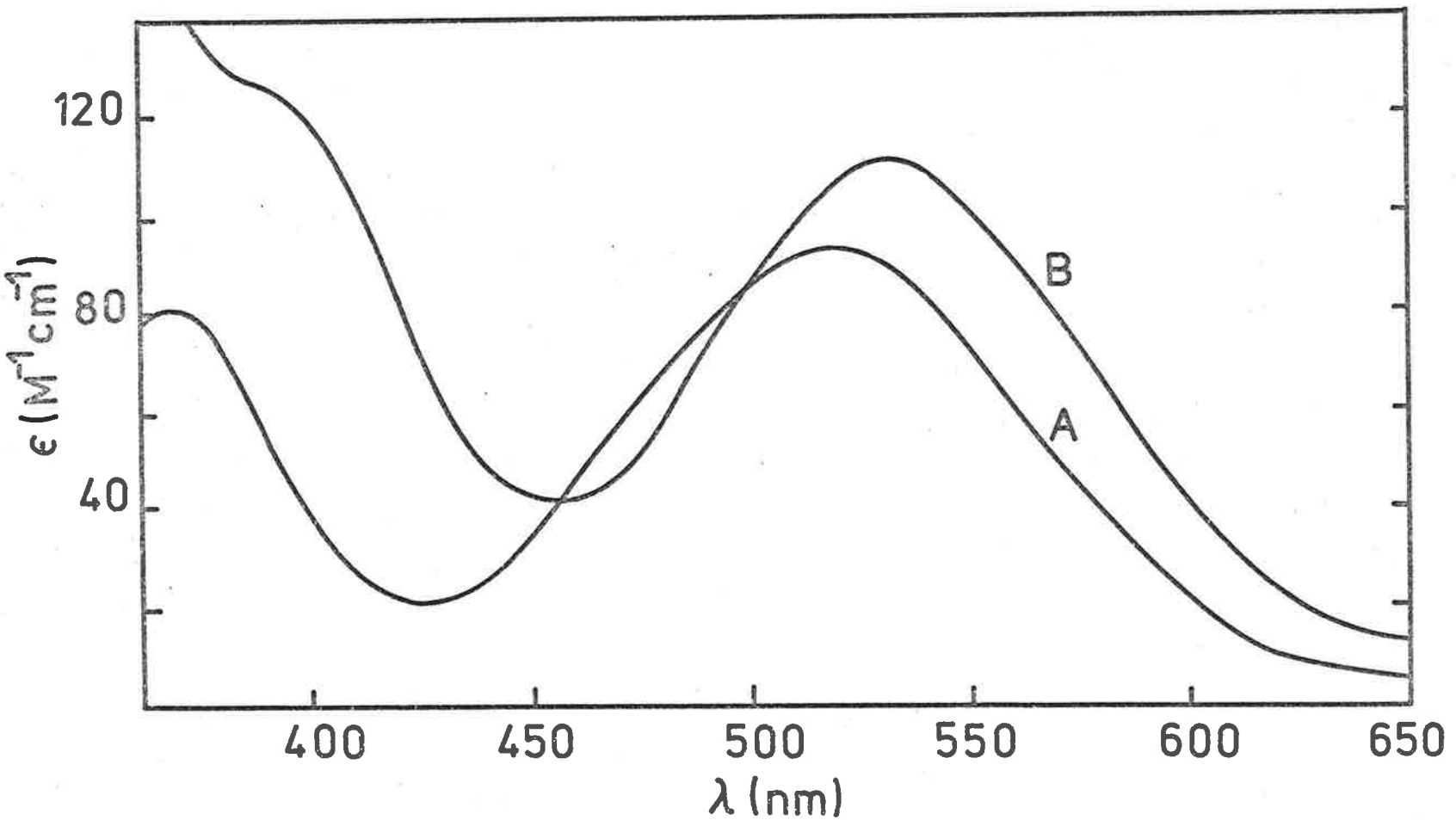

Fig. 4.6 U.V. - Visible Spectra of (A) *cis*-$[Co(en)_2(OH)(OH_2)]^{2+}$,

(B) *cis*-$[Co(en)_2(OH_2)OSeO_2]^{2+}$ at pH ∿ 7.

Table 4.11 Rate Data for Substitution of *cis*-$[Co(en)_2(OH)(OH_2)]^{2+}$ by Se(IV)

10^2[Se(IV)](M)	k25°(sec^{-1})	k30°(sec^{-1})	k35°(sec^{-1})	k40°(sec^{-1})
5.0	0.74 ± 0.04	0.93 ± 0.03	-	-
7.5	1.43 ± 0.04	1.88 ± 0.06	2.38 ± 0.11	2.83 ± 0.10
10	-	2.68 ± 0.11	3.50 ± 0.14	4.27 ± 0.21
15	4.90 ± 0.18	6.24 ± 0.17	7.66 ± 0.37	9.06 ± 0.32
20	7.11 ± 0.19	8.70 ± 0.25	10.9 ± 0.4	13.0 ± 0.4
25	7.90 ± 0.45	10.2 ± 0.6	12.4 ± 0.5	15.0 ± 1.0

([aquo complex] = 5 x 10^{-3} M ; μ = 1.0 M, ClO_4^- medium)

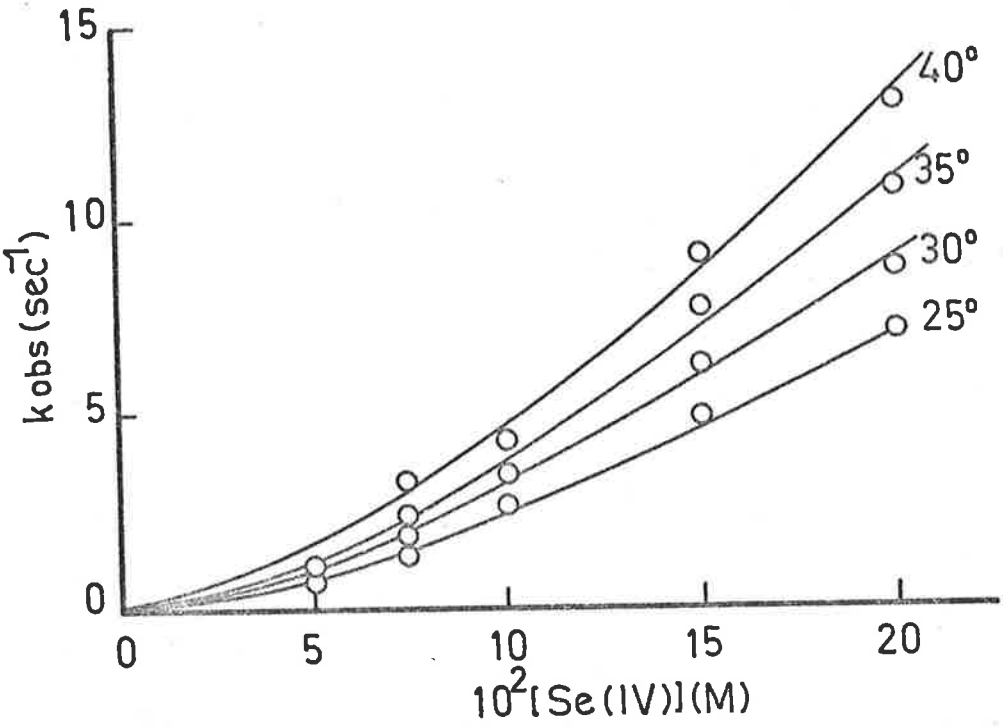

Fig. 4.7 Plots of k_{obs} vs [Se(IV)] for Substitution of *cis*-$[Co(en)_2(OH)(OH_2)]^{2+}$ with Selenite at pH 7.

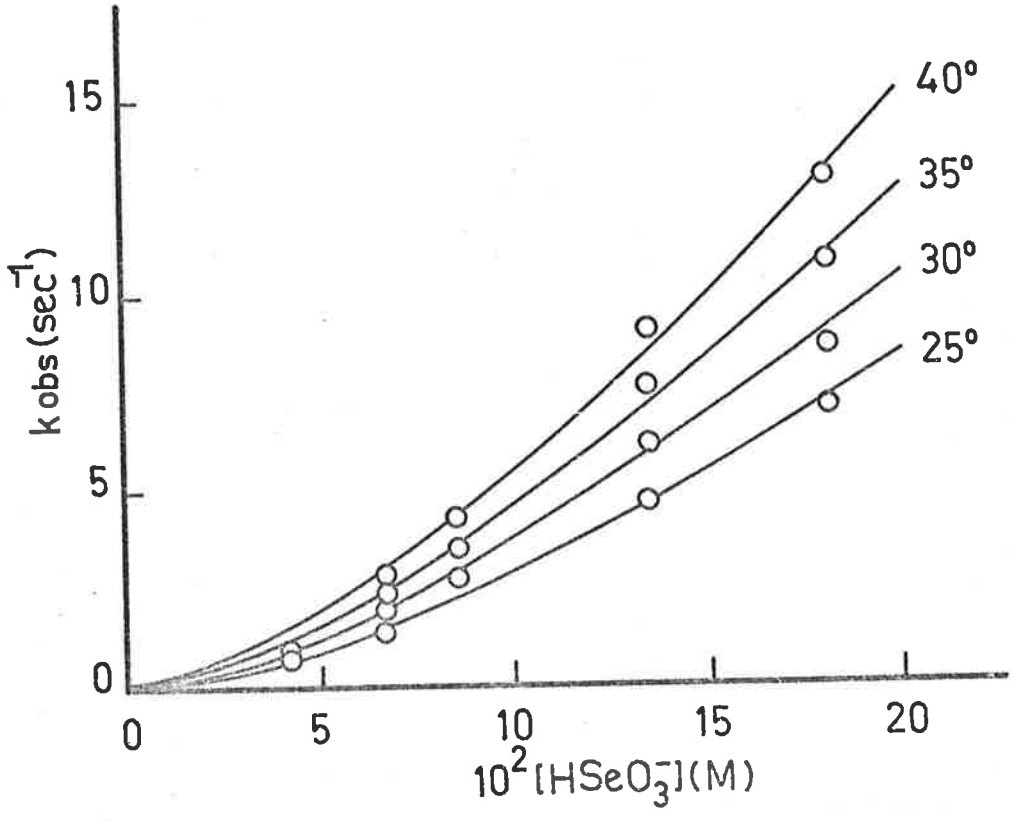

Fig. 4.8 Plots of k_{obs} vs $[HSeO_3^-]$ for Substitution of *cis*-$[Co(en)_2(OH)(OH_2)]^{2+}$ with Selenite at pH 7.

Fig. 4.9 Plots of k_{obs} vs $[Se(IV)]^2$ for Substitution of *cis*-$[Co(en)_2(OH)(OH_2)]^{2+}$ with Selenite at pH 7.

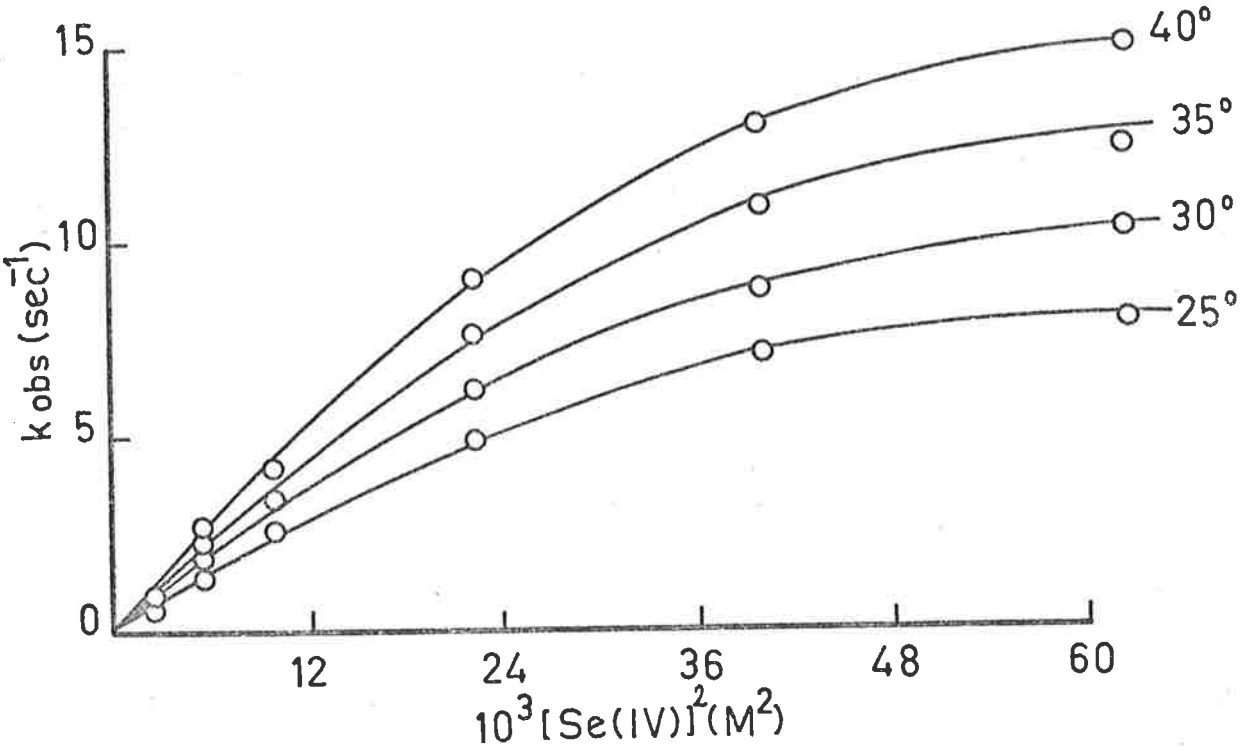

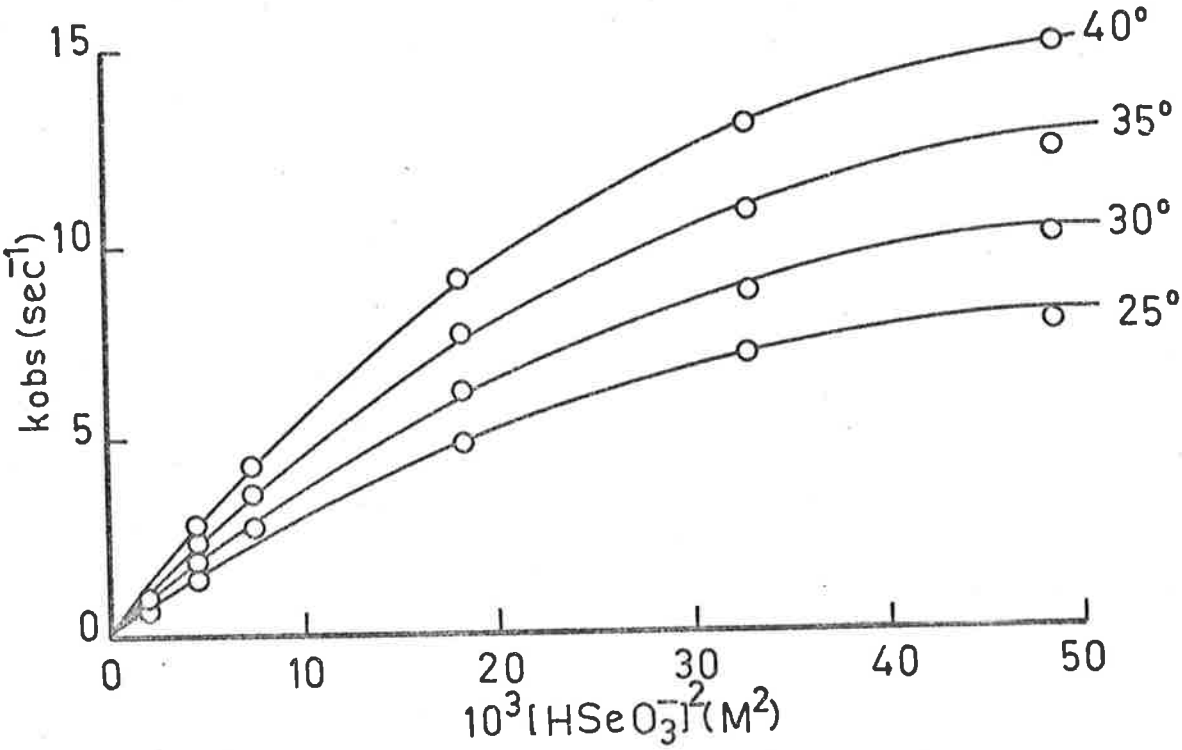

Fig. 4.10 Plots of k_{obs} vs $[HSeO_3^-]^2$ for Substitution of *cis*-$[Co(en)_2(OH)(OH_2)]^{2+}$ with Selenite at pH 7.

$1/[HSeO_3^-]^2$, are shown in Fig. 4.11. The k_{an} and K_{IP} values, derived from the intercepts and slopes respectively, are summarized in Table 4.12. From the plots of k_{an} vs 1/T and K_{IP} vs 1/T,

$$\Delta H^{\ddagger}_{an} = 25.5 \pm 1.0 \text{ kJ mol}^{-1}, \quad \Delta S^{\ddagger}_{an} = -126 \pm 4 \text{ J K}^{-1} \text{ mol}^{-1};$$

$$\Delta H_{IP} = 11.6 \pm 0.4 \text{ kJ mol}^{-1}, \quad \Delta S_{IP} = -175 \pm 4 \text{ J K}^{-1} \text{ mol}^{-1};$$

respectively, for the anation of *cis*-$[Co(en)_2OH(OH_2)]^{2+}$ ion by selenite.

In addition to the temperature dependence study carried out simultaneously with the concentration dependence study for the *cis*-$[Co(en)_2OH(OH_2)]^{2+}$ complex, temperature dependence studies were performed at pH 6 on the *trans*-$[Co(en)_2OH(OH_2)]^{2+}$, and *cis*- and *trans*-$[Co(tn)_2OH\ (OH_2)]^{2+}$ species. This pH was selected because it coincides with an optimum concentration of the hydroxo-aquo form of the above complex species. In each case the concentration of the complex species was 1×10^{-2} M and the selenite concentration was 10^{-1} M. The rate data from these studies are presented in Table 4.13 and the activation parameters, $\Delta H^{\ddagger}_{an}$ and $\Delta S^{\ddagger}_{an}$, derived from them are shown in Table 4.14 together with the values obtained for *cis*-$[Co(en)_2OH.OH_2]^{2+}$.

An analysis of the $\Delta H^{\ddagger}_{an}$ values reveals that they fall in the range 32 - 42 kJ mol^{-1} which is significantly lower than the 46 - 54 kJ mol^{-1} range of values found at pH 1 and pH 3.

A comparison of the rate data for the various complex species shows

1. a marked similarity between the rates of substitution for the

Substitution of *cis*-$[Co(en)_2(OH)(OH_2)]^{2+}$ with Selenite at pH 7.

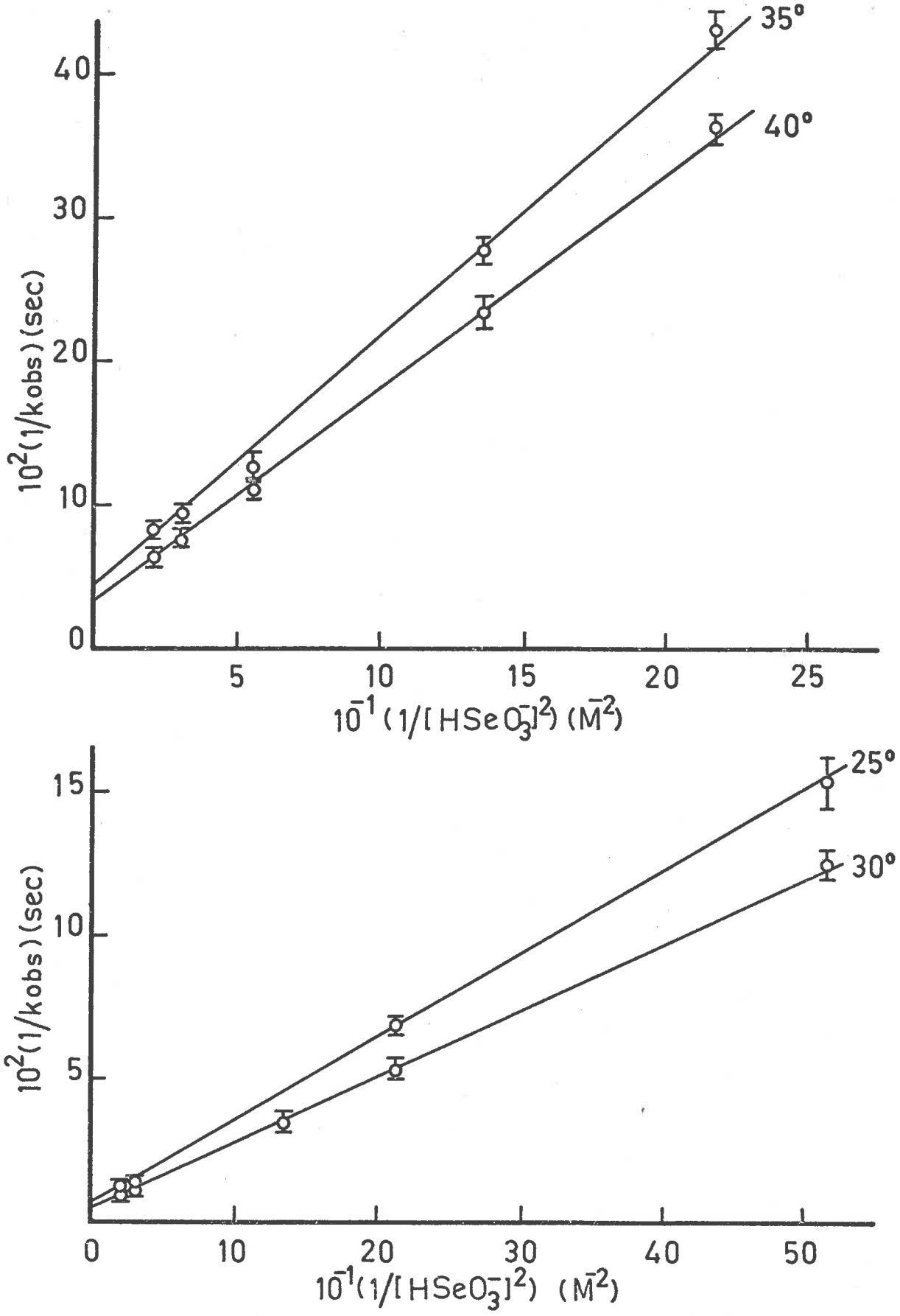

Fig. 4.11 Plots of k_{obs} vs $1/[HSeO_3^-]^2$

Table 4.12 k_{an} *and* $K_{I.P.}$ *Values for Se(IV) Substitution of* *cis*-$[Co(en)_2OH.(OH_2)]^{2+}$

Temp (±0.1°)	k_{an} (sec^{-1})	$K_{I.P.}$ (M^{-1})
25.1	20.0 ± 1.8	15.7 ± 5.3
30.4	25.0 ± 3.6	17.1 ± 4.8
35.0	28.6 ± 3.6	18.9 ± 1.1
40.0	34.5 ± 4.0	20.4 ± 1.9

(pH = 7.20 ± 0.01 ; μ = 1.0 M, ClO_4^- medium)

Table 4.13 Temperature Dependence of Se(IV) Substitution for Various Aquo-Metal Complexes

Temp (°C)	k_{obs} (sec^{-1})		
	cis-$Co(tn)_2(OH)(OH_2)^{2+}$	*trans*-$Co(tn)_2(OH)(OH_2)^{2+}$	*trans*-$Co(en)_2(OH)(OH_2)^{2+}$
10		1.00 ± 0.05	1.18 ± 0.04
15		1.38_4 ± 0.04_0	1.55_0 ± 0.05_0
20		1.90 ± 1.10	2.01 ± 0.07
25	2.65 ± 0.15		
30	3.56 ± 0.29		
35			
40	5.70 ± 0.30		

([aquo complex] = 1 x 10^{-2} M; [Se(IV)] = 10^{-1} M; μ = 1.0 M, ClO_4^- medium).

Table 4.14 Activation Parameters for Substitution of Se(IV) at pH 6.

Aquo Complex	$\Delta H^{\ddagger}$ (kJ mol^{-1})	$\Delta S^{\ddagger}_{298}$ (J $K^{-1}mol^{-1}$)	$\Delta G^{\ddagger}_{298}$ (kJ mol^{-1})
**cis*-$Co(en)_2(OH)(H_2O)^{2+}$	36.2 ± 2.4	-109 ± 7	68.7 ± 4.5
trans-$Co(en)_2(OH)(OH_2)^{2+}$	34.8 ± 0.5	-112 ± 2	68.2 ± 1.1
cis-$Co(tn)_2(OH)(OH_2)^{2+}$	37.4 ± 1.3	-103 ± 3	68.1 ± 2.2
trans-$Co(tn)_2(OH)(OH_2)^{2+}$	42.6 ± 2.8	-86.0 ± 5.9	68.2 ± 4.6

* measured at pH 7.

en and *tn* complexes and,

2. the absence of any significant *trans*- effect in this pH region.

The initial linear dependence of the plots of k_{obs} vs [Se(IV)] and $[HSeO_3^-]$ indicated that the reaction was probably proceeding by a monomeric as well as a dimeric pathway, at least at the lower selenite concentrations, giving an overall rate law

$$k_{obs} = k_1[HSeO_3^-] + k_2[HSeO_3^-]^2 \qquad 4.9$$

The quantity $k_{obs}/[HSeO_3^-]$ was plotted as a function of $[HSeO_3^-]$, as shown in Fig. 4.12. From the intercepts and initial slopes, the respective monomeric and dimeric rate constants, k_1 and k_2, can be calculated and these are summarized in Table 4.15.

The predominant complex form in the pH region 6-7 is the hydroxo or hydroxo-aquo ion. In the case of the *cis*-$[Co(en)_2(OH_2)_2]^{3+}$ system, the hydroxo-aquo ion is present to the extent of about 86% at pH 7. The contributions from the hydroxo-aquo forms at pH 6 for the *cis*- and *trans*-$[Co(tn)_2(OH_2)_2]^{3+}$ systems are about 90% and for the *trans*-$[Co(en)_2(OH_2)_2]^{3+}$ system about 96%.

The Se distribution data of Barcza and Sillén indicate that 80 - 90% of the Se(IV) concentration in the pH range 6 - 7 exists in the monomeric form for [Se(IV)] = 0.1 M in 1 M $NaClO_4$ as supporting electrolyte. The predominant monomeric form is the $HSeO_3^-$ ion which is present to the extent of 70 - 80% and the predominant dimeric form is the $H_2L_2^{2-}$ ion which contributes about 18% giving a total biselenite concentration of between 90 and 100%.

Substitution of *cis*-$[Co(en)_2(OH)(OH_2)]^{2+}$ with Selenite at pH 7.

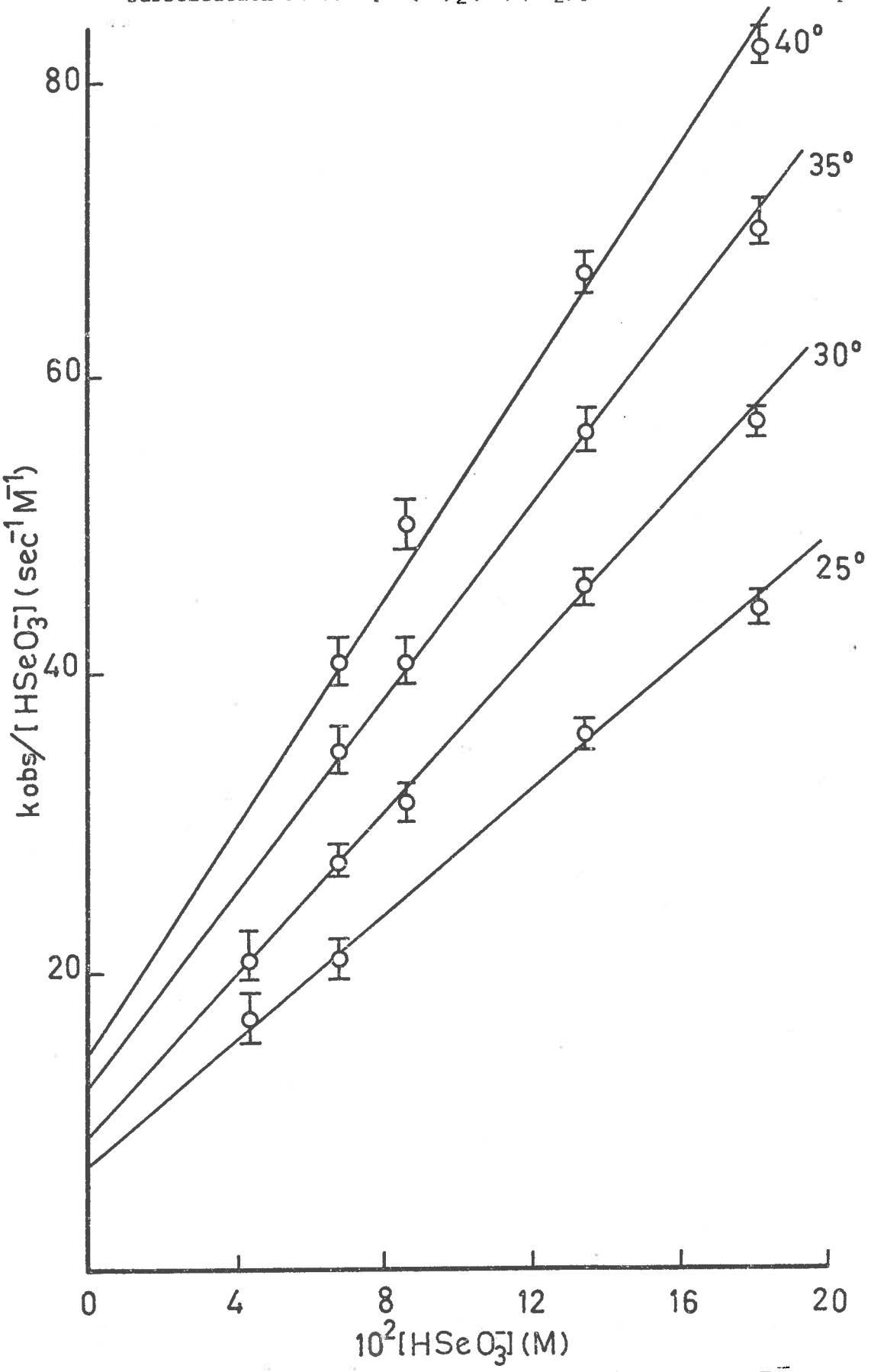

Fig. 4.12 Plots of $k_{obs}/[HSeO_3^-]$ vs $[HSeO_3^-]$

Table 4.15 Monomeric and Dimeric Rate Constants for the Reaction of cis-$[Co(en)_2OH(OH_2)]^{2+}$ with Se(IV).

Temp (± 0.1°)	$k_1(sec^{-1}M^{-1})$	$10^2k_2(sec^{-1}M^{-2})$
25.1	7 ± 1	2.1 ± 0.1
30.4	9 ± 1	2.8 ± 0.2
35.0	13 ± 2	3.3 ± 0.2
40.0	15 ± 2	4.0 ± 0.3

It is apparent from the kinetic data that substitution by selenite in this pH region proceeds by two major pathways which can now be written as

$$ROH_2^{2+} + HSeO_3^- \xrightarrow{k_{an}} ROSeO_2^+ + H_2O \qquad 4.10$$

$$ROH_2^{2+} + H_2(SeO_3)_2^{2-} \xrightarrow{k_{2an}} ROSeO_2^+ + HSeO_3^- \qquad 4.11$$

Path 4.10 is only important at relatively low [Se(IV)].

The observed kinetics for the *cis*-$[Co(en)_2OH(OH_2)]^{2+}$ anation are consistent with an S_NIP mechanism proceeding through the precursor ion-pair species, *cis*-$[Co(en)_2OH(OH_2)]^{2+}.H_2(SeO_3)_2^{2-}$.

The enhanced reactivity of the dimeric species, $H_2(SeO_3)_2^{2-}$, over the monomeric species, $HSeO_3^-$, in this pH region is presumably related to the more favourable ion-association constant between a +2 and a -2 species than between a +2 and a -1 species.

B. pH 8 - 8.5

A concentration dependence study was carried out at 25, 30, 35, and 40° for the substitution of $[Co(NH_3)_5OH]^{2+}$ by selenite and at 25, 30, and 35° for the substitution of $[Rh(NH_3)_5OH]^{2+}$ by selenite. The $[Co(NH_3)_5OH]^{2+}$ concentration was maintained at 1×10^{-2} M and the selenite concentration varied from $5 - 25 \times 10^{-2}$ M. In the case of $[Rh(NH_3)_5OH]^{2+}$, the complex concentration was held at 5×10^{-3} M and the selenite concentration varied from $3.75 - 25 \times 10^{-2}$ M. The reactant solutions were prepared in 0.5 M Trizma Base buffer. Table 4.16 shows the measured pH values of the reaction solutions at each selenite concentration used for the $[Co(NH_3)_5OH]^{2+}$ and $[Rh(NH_3)_5OH]^{2+}$

Table 4.16 pH of Reaction Solutions for Substitution of $[Co(NH_3)_5(OH_2)]^{3+}$ and $[Rh(NH_3)_5(OH_2)]^{3+}$ by Se(IV)

10^2[Se(IV)](M)	pH(±0.01) 25.2°	30.2°	34.8°	40.0°
3.75	8.16	7.97	7.86	7.74
5.0	8.18	8.00	7.90	7.78
7.5	8.20	8.05	7.96	7.85
10	8.22	8.09	7.99	7.90
15	8.32	8.20	8.13	8.00
25	8.40	8.31	8.20	8.10

([aquo complex] = 1 x 10^{-2} M for Co(III), 5 x 10^{-3} M for Rh(III); μ = 1.0 M, ClO_4^- medium).

systems. The large variation in pH with temperature attributable to the Trizma Base buffer is a complicating factor which led to the eventual removal of this buffer in favour of adjusting the pH at the time of mixing as previously described in section 4.3.4.

The U.V. - visible spectra of the $[Co(NH_3)_5OH]^{2+}$ and $[Rh(NH_3)_5OH]^{2+}$ ions and their selenito products are shown in Figs. 4.13 and 4.14, respectively. Kinetic runs were followed at 550 nm and 460 nm for the substitution of $[Co(NH_3)_5OH]^{2+}$, corresponding with an increase and decrease in optical absorbance from reactants to products respectively, and at 350 nm for the substitution of $[Rh(NH_3)_5OH]^{2+}$ which corresponds with an increase in optical absorbance from reactants to products.

The rate data derived from the substitution studies are shown in Table 4.17 and 4.18, for the $[Co(NH_3)_5OH]^{2+}$ and $[Rh(NH_3)_5OH]^{2+}$ systems, respectively. The outstanding feature is the remarkable similarity of substitution rates for the different transition metal systems.

Plots of k_{obs} vs [Se(IV)] and k_{obs} vs $[HSeO_3^-]$ are shown in Figs. 4.15 and 4.16 for each system. The plots show an approximate linear dependence at first but then increase sharply with anion concentration around [Se(IV)] = 0.10 M.

When k_{obs} is plotted as a function of the square of the anion concentration, however, there is a linear dependence up to the highest anion concentration used. These plots are shown in Figs. 4.17 and 4.18, respectively, for the $[Co(NH_3)_5OH]^{2+}$ and $[Rh(NH_3)_5OH]^{2+}$ ions.

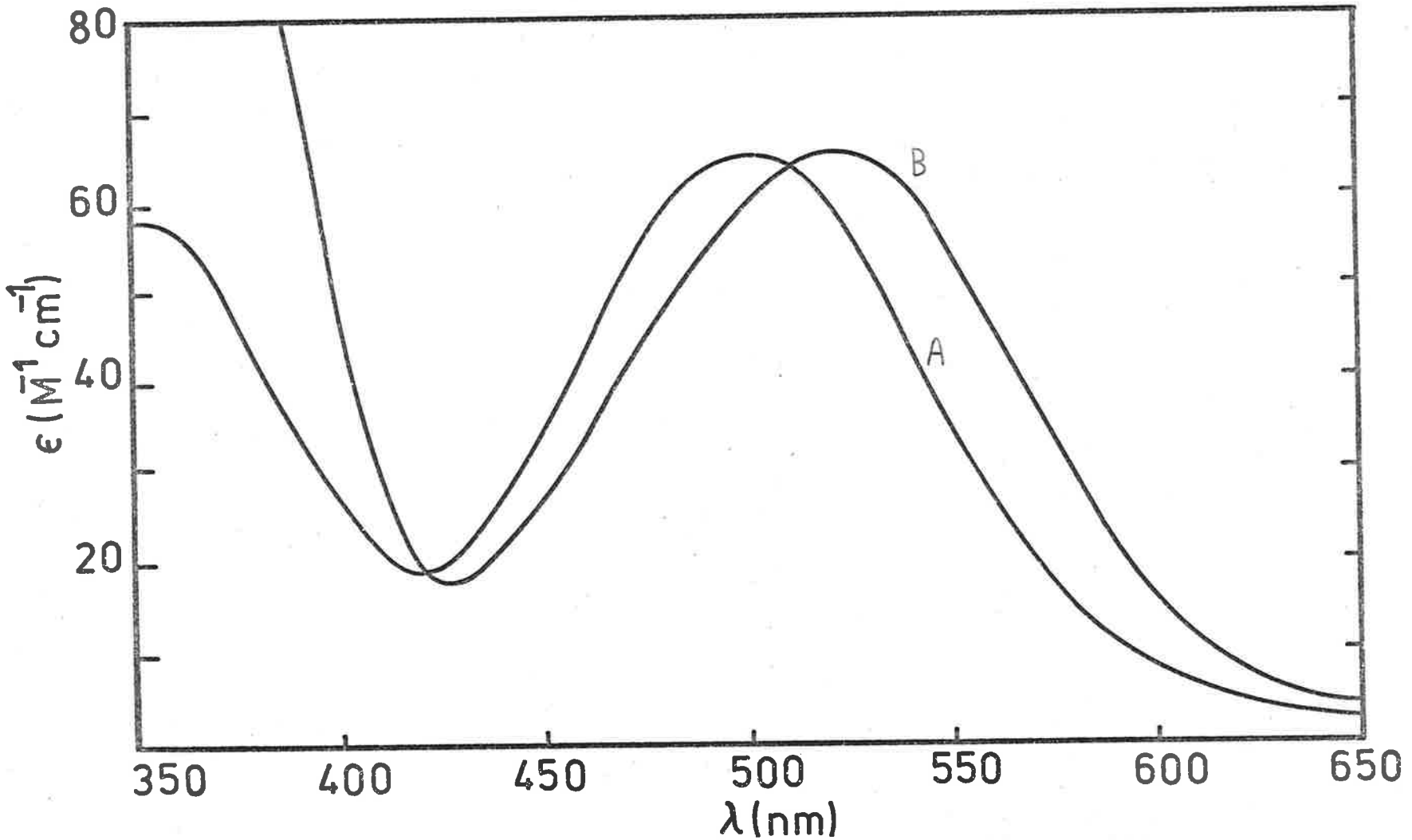

Fig. 4.13 U.V. - Visible Spectra of (A) $[Co(NH_3)_5OH]^{2+}$,

(B) $[Co(NH_3)_5OSeO_2]^+$ at pH ∿ 8.

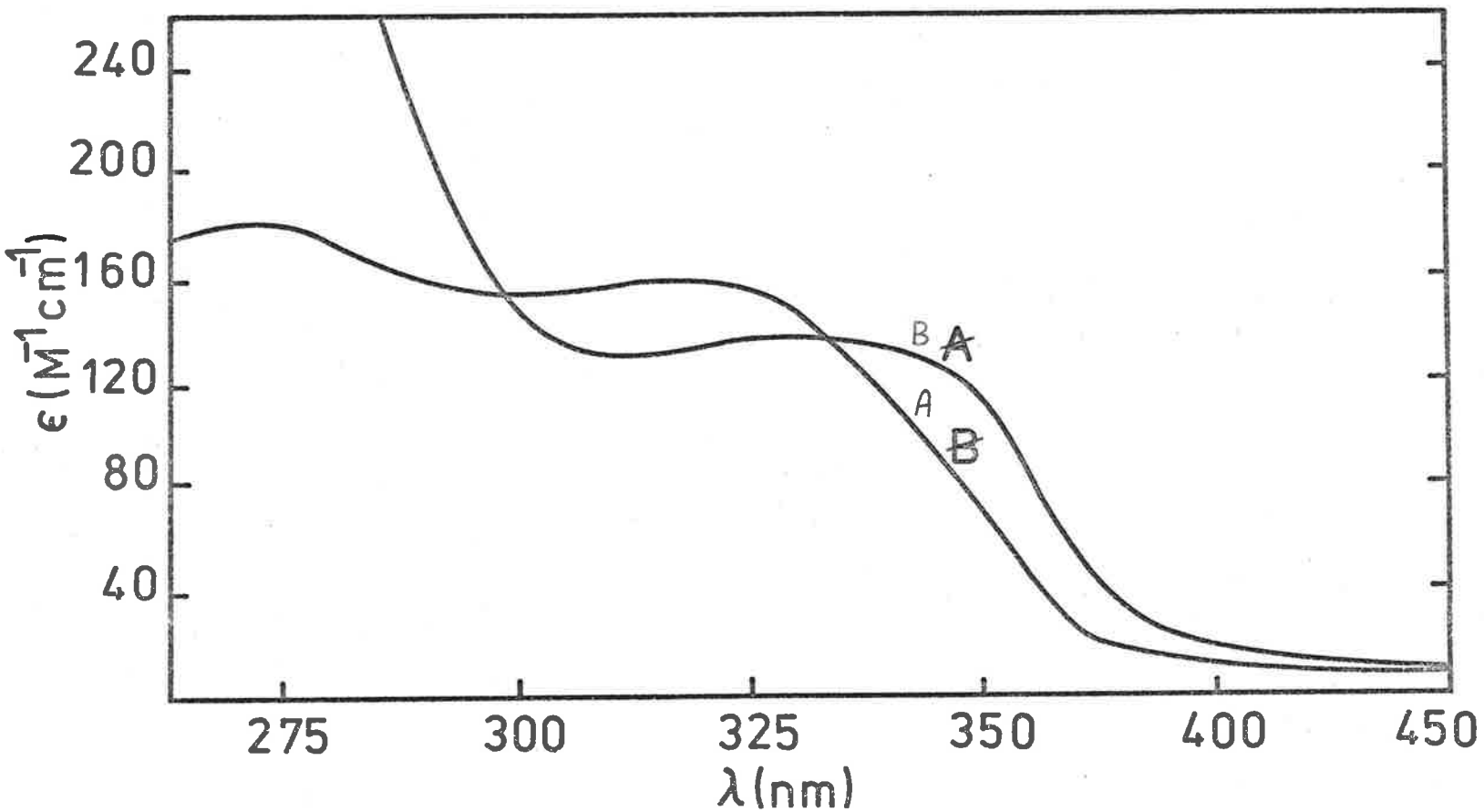

Fig. 4.14 U.V. - Visible Spectra of (A) $[Rh(NH_3)_5OH]^{2+}$,

(B) $[Rh(NH_3)_5OSeO_2]^+$ at pH ∿ 8.

Table 4.17 Rate Data for Substitution of $[Co(NH_3)_5(OH)]^{2+}$ *by Se(IV).*

10^2[Se(IV)]	$k_{25°}(sec^{-1})$	$k_{30°}(sec^{-1})$	$k_{35°}(sec^{-1})$	$k_{40°}(sec^{-1})$
5.0	0.40 ± 0.03	0.63 ± 0.04	1.18 ± 0.07	1.74 ± 0.06
7.5	0.78 ± 0.05	1.17 ± 0.05	1.92 ± 0.09	3.42 ± 0.19
10	1.25 ± 0.06	2.10 ± 0.10	3.19 ± 0.24	4.85 ± 0.30
15	2.37 ± 0.06	3.51 ± 0.39	5.57 ± 0.25	9.09 ± 0.41
25	4.35 ± 0.15	6.92 ± 0.16	11.8 ± 0.6	20.2 ± 1.3

([hydroxo-complex] = 1 x 10^{-2} M; μ= 1.0 M, ClO_4^- medium)

Table 4.18 Rate Data for Substitution of $[Rh(NH_3)_5(OH)]^{2+}$ by Se(IV)

10^2[Se(IV)](M)	$k_{25°}(sec^{-1})$	$k_{30°}(sec^{-1})$	$k_{35°}(sec^{-1})$
3.75	0.43 ± 0.02	0.79 ± 0.04	1.33 ± 0.11
5.0	0.82 ± 0.03	1.33 ± 0.05	2.07 ± 0.06
7.5	1.53 ± 0.05	2.80 ± 0.11	3.85 ± 0.11
10	2.55 ± 0.19	4.39 ± 0.37	7.32 ± 0.29
15	4.72 ± 0.22	7.16 ± 0.25	12.4 ± 0.4
25	10.3 ± 0.5	17.9 ± 0.8	27.5 ± 2.1

([hydroxo complex] = 5 x 10^{-3} M ; μ = 1.0 M, ClO_4^- medium)

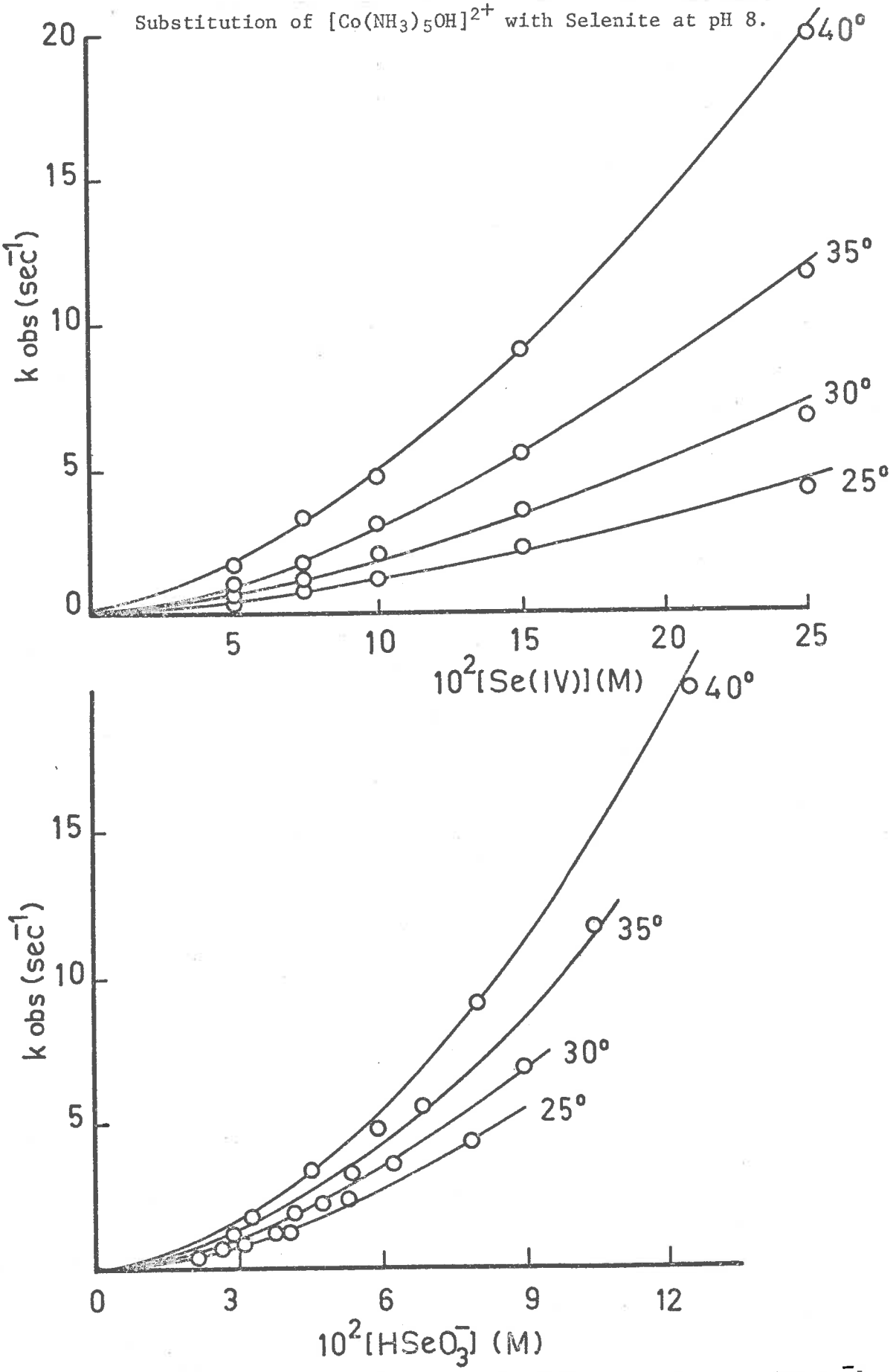

Fig. 4.15 Plots of (a) k_{obs} vs [Se(IV)], (b) k_{obs} vs $[HSeO_3^-]$

Fig. 4.16 Plots of (a) k_{obs} vs [Se(IV)], (b) k_{obs} vs $[HSeO_3^-]$ for Substitution of $[Rh(NH_3)_5OH]^{2+}$ with Selenite at pH 8.

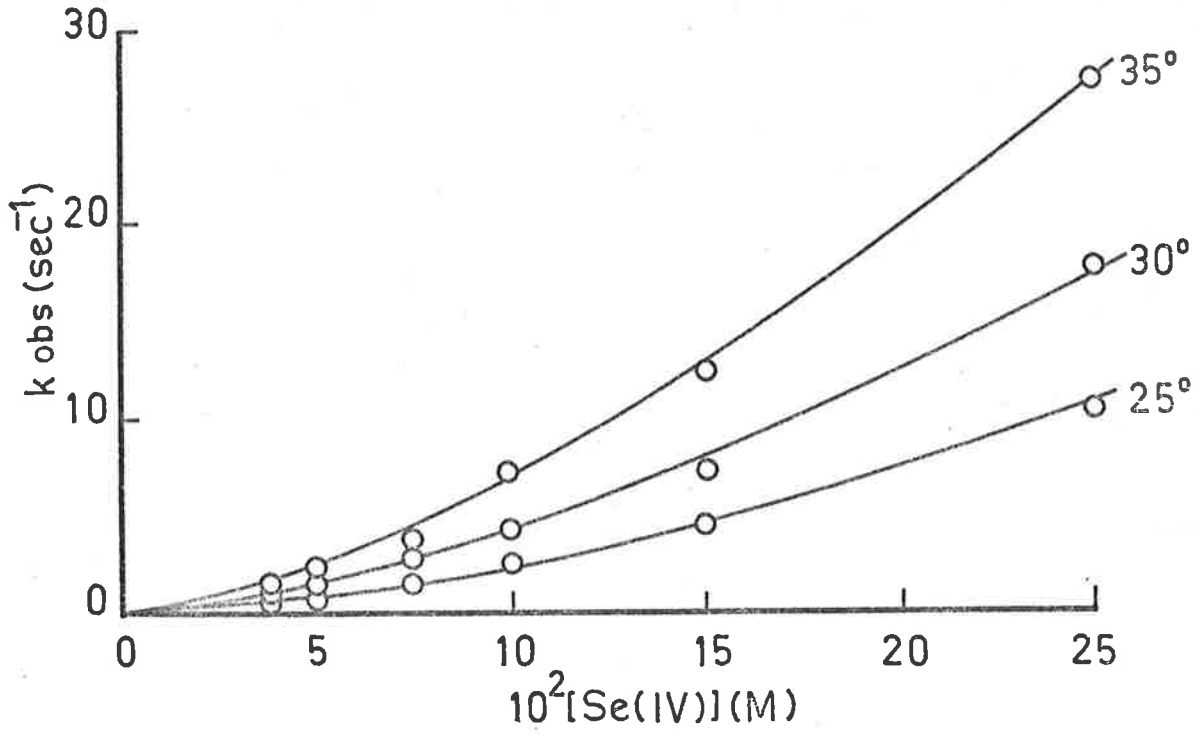

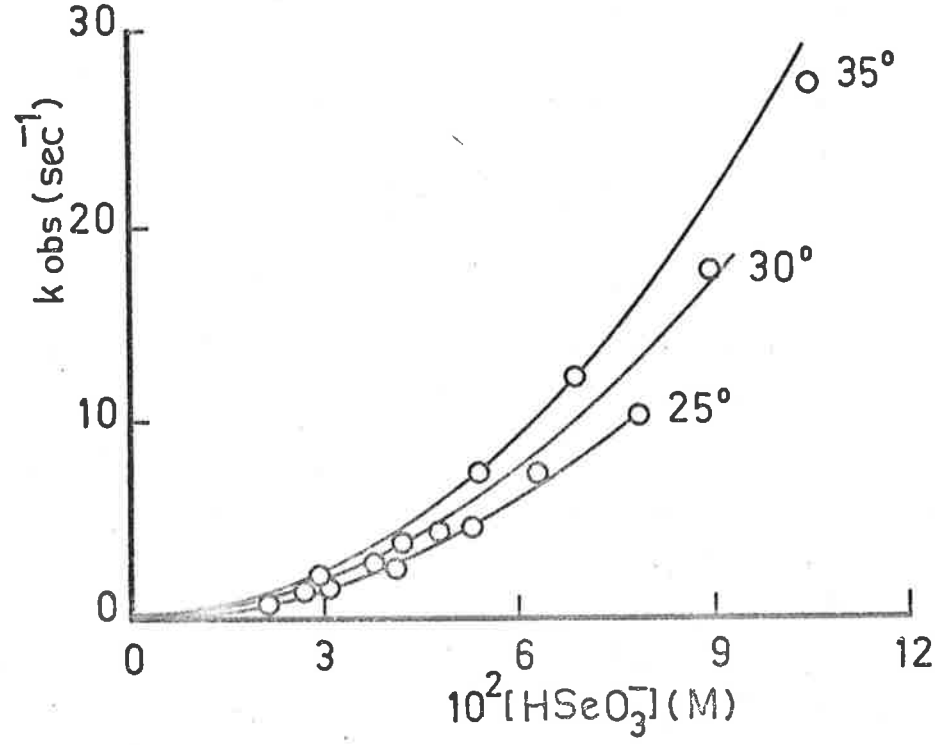

Fig. 4.17 Plots of k_{obs} vs $[HSeO_3^-]^2$ for Substitution of $[Co(NH_3)_5OH]^{2+}$ with Selenite at pH 8.

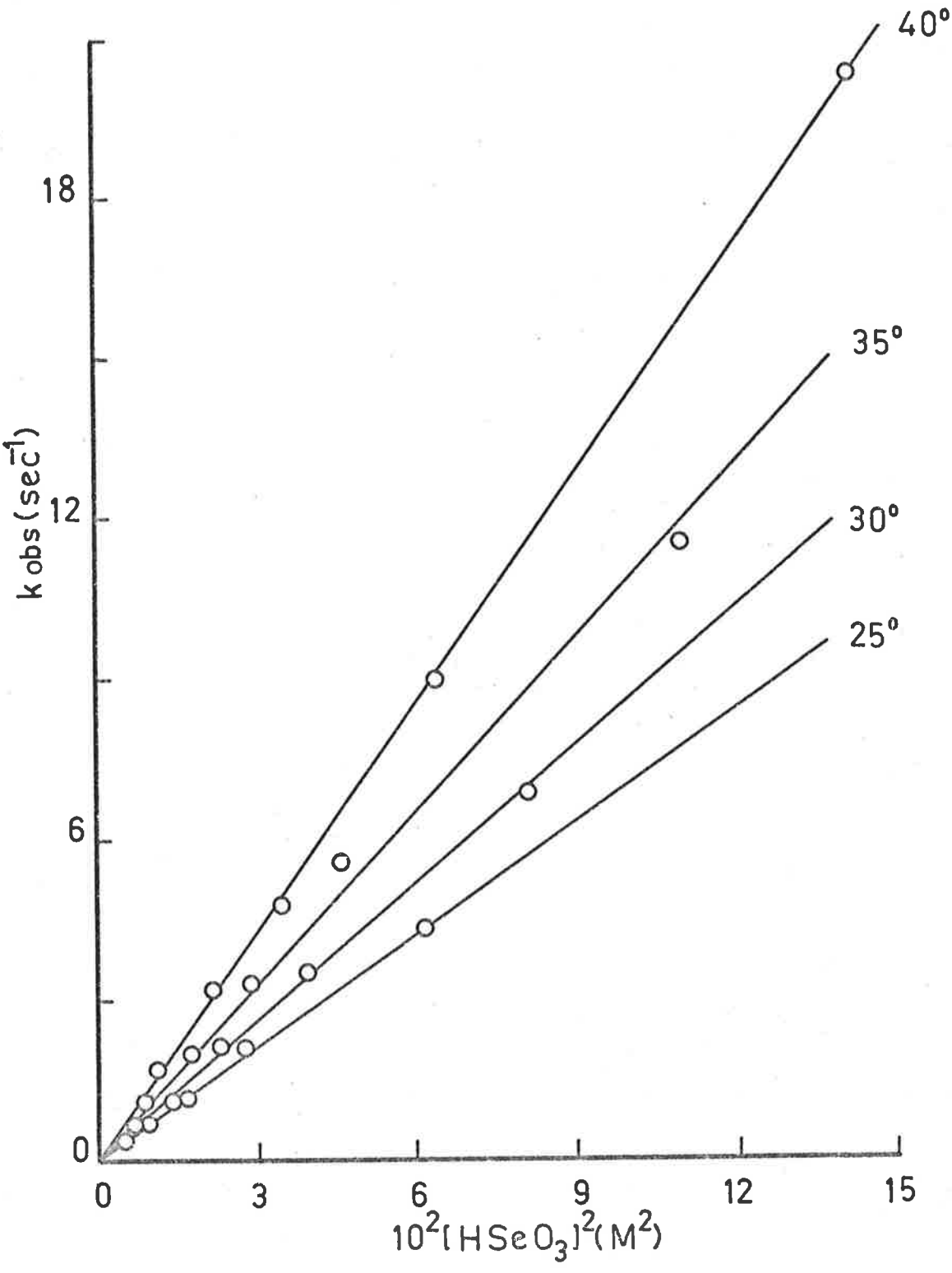

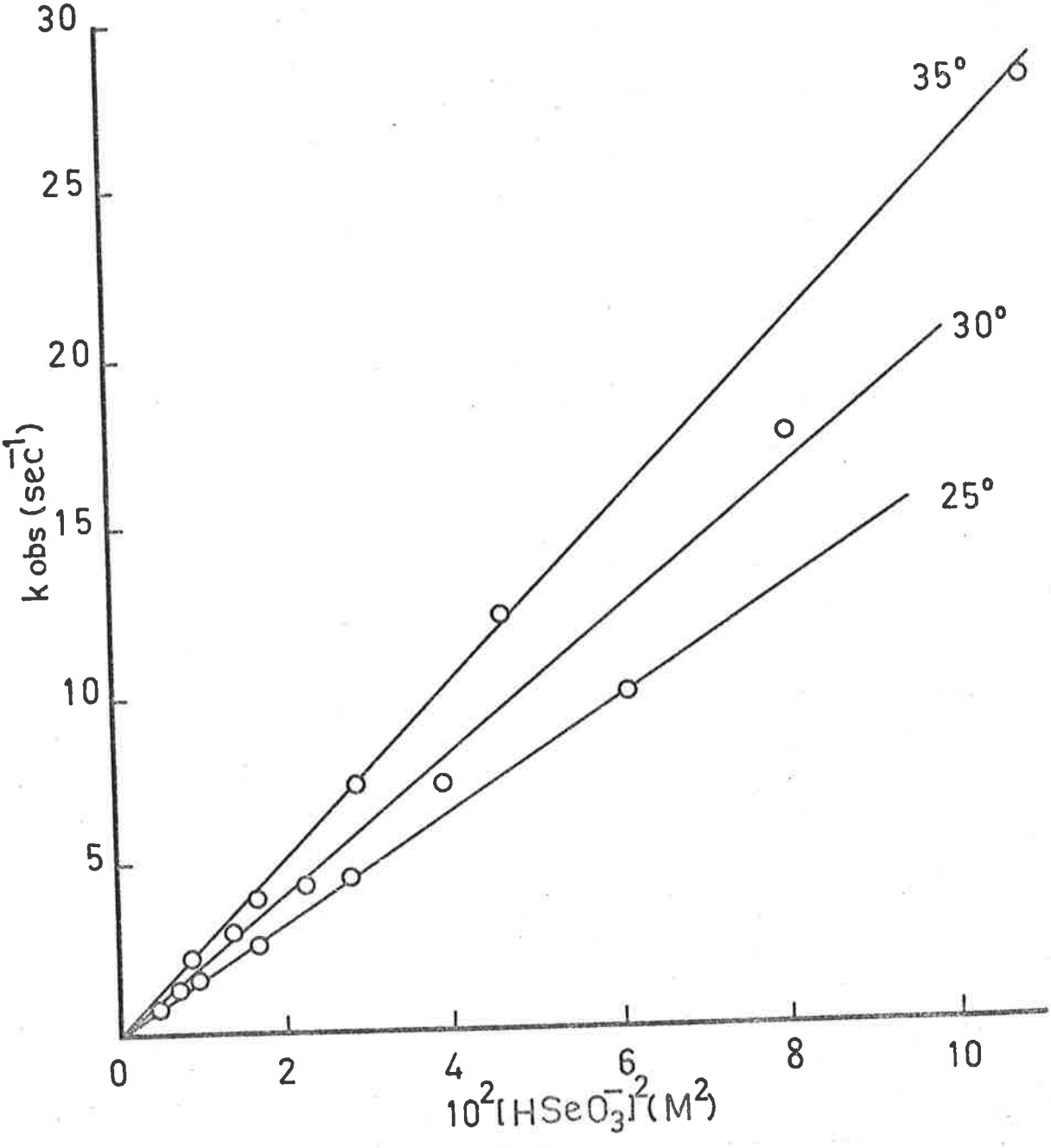

Fig. 4.18 Plots of k_{obs} vs $[HSeO_3^-]^2$ for Substitution of $[Rh(NH_3)_5OH]^{2+}$ with Selenite at pH 8.

The k_{subs} values derived from the slopes are shown in Table 4.19. The activation parameters derived from plots of k_{subs} vs 1/T are for the $[Co(NH_3)_5OH]^{2+}$ ion,

$$\Delta H^{\ddagger}_{subs} = 33.2 \pm 1.2 \text{ kJ mol}^{-1}, \quad \Delta S^{\ddagger}_{subs} = -70.8 \pm 1.7 \text{ J K}^{-1} \text{ mol}^{-1}$$

and for the $[Rh(NH_3)_5OH]^{2+}$ ion,

$$\Delta H^{\ddagger}_{subs} = 32.6 \pm 1.0 \text{ kJ mol}^{-1}, \quad \Delta S^{\ddagger} = -66.0 \pm 1.3 \text{ J K}^{-1} \text{ mol}^{-1}.$$

The $\Delta H^{\ddagger}_{subs}$ values are similar in magnitude to those found in the region pH 6 - 7.

The initial linearity of the plots of k_{obs} vs [Se(IV)] and k_{obs} vs $[HSeO_3^-]$ suggested that the substitution reaction may be proceeding by a two-step reaction pathway described by the rate-law

$$k_{obs} = k_1[HSeO_3^-] + k_2[HSeO_3^-]^2$$

Figs. 4.19 and 4.20 show the plots of $k_{obs}/[HSeO_3^-]$ vs $[HSeO_3^-]$ for the cobalt(III) and rhodium(III) systems respectively. The plots are linear with intercept = k_1 and slope = k_2. The relative magnitudes of the two rate constants, k_1 and k_2, which are shown in Table 4.20, indicate that at low $[HSeO_3^-]$ the monomeric and dimeric paths are competitive, but at higher $[HSeO_3^-]$ the k_2 term takes over and the rate law becomes simplified to

$$k_{obs} = k_2[HSeO_3^-]^2 \qquad 4.12$$

Around pH 8 the predominant complex form is the hydroxo ion which is present to the extent of about 95% for the $[Co(NH_3)_5OH_2]^{3+}$

Table 4.19 k_{subs} *Values for Se(IV) Substitution of* $Co(NH_3)_5OH^{2+}$ and $Rh(NH_3)_5OH^{2+}$

Temp (± 0.1°)	$10^2 k_{subs}$ (sec^{-1} M^{-2})	
	$Co(NH_3)_5OH^{2+}$	$Rh(NH_3)_5OH^{2+}$
25.2	7.2 ± 0.3	16.2 ± 0.8
30.3	8.9 ± 0.4	20.4 ± 1.4
34.9	11.0 ± 0.5	25.3 ± 1.8
40.0	14.2 ± 0.7	

([aquo complex] = 1 x 10^{-2} M for Co(III), 5 x 10^{-3} M for Rh(III); pH = 8.0 ± 0.4; μ = 1.0 M, ClO_4^- medium)

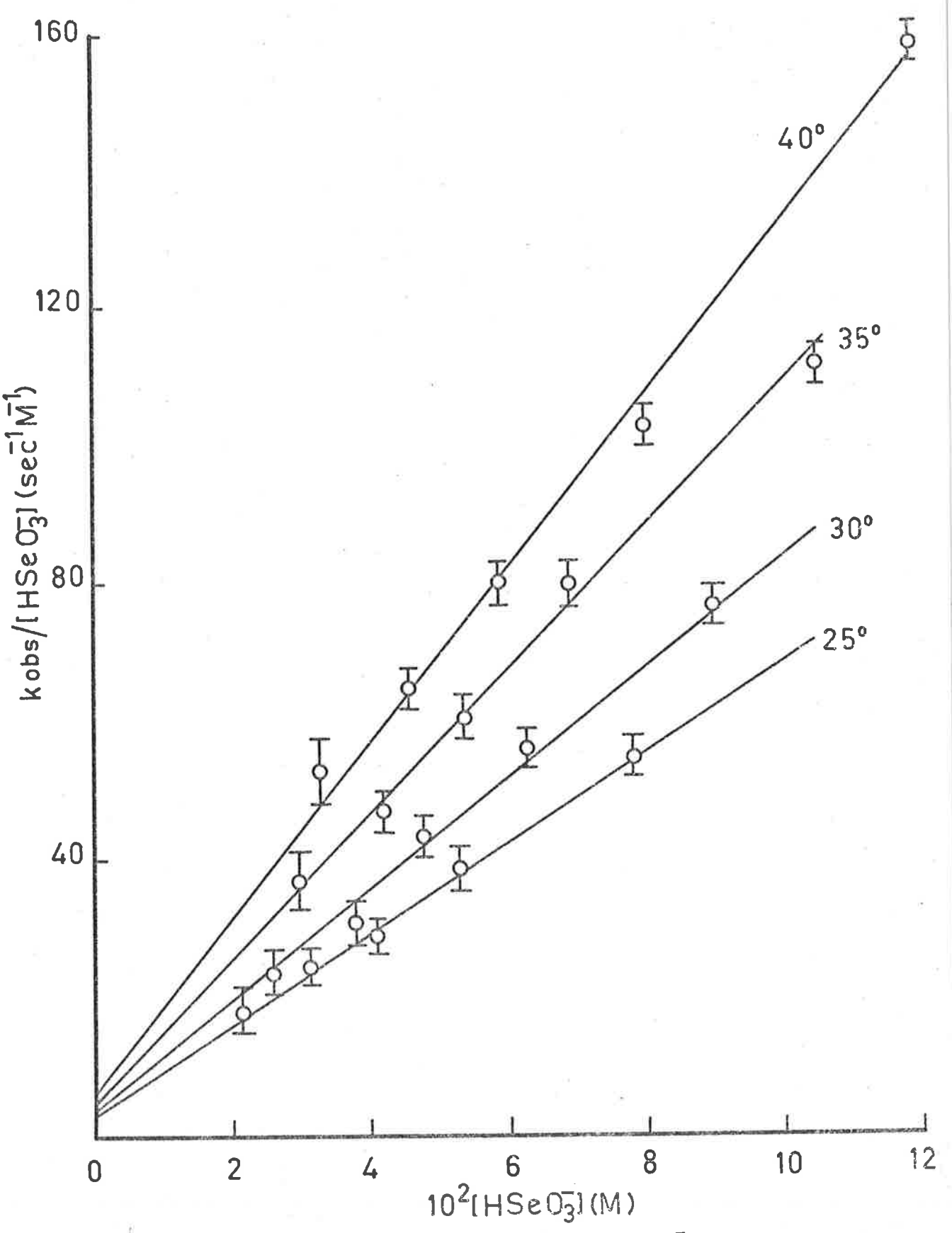

Fig. 4.19 Plots of $k_{obs}/[HSeO_3^-]$ vs $[HSeO_3^-]$ for Substitution of $[Co(NH_3)_5OH]^{2+}$ with Selenite at pH 8.

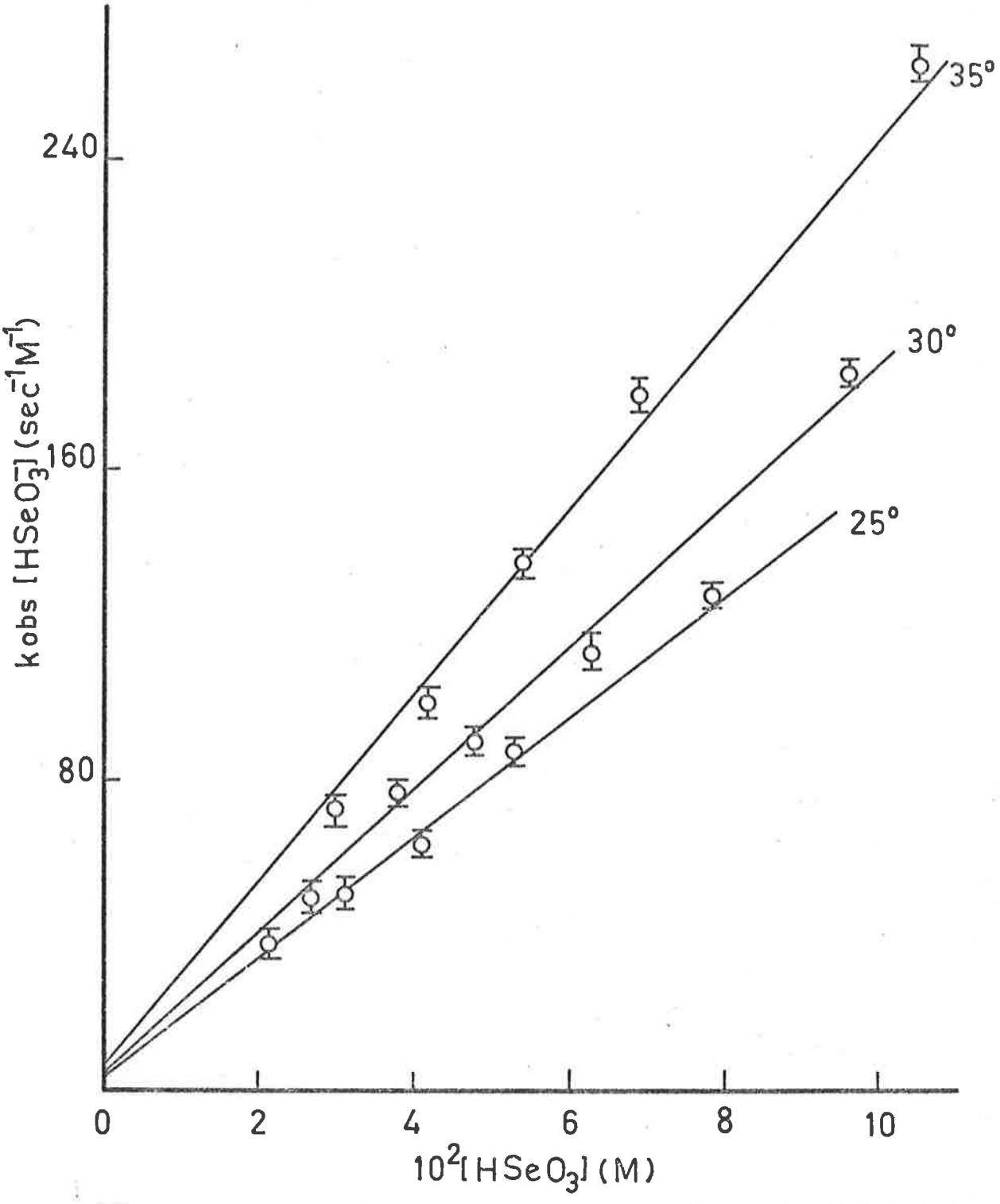

Fig. 4.20 Plots of $k_{obs}/[HSeO_3^-]$ vs $[HSeO_3^-]$ for Substitution of $[Rh(NH_3)_5OH]^{2+}$ with Selenite at pH 8.

Table 4.20 Monomeric and Dimeric Rate Constants for the Reaction of $[Co(NH_3)_5OH]^{2+}$ and $[Rh(NH_3)_5OH]^{2+}$ with Se(IV)

Temp (± 0.1°)	$Co(NH_3)_5OH^{2+}$		$Rh(NH_3)_5OH^{2+}$	
	$k_1(sec^{-1}M^{-1})$	$10^2k_2(sec^{-1}M^{-2})$	$k_1(sec^{-1}M^{-1})$	$10^2k_2(sec^{-1}M^{-2})$
25.2	3 ± 1	7.2 ± 0.2	2 ± 1	16 ± 2
30.3	4 ± 1	8.9 ± 0.5	3 ± 1	20 ± 4
34.9	5 ± 2	11 ± 1	5 ± 2	25 ± 6
40.0	7 ± 2	14 ± 2		

system and 99% for the $[Rh(NH_3)_5OH_2]^{3+}$ system.

The Se distribution data of Barcza and Sillén indicate that at this pH about 90% of the total Se(IV) concentration is in the monomeric form, of which 55% is contributed by the SeO_3^{2-} ion, for [Se(IV)] = 0.1 M, $NaClO_4$ as supporting electrolyte. The principal dimeric form is the HL_2^{3-} ion which reaches its maximum concentration at pH 8.

Thus the dual reaction path mechanism indicated from the kinetic data can now be written as

$$ROH_2^{2+} + H\,SeO_3^- \xrightarrow{k_{1an}} ROSeO_2^+ + H_2O \qquad 4.13$$

$$ROH_2^{2+} + H(SeO_3)_2^{3-} \xrightarrow{k_{2an}} ROSeO_2^+ + SeO_3^{2-} \qquad 4.14$$

Again path 4.13 is only important at low [Se(IV)].

Unlike the anation of the *cis*-$[Co(en)_2OH(OH_2)]^{2+}$ species at pH7 where a limiting rate of substitution is attained at high [Se(IV)], no such limiting rate is observed for the anation reactions at pH 8 of the $[Co(NH_3)_5OH]^{2+}$ and $[Rh(NH_3)_5OH]^{2+}$ species. This may be attributed to the considerable decrease in the $HSeO_3^-$ ion concentration from pH 7 to pH 8 (a drop of about 40%) which reduces substantially the number of $HSeO_3^-$ ions available for dimerization. In other words the total biselenite concentration is much higher at pH 7 than at pH 8.

4.3.3 High pH Region : pH 10

No concentration dependence study was undertaken in this region but temperature dependence studies were carried out for the *cis*- and *trans*-$[Co(en)_2(OH)_2]^+$, *cis*- and *trans*-$[Co(tn)_2(OH)_2]^+$, and $[Co(NH_3)_5OH]^{2+}$ ions. In each case the complex concentration was

1×10^{-2} M and the selenite concentration was 10^{-1} M.

The rate data obtained are listed in Table 4.21 and the activation parameters derived from them are summarized in Table 4.22. Once again the remarkable feature is the similarity of the substitution rates between the different systems. There is also no significant *trans*-effect in this pH region.

A comparison of the k_{obs} values at pH 10 and pH 8 for the $[Co(NH_3)_5OH]^{2+}$ ion shows that there is a sharp drop in the substitution rate at the higher pH value. At pH 8, $k_{obs} = 1.25\ sec^{-1}$, and at pH 10, $k_{obs} = 0.21\ sec^{-1}$ at 25° and [Se(IV)] = 0.1 M. The $HSeO_3^-$ concentration at pH 10 (< 2%) is too small to fully account for the observed rate of substitution at this pH - k_{subs}(calc) $\sim 0.025\ sec^{-1}$ (determined from k_{obs} at pH 8), which is only one tenth of the actual k_{obs} value at pH 10 for $[Co(NH_3)_5OH]^{2+}$. There is also a measurable substitution rate at pH 11.5 (see 3.6.3) where $[HSeO_3^-] = 0$, which means that the SeO_3^{2-} ion does undergo substitution, although at a much slower rate than the $HSeO_3^-$ ion. Thus at pH 10, substitution of the hydroxo-ligand probably proceeds by two concurrent paths, viz.,

$$ROH^+ + HSeO_3^- \underset{k_{hyd}}{\overset{k_{1subs}}{\rightleftharpoons}} ROSeO_2 + H_2O \qquad 4.15$$

$$ROH^+ + SeO_3^{2-} \underset{k_{hyd}}{\overset{k_{2subs}}{\rightleftharpoons}} ROSeO_2 + OH^- \qquad 4.16$$

At pH > 11, substitution would proceed only by reaction 4.16. The decrease in the rate of substitution with increasing pH can therefore be attributed to the fact that the leaving group in reaction 4.16,

Table 4.21 Temperature Dependence of Se(IV) Substitution with Various Hydroxo-Metal Complexes

Temp. (°C)	k_{obs} (sec^{-1})				
	cis $Co(tn)_2(OH)_2^+$	*trans* $Co(tn)_2(OH)_2^+$	*cis* $Co(en)_2(OH)_2^+$	*trans* $Co(en)_2(OH)_2^+$	$Co(NH_3)_5OH^{2+}$
10		$0.02_1 \pm 0.00_1$			
15		$0.05_5 \pm 0.00_1$		$0.05_0 \pm 0.00_1$	
20		$0.13_2 \pm 0.00_7$		$0.11_0 \pm 0.00_6$	
25	$0.11_0 \pm 0.00_1$		$0.13_0 \pm 0.00_4$	$0.19_4 \pm 0.00_4$	$0.21_0 \pm 0.00_5$
30	$0.17_8 \pm 0.00_4$		$0.19_1 \pm 0.00_4$		0.31 ± 0.02
35	$0.26_0 \pm 0.00_3$		$0.24_5 \pm 0.00_3$		
40	$0.37_5 \pm 0.00_5$		$0.34_7 \pm 0.00_6$		$0.59_9 \pm 0.00_9$

([hydroxo complex] = 1×10^{-2} M; [Se(IV)] = 10^{-1} M; μ = 1.0 M, ClO_4^- medium)

Table 4.22 Activation Parameters for Substitution of Se(IV) at pH 10.

Hydroxo-Complex	$\Delta H^{\ddagger}$ (kJ mol^{-1})	$\Delta S^{\ddagger}_{298}$ (J $K^{-1}mol^{-1}$)	$\Delta G^{\ddagger}_{298}$ (kJ mol^{-1})
cis -$Co(en)_2(OH)_2^+$	48.1 ± 1.0	-92.1 ± 2.2	75.6 ± 1.7
trans-$Co(en)_2(OH)_2^+$	59.2 ± 3.0	-52.4 ± 2.9	74.8 ± 3.9
cis-$Co(tn)_2(OH)_2^+$	61.8 ± 1.0	-47.4 ± 0.9	76.0 ± 1.3
trans-$Co(tn)_2(OH)_2^+$	45.1 ± 1.3	-114 ± 4	79.1 ± 2.5
$Co(NH_3)_5(OH)^{2+}$	52.3 ± 1.2	-74.1 ± 1.7	74.4 ± 1.7

which becomes increasingly important at high pH, is the OH^- ion which is a much poorer leaving group than H_2O.

The $\Delta H^{\ddagger}$ values for substitution in this region fall in the range 46 - 61 kJ mol^{-1} which is in good agreement with the range of the values observed at low pH. This is again consistent with Se-O bond formation or cleavage in the rate-determining step.

4.5 Summary

From an analysis of the kinetic data for the substitution by selenite of various aquo-ligands over the pH range 1 - 10, the following general conclusions can be made:

1. the substitution rate attains its maximum value around pH 3 - 4, corresponding with optimum concentrations of the diaquo (in the case of the *en* and *tn* systems) or aquo (in the case of the pentaammine systems) species and the $HSeO_3^-$ species. The substitution rate is lowest at high pH ($\gtrsim$ 10), corresponding with optimum concentrations of the dihydroxo or hydroxo species and the SeO_3^{2-} species;
2. the nature of the nitrogen bases (NH_3, *en*, and *tn*) coordinated to the metal has only a secondary effect on reaction rate;
3. the nature of the metal does not appear to greatly influence the reaction rate, as is evidenced by the remarkable similarity in the $[Co(NH_3)_5OH]^{2+}$ and $[Rh(NH_3)_5OH]^{2+}$ substitution rates;
4. there is a slight but significant *trans*-effect at pH 1 and pH 3 (cf. the strong *trans*-effect exhibited by the analogous sulphite group[5]) which, however, becomes less important at higher pH and is in fact entirely absent at pH 10;
5. the substitution mechanism is complicated at neutral pH (6 - 8.5) by the emergence of a dimeric pathway, in addition to the monomeric pathway observed at low (1 - 4) and high (10) pH;
6. the activation enthalpies for hydrolysis and substitution are generally in the range 46 - 60 kJ mol^{-1} which is indicative of

Se-O bond rupture and formation in the rate-determining step (cf. base hydrolysis of $[Co(NH_3)_5OSeO_2]^+$ which proceeds by Se-O bond rupture and has $\Delta H^{\ddagger} = 48.1 \pm 1.4$ kJ mol^{-1}); however in the neutral pH region the activation enthalpy for substitution falls to around 35 kJ mol^{-1}.

The substitution half-times at 25°, which vary from a few seconds to about 30 millisecs depending on pH, can be contrasted with the half-times of many hours for the exchange of oxygen between the aquo-ligand and solvent water in the case of the $[Co(en)_2(OH_2)_2]^{3+}$ and $[Co(NH_3)_5OH_2]^{3+}$ complex systems.

The substitution half-times at pH 10 which are of the order of 5 - 10 secs at 25° can also be compared with the half-time of about 2 hrs. for the oxygen exchange reaction on selenite itself at the same pH.

In view of these comparative reaction rates and the fact that the metal-oxygen bond remains intact during substitution the substitution reaction can be conceived as proceeding by an associative mechanism which involves nucleophilic attack of the aquo-ligand on the Se(IV) centre. A similar mechanism has been proposed for the anation reaction between $[Co(NH_3)_5OH_2]^{3+}$ and arsenate.[2] A possible reaction scheme for the substitution at Se(IV) in the low pH region is shown below.

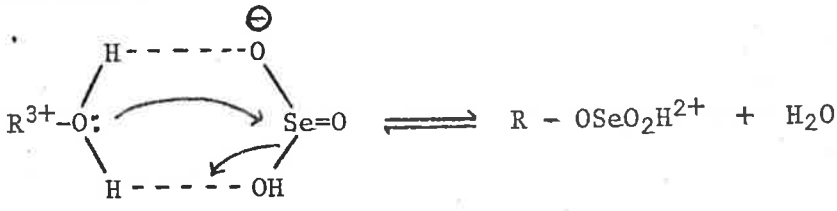

At neutral pH, substitution occurs mainly through the dimeric species, $H_2(SeO_3)_2^{2-}$ and $H(SeO_3)_2^{3-}$, so that the leaving group will be $HSeO_3^-$, and at high pH, substitution proceeds mainly through SeO_3^{2-}, with OH^- as the leaving group.

B. *Isomerization at Selenium(IV) : Selenito - Complex Isomerization.*

4.6 Introduction

Investigations into the substitution reactions of *trans*-$[Co(en)_2(OH_2)_2]^{3+}$ and *trans*-$[Co(tn)_2(OH_2)_2]^{3+}$ with selenite, as described in section A, subsequently led to the detection of a second slower reaction step which occurred after the initial fast substitution process.

When *trans*-$[Co(en)_2(OH_2)_2]^{3+}$ was reacted with excess selenite at pH $\sim$ 3 there was an immediate colour change from red to green followed by a gradual conversion (completed within $\sim$ 3 hrs. at 25°) to red-purple on standing. This contrasted with the analogous substitution reaction of *cis*-$[Co(en)_2(OH_2)_2]^{3+}$ with selenite where there was no visually detectable colour change after the initial immediate conversion from red to red-purple. Subsequent spectrophotometric analysis, however, revealed a slight shift in the visible spectrum of the *cis*-selenito product over a similar time period as above.

A similar 2-step reaction sequence was also found in the case of the *trans*-$[Co(tn)_2(OH_2)_2]^{3+}$ substitution reaction with selenite, but here step II was considerably faster than for the analogous *en* system and completed within a matter of seconds at 25°.

The final spectra after completion of step II in the case of the *trans*-diaquo complexes were found to be identical with those of the analogous *cis*-diaquo complexes on completion of step II. This

indicated that step II involved isomerization of the respective selenito products to an equilibrium mixture of *cis*- and *trans*-isomers.

The isomerization reaction

$$trans\text{-}[Co(en)_2(OH_2)OSeO_2H]^{2+} \underset{\leftarrow}{\overset{pH\ 3.3}{\rightarrow}} cis\text{-}[Co(en)_2(OH_2)OSeO_2H]^{2+} \quad 4.17$$

is sufficiently slow to enable the isolation of the *trans*-selenito complex at low temperature, as described in ch. 2. A temperature and pressure dependence study of this isomerization reaction was subsequently performed in these laboratories by Vanderhoek[23] using the pure *trans*-$[Co(en)_2(OH_2)OSeO_2H]^{2+}$ complex.

A temperature dependence study was also carried out for the isomerization reaction

$$trans\text{-}[Co(tn)_2(OH_2)OSeO_2H]^{2+} \underset{\leftarrow}{\overset{pH\ 3.3}{\rightarrow}} cis\text{-}[Co(tn)_2(OH_2)OSeO_2H]^{2+} \quad 4.18$$

by preparing the *trans* selenito complex *in situ* in the mixing chamber of the stopped-flow apparatus and following the resultant isomerization process on completion of the initial substitution reaction.

4.7 Experimental

4.7.1 Materials

trans-$[Co(en)_2(OH_2)\ OSeO_2H]^{2+}$ was prepared by the method described in 2.2.3.

trans-$[Co(tn)_2(OH_2)OSeO_2H]^{2+}$ was prepared *in situ* from *trans*-$[Co(tn)_2(OH_2)_2]^{2+}$ (see 2.2.3 and 4.3.4) and excess selenite.

4.7.2 Optical Absorbance and pH Measurements

These were carried out using the methods previously described in 3.2.2 and 3.2.3.

4.7.3 Kinetics

All kinetic runs involved in the isomerization study of the *trans*-$[Co(en)_2(OH_2)OSeO_2H]^{2+}$ complex system were performed with a Unicam SP 800 continuous scan spectrophotometer linked to an external recorder through an expanded scale control. Constant temperature was maintained by rapidly pumping water from an external thermostat through the metal block containing the reaction cell. This instrument was also used in the determination of isosbestic points for the isomerization reactions.

The kinetic study of the *trans*-$[Co(tn)_2(OH_2)OSeO_2H]^{2+}$ isomerization reaction was performed using the stopped-flow apparatus previously described.

All reaction solutions were adjusted to 1 M ionic strength with sodium perchlorate.

4.8 Results and Discussion

The relevant spectral data for the isomerization process in the *en* and *tn* systems are summarized in Tables 4.23 and 4.24 respectively, at 4 different pH values, viz. pH 1, 3, 7 and 10. These data can be compared with those obtained for the pure monodentate and bidentate selenito complexes (2.3.3). The important conclusion is that only monodentate selenito complex formation is important under the conditions used during the kinetic investigation.

The rate data obtained from the temperature dependence studies of the *trans*-$[Co(en)_2(OH_2)OSeO_2H]^{2+}$ and *trans*-$[Co(tn)_2(OH_2)OSeO_2H]^{2+}$ isomerization reactions at pH 3.3 are shown in Table 4.25, and the activation parameters, $\Delta H^{\ddagger}$ and $\Delta S^{\ddagger}$, are presented in Table 4.26, together with the $\Delta V^{\ddagger}$ values for the *trans*-$[Co(en)_2(OH_2)OSeO_2H]^{2+}$ system measured at pH 3.3 and pH 7.0.

A comparison of the rate data for isomerization with that for substitution at the same pH reveals that the isomerization rate is a factor of 10^5 slower than the substitution rate in the case of the *en* system and 10^2 slower in the case of the *tn* system.

In contrast to the substitution step where there is only a secondary dependence of reaction rate on the nature of the nitrogen base coordinated to the metal, the rate of isomerization is greatly accelerated on the insertion of an extra CH_2 group into the amine ring. The rate of isomerization for the *trans*-$[Co(tn)_2(OH_2)OSeO_2H]^{2+}$ complex is a factor of 10^3 greater than for the *trans*-$[Co(en)_2(OH_2)OSeO_2H]^{2+}$ complex whereas the rates of substitution by selenite

Table 4.23 *Isomerization of trans-*$[Co(en)_2(OH_2)OSeO_2H]^{2+}$

pH	Complex Species		equilibrium mixture
	trans-$[Co(en)_2(OH_2)OSeO_2H]^{2+}$	*cis*-$[Co(en)_2(OH_2)OSeO_2H]^{2+}$	
1	λ_{max1}= 573 nm (ε=33 $M^{-1}cm^{-1}$)	500 (84)	500 (72)
	λ_{max2}= 440 nm (ε=33 $M^{-1}cm^{-1}$)	360 (70)	
isosbestic points:	563, 445, 380 nm.		
3	590 (39)	520 (96)	520 (88)
	438 (31)	356 (84)	367 (87)
isosbestic points:	584, 453, 425, 378 nm.		
6	590 (50)	530(110)	530(103)
isosbestic points:	589, 450, 403 nm.		
10	570 (49)	524(100)	526 (90)
	470 (32)		
isosbestic points:	566, 470 nm.		

([aquo-complex] = 1 x 10^{-2}M; [Se(IV)] = 10^{-1} M; μ = 1.0 M, ClO_4^- medium; Temp = 25.0 ± 0.1°)

Table 4.24 *Isomerization of trans-*$[Co(tn)_2(OH_2)OSeO_2H]^{2+}$

pH	Complex Species		equilibrium mixture
	trans-$[Co(tn)_2(OH_2)OSeO_2H]^{2+}$	*cis*-$[Co(tn)_2(OH_2)OSeO_2H]^{2+}$	
1	λ_{max1} = 500 nm(ε= 48 $M^{-1}cm^{-1}$)	520 (68)	517 (61)
	λ_{max2} = 362 nm(ε= 87 $M^{-1}cm^{-1}$)	365 (82)	365 (73)
isosbestic points:	577, 477 nm.		
3	548 (43)	539 (80)	539 (78)
		372 (76)	372 (73)
isosbestic points:	600, 483, 424, 403 nm.		
6	520 (64)	546 (92)	545 (89)
	368 (80)	399 (80)	399 (76)
isosbestic points:	510, 446, 374 nm.		
10	534 (72)	535 (76)	534 (75)
isosbestic points:	500, 415 nm.		

([aquo-complex] = 1 x 10^{-2} M; [Se(IV)] = 10^{-1} M; μ = 1.0 M, ClO_4^- medium, Temp. = 25.0 ± 0.1°)

Table 4.25 Temperature Dependence Studies of en and tn Isomerization Reactions at pH 3.3.

Temp. (± 0.1°)	k_{obs} (sec^{-1})	
	trans-$[Co(en)_2(OH_2)OSeO_2H]^{2+}$	*trans*-$[Co(tn)_2(OH_2)OSeO_2H]^{2+}$
15.1		$(5.7 \pm 0.2) \times 10^{-2}$
19.9	1.20×10^{-4}	$(12.2 \pm 0.6) \times 10^{-2}$
25.1	2.42×10^{-4}	$(22.0 \pm 1.0) \times 10^{-2}$
30.3	4.77×10^{-4}	
34.9	9.87×10^{-4}	

Table 4.26 Activation Parameters for en and tn Isomerization Reactions at pH 3.3.

Complex	$\Delta H^{\ddagger}$ (kJ mol^{-1})	$\Delta S^{\ddagger}_{298}$ (J K^{-1} mol^{-1})	$\Delta G^{\ddagger}_{298}$ (kJ mol^{-1})
trans-$[Co(tn)_2(OH_2)OSeO_2H]^{2+}$	110.0 ± 2.1	107.5 ± 10.5	82.0 ± 5.1
trans-$[Co(en)_2(OH_2)OSeO_2H]^{2+}$	109.2 ± 1.3	52.7 ± 4.2	97.5 ± 2.5
	$\Delta V^{\ddagger}$ t→c ($cm^3 mol^{-1}$)	$\Delta V^{\ddagger}$ c→t (cm^3 mol^{-1})	pH
trans-$[Co(en)_2(OH_2)OSeO_2H]^{2+}$	7.5 ± 0.2	12.7 ± 1.0	3.3
	7.3 ± 0.2	7.3 ± 0.2	7.0

are comparable for both complexes.

The high $\Delta H^{\ddagger}$ values observed for step II are consistent with Co-O bond cleavage in the rate-determining step. It can be seen from Table 4.26 that the $\Delta H^{\ddagger}$ values for the *en* and *tn* isomerizations are almost the same and that the large difference in rates of isomerization between the two systems is therefore almost entirely due to the differences in the entropy of activation term. At pH 3.3 the difference in $T\Delta S^{\ddagger}$ between the two systems is 16.4 kJ mol^{-1}. The entropy difference can be attributed to the relatively greater freedom for the six-membered *tn* ring in a dissociated transition state involving release of the aquo-ligand.

This large difference in isomerization rates between the *en* and *tn* complexes is consistent with previous observations for other reactions involving these complexes where there is Co-O bond cleavage in the rate-determining step. For instance, the base hydrolysis of the $Co(tn)_3^{3+}$ complex[24] has been found to proceed by a factor of 10^4 faster than the base hydrolysis of the $Co(en)_3^{3+}$ complex,[25] and the isomerization rate for *trans*-$[Co(tn)_2(OH_2)_2]^{3+}$ is 10^3 times greater than that of the *trans*-$[Co(en)_2(OH_2)_2]^{3+}$ complex (see 1.8).

The equilibrium constant, K_{isom} (= kt/kc), was measured at two pH values, viz., pH 3.3 and 7.0, for the reaction

$$trans\text{-}[Co(en)_2(OH_2)OSeO_2H]^{2+} \underset{\longleftarrow}{\xrightarrow{K_{isom}}} cis\text{-}[Co(en)_2(OH_2)OSeO_2H]^{2+}$$

K_{isom} = 13.5 ± 1 at pH 3.3 (25°, 1 M ionic strength);

K_{isom} = 70 ± 20 at pH 7.0 (25°, 1 M ionic strength).

A qualitative analysis of the equilibrium properties for the analogous *tn* system indicated that the *cis*-selenito complex was again strongly predominant and similar K_{isom} values would be expected to those quoted above.

The *cis*-selenito products are favoured over the entire pH range although K_{isom} progressively decreases with decreasing pH. The increased stability of the *cis*-selenito complex relative to the *trans*-isomer can probably be attributed to the presence of hydrogen bonding in the *cis*-isomer, leading to the formation of a pseudo six-membered ring:

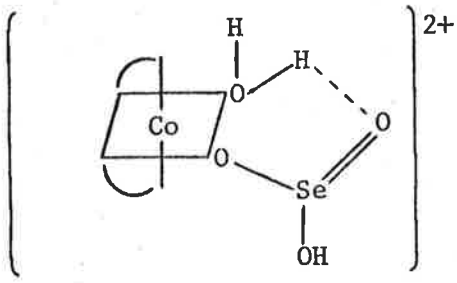

This supposition is strongly supported by the respective $\Delta V^{\ddagger}$ values at pH 3.3, $\Delta V^{\ddagger}_{tc}$ = +7.5 $cm^3\ mol^{-1}$ and $\Delta V^{\ddagger}_{ct}$ = + 12.7 $cm^3\ mol^{-1}$, for the *trans* → *cis* and *cis* → *trans* isomerization pathways in the case of the *en* system.[23] The higher $\Delta V^{\ddagger}_{ct}$ value has been interpreted as arising from the necessity to achieve virtually complete removal of the aquo-ligand in the transition state leading to *cis* → *trans* isomerization, whereas the lower $\Delta V^{\ddagger}_{tc}$ value is taken as an indication that only stretching of the metal-water bond is required in the transition state leading to *trans* → *cis* isomerization. The difference between the two $\Delta V^{\ddagger}$ values $\Delta(\Delta V^{\ddagger})$ =

+ 5.2 $cm^3\ mol^{-1}$, thus represents the additional volume increase required to overcome hydrogen bonding.

The increase in the proportion of the *trans*-isomer at low pH is presumably a reflection of the increasing importance of acid hydrolysis which would make the formation of the *trans*-selenito complex statistically more favourable than that of the *cis*-selenito complex.

4.9 Summary

When *cis* and *trans* diaquo complexes are reacted with selenite, there is a two-step reaction sequence

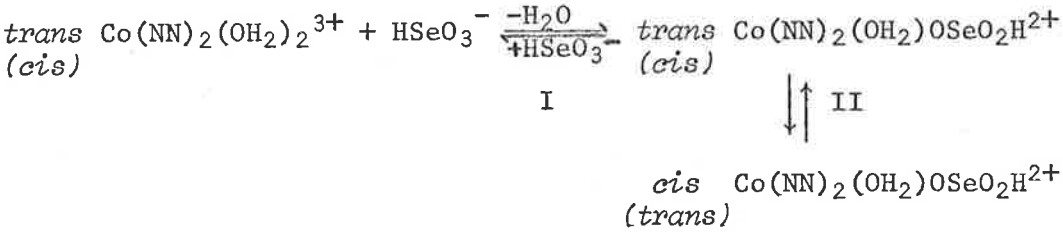

Step I, which is substitution by selenite, is up to 10^5 times faster than step II, which is isomerization to an equilibrium mixture of *cis* and *trans* isomers, when NN = *en* and up to 10^2 times faster when NN = *tn*.

The substitution by selenite occurs with half-times of seconds or less and is fastest around pH 3 - 4. The slower isomerization reaction has its maximum rate in the neutral pH region.

Whereas step I is virtually unaffected by ring size (e.g. NN = *en* or *tn*), step II is markedly accelerated with 6-membered *tn* rings as opposed to 5-membered *en* rings, the difference in the respective isomerization rates being of the order of 10^3.

Step I is thought to proceed by associative attack on the Se(IV) centre by an aquo-ligand, resulting in Se-O bond breakage in the rate-determining step. Step II is proposed as proceeding by dissociative release of water from the selenito complex involving Co-O bond cleavage in the rate-determining step.

Formation of the *cis*-selenito product is favoured over the *trans* isomer for the entire pH range 1 - 12 because of the added

stability imparted to the *cis* complex through intramolecular hydrogen bonding.

References to Chapter 4.

1. S.F. Lincoln and D.R. Stranks, *Aust. J. Chem.*, 1968, 21, 1745.
2. T.A. Beech, N.C. Lawrence, and S.F. Lincoln, *in press.*
3. H. Taube and F.A. Posey, *J. Am. Chem. Soc.*, 1953, 75, 1463.
4. R.S. Murray, *Ph.D. Thesis, University of Adelaide*, 1967.
5. D.R. Stranks and J.K. Yandell, *J. Phys. Chem.*, 1969, 73, 840.
6. N.F. Hall and O.R. Alexander, *J. Am. Chem. Soc.*, 1940, 62, 3455.
7. A.I. Brodskii and N.A. Vysotzkaya, *Zh. Fiz. Kim.*, 1958, 32, 1521.
8. A.T. Davies, *Ph.D. Thesis, University of Melbourne*, 1971.
9. J.O. Edwards, *"Inorganic Reaction Mechanisms", W.A. Benjamin Inc., New York*, 1965.
10. A. Okumura and N. Okazaki, *Bull. Chem. Soc. Jap.*, 1973, 46, 1084.
11. N. Vanderhoek, *Honours Report, University of Adelaide*, 1969.
12. P.A. Tregloan and G.S. Laurence, *J. Scient. Instrum.*, 1965, 42, 869.
13. J.M. Sturtevant, *"Rapid Mixing and Sampling Techniques in Biochemistry", ed. B. Chance, New York Acad. Press.*, 1964, 89.
14. P.R. Sibly, *Honours Report, University of Adelaide*, 1969.
15. W. Kruse and H. Taube, *J. Am. Chem. Soc.*, 1961, 83, 1280.
16. F. Basolo and R.K. Murmann, *Inorg. Synthesis*, 4, 171.
17. T.W. Swaddle and D.R. Stranks, *J. Am. Chem. Soc.*, 1972, 94, 8357.
18. L. Barcza and L.G. Sillén, *Acta. Chem. Scand.*, 1971, 25, 1250.
19. J. Bjerrum and S.E. Rasmussen, *ibid.*, 1952, 6, 1265.
20. I.R. Jonasson, *unpublished data.*
21. F. Basolo and R.G. Pearson, *"Mechanisms of Inorganic Reactions", 2nd edn., John Wiley and Sons Inc., New York*, 1967, 33.

22. R. Arnek and L. Barcza, *Acta. Chem. Scand.*, 1972, 26, 1.

23. N. Vanderhoek, *Ph.D. Thesis, University of Adelaide*, 1973.

24. A.D. Fowless, *Honours Report, University of Adelaide*, 1969.

25. J.A. Friend and E.K. Nunn, *J. Chem. Soc.*, 1958, 1567.

Chapter 5 Selenite Substitution With Sterically-Hindered Aquo-Ligands.

5.1 Introduction

The previous chapters (2 - 4) have dealt with the substitution reactions between Se(IV) and relatively inert octahedral aquo-complexes. As stated in chapter 1, it was decided to conclude the overall investigation into selenite substitution by making a preliminary survey of selenito formation with two other aquo-complexes of quite different stereochemical environments, viz., the 5-coordinate trigonal-bipyramidal nickel(II) complex, $[Ni(Me_6tren)\ OH_2]^{2+}$, and the macrocyclic cobalt(III) corrinoid, $C_{62}\ H_{90}\ N_{13}\ O_{15}\ P\ Co$ (aquocobalamin or Vitamin B12a).

5.1.1 $[Ni(Me_6tren)OH_2]^{2+}$

The ligand, Me_6tren, $[N(CH_2CH_2N(CH_3)_2)_3]$, forms high spin complexes of divalent first row transition metals and has little tendency to ~~π~~ π-bond with metals. The 5-coordination appears to be rigidly maintained by the steric crowding about the $N(CH_3)_2$ groups which effectively prevents the possibility of attaining a 6-coordinate configuration. The structure of the $[Ni(Me_6tren)NCS]^+$ species is shown below.

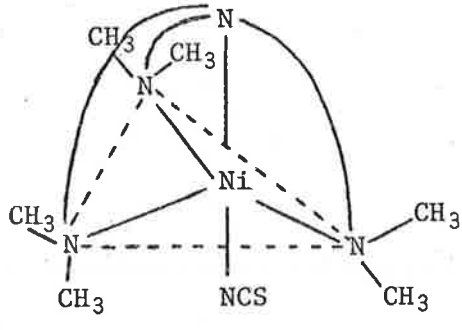

This can be contrasted with the complex, $[Ni(tren)(SCN)_2]^0$, which has a *cis*-octahedral configuration and a visible spectrum which differs markedly ~~form~~ from the more strongly absorbing 5-coordinate $[Ni(Me_6tren)\ OH_2]^{2+}$ complex.

West[1] has recently studied the solvent exchange reactions of $[Co(tren)CH_3CN]^{2+}$ and $[Co(Me_6tren)CH_3CN]^{2+}$. He found that the more loosely 5-coordinate tren complex exhibited a similar lability to other solvated Co(II) species but that the more rigidly 5-coordinate Me_6tren complex underwent solvent exchange at a rate which was too slow to measure on the N.M.R. time scale. The analogous solvent exchange process for the $[Ni(Me_6tren)CH_3CN]$ complex was also too slow to be measured by N.M.R.

This unusual kinetic behaviour prompted Weatherburn[2] to carry out some preliminary experiments on the substitution reactions of the Ni(II), Co(II), and Cu(II) Me_6tren complexes with Br^-, Cl^-, and SCN^-. These reactions could be followed in the visible region using the stopped-flow method and the reaction half-times at 25° were in the 100 msec range.

Since no data has yet been published on the substitution reactions of Me_6tren complexes, it was decided to repeat the reactions with Cl^- and Br^- for the $[Ni(Me_6tren)OH_2]^{2+}$ complex in these laboratories and to also include a study of the substitution reaction with the azide ion, N_3^-. This would then allow a comparison to be made between the substitution reactions of these representative nucleophiles and the substitution reaction with selenite.

5.1.2 Aquocobalamin

The structure of the aquocobalamin molecule is shown in Fig. 5.1. Chelation with the benzimidazole side chain prevents the formation of 2:1 complexes. The cobalt(III) ion is in an octahedral environment, being surrounded by 5 nitrogen atoms and 1 oxygen atom. Thus the macrocyclic aquocobalamin compound may be compared with the kinetically inert model cobalamin complexes, iodo- and nitroaquobis(dimethyl-glyoximato) cobalt(III), where the cobalt(III) ion is in a similar octahedral environment. The structures of these model cobalamin complexes are shown below.

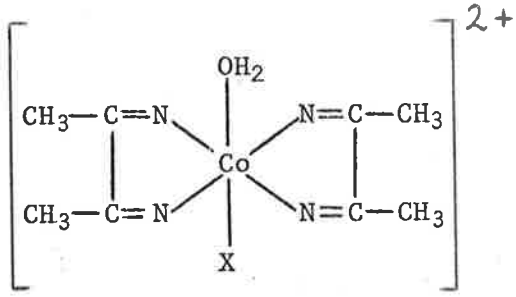

X = I^- or NO_2^-

Although the cobalt(III) ion is considered to be 6-coordinate in aquocobalamin, it seems likely that the sterically hindered aquo-ligand is only weakly bound to the metal centre. Recent studies[3] on the substitution reactions of aquocobalamin with SCN^-, SO_3^{2-}, $S_2O_3^{2-}$, NCO^-, N_3^-, I^-, and Br^- have indicated that the aquo-ligand is particularly labile towards substitution. The dissociation rate constants for the reactions

$$L + CBM - OH_2 \underset{k_d}{\overset{k_f}{\rightleftharpoons}} CBM - L + H_2O \qquad 5.1$$

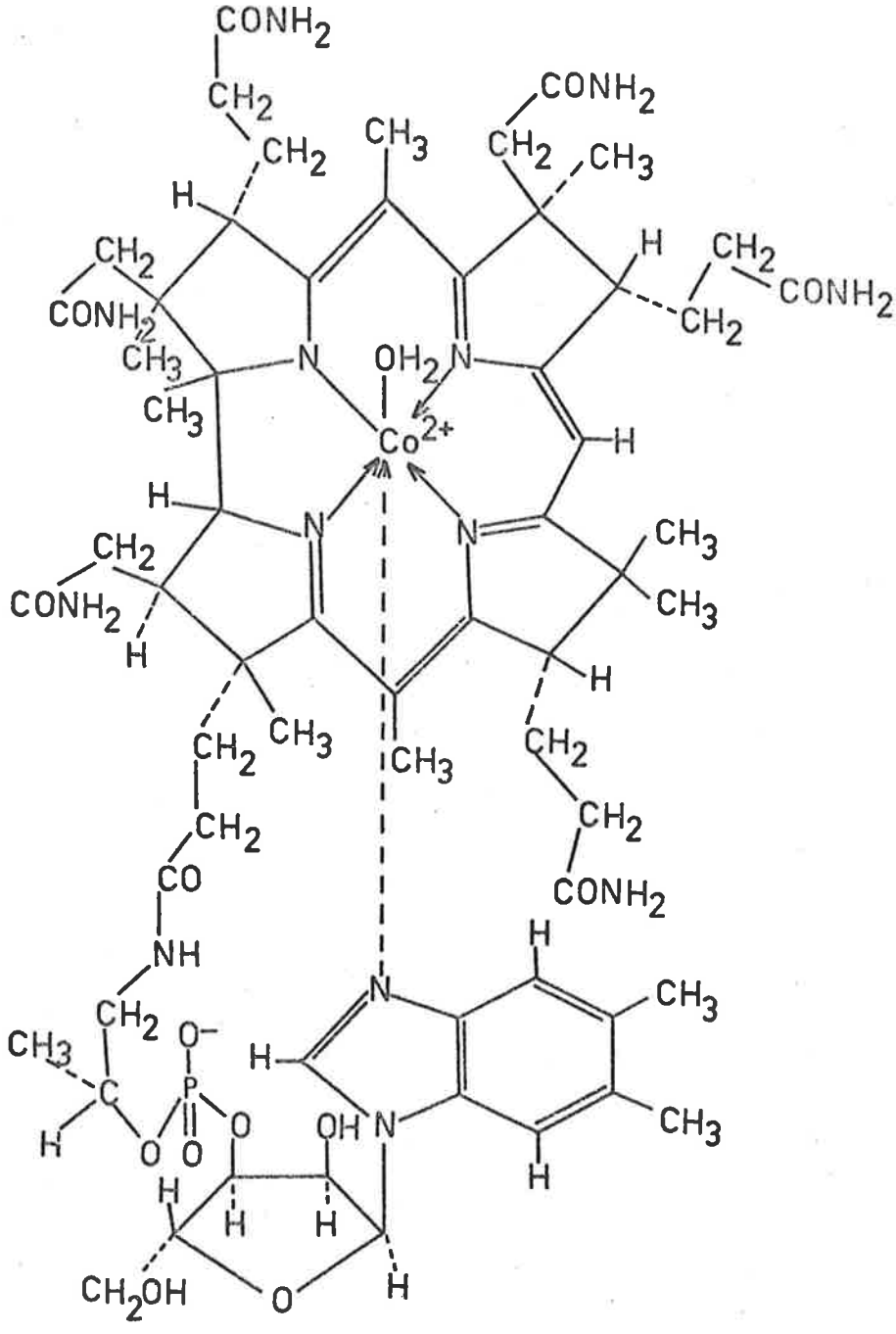

Fig. 5.1 Structure of Aquocobalamin (Vitamin B12a).

varied from 5.9×10^{2} - < 10^{-5} sec^{-1} at 25°. When L = HSO_3^-, the reaction pathway was found to be

$$HSO_3^- + CBM - OH_2 \underset{k_d^*}{\overset{k_f}{\rightleftharpoons}} CBM - SO_3^{2-} + H_3O^+ \qquad 5.2$$

No significant change in the anation rate was found on varying the pH between 3.7 and 5.8, indicating that kinetic paths involving H_2SO_3 or SO_3^{2-} are unimportant. This can be compared with the similar result obtained for the anation reactions of cobalt(III) aquo-complexes with $HSeO_3^-$, as described in chapter 4.

In view of the sterically hindered nature of the aquo-ligand in aquocobalamin and the fact that selenite substitution with aquo-complexes appears to proceed through nucleophilic attack of the aquo-ligand at Se(IV), the reaction of aquocobalamin with selenite was thought to be of particular interest.

5.2 *Experimental*

5.2.1 *Materials*

A. $[Ni(Me_6tren)ClO_4]ClO_4$ was prepared by the method of Ciampolini and Nardi.[4] In aqueous solution, this species generates $[Ni(Me_6tren)OH_2]^{2+}$ which has a pKa = 9.53 at 25°.[5]

Anhydrous LiBr(B.D.H.) and LiCl(B.D.H.) were dried in vacuo at 50° and used without further purification.

Sodium azide (B.D.H.) was recrystallized from concentrated aqueous solution and dried *in vacuo* at 50°.

Sodium selenite (B.D.H.) was purified and dried as previously described.

Anhydrous $LiClO_4$ (G.F.S.) and $NaClO_4.H_2O$ (Fluka) were used without further purification.

All solutions were prepared from doubly distilled water.

B. Crystalline hydroxocobalamin chloride (Glaxo) was the source of aquocobalamin. A stock solution was made up by dissolving approximately 1 g. of the chloride in 1 litre of 0.01 M $HClO_4$. The absorption at 350 nm was used to determine the concentration of this stock solution.[6]

5.2.2 *Kinetics*

A. $[Ni(Me_6tren)OH_2]^{2+}$

All substitution reactions were followed in the visible region using the stopped-flow apparatus previously described. In order to maintain pseudo first order reaction conditions the ligand

concentration after mixing was at least 10 times greater than that of the aquo complex, this being 5×10^{-3} M. The ligand concentration was varied up to 0.5 M.

The pH remained constant at 8.40 ± 0.1 before and after reaction over the whole range of ligand concentration for the Br^-, Cl^-, and N_3^- reactions without the need for an external buffer. In the case of the selenite reaction, the self-buffering property of the ligand itself was used to maintain the pH at 8.55 ± 0.05 over the entire Se(IV) concentration range. The original buffer used, Trizma Base, was discarded when it was found to react with the $[Ni(Me_6tren)OH_2]^{2+}$ complex over a relatively short period of time.

The ionic strength was adjusted to 1 M with the appropriate metal perchlorate salt.

All kinetic runs were performed at a temperature of 25.2 ± 0.1°.

B. *Aquocobalamin*

Preliminary kinetic investigations were performed in the U.V.-visible region on a Unicam SP 800 scanning spectrophotometer over the wavelength range 250 - 650 nm and a pH range 1-10. Further experiments were then conducted on the stopped-flow apparatus previously described at pH ∿ 3 and pH ∿ 10 over the wavelength range 250 - 850 nm. In all cases, [aquocobalamin] = 1.4×10^{-4} M, [Se(IV)] = 1.4×10^{-2} M and μ = 1 M, adjusted with perchlorate ion. No external buffer was used, the pH of the reactant solutions being adjusted prior to mixing.

5.3 *Results for* $[Ni(Me_6tren)OH_2]^{2+}$ *System*

5.3.1 *Nature of Reaction Products*

The visible spectra of the $[Ni(Me_6tren)OH_2]^{2+}$ complex with Cl^-, Br^-, and N_3^- ions are shown in Fig. 5.2. In each case there is a slight increase in optical absorbance and shift away from λ_{max} on addition of the anion. Kinetic runs were performed at 435, 440, and 410 nm for the Cl^-, Br^-, and N_3^- ions, respectively, corresponding with the increase in optical absorbance from reaction to product. Under the reaction conditions employed in the kinetic study ([anion] $\geq$ 10 x $[Ni(Me_6tren)OH_2^{2+}]$), substitution proceeds virtually to completion. The spectra obtained from the reactions of Cl^-, Br^-, and N_3^- with $[Ni(Me_6tren)OH_2]^{2+}$ are consistent with the formation of 5-coordinate chloride, bromide, and azide substituted Me_6tren complexes.

The visible spectra of the $[Ni(Me_6tren)OH_2]^{2+}$ complex with $HSeO_3^-$ and Trizma Base are shown in Fig. 5.3. There is a large decrease in optical absorbance around 410 nm with the $HSeO_3^-$ ion and an even larger decrease in the same region with Trizma Base, corresponding to a visually detectable colour change from bright green to very pale blue-green. The spectra of the $HSeO_3^-$ and Trizma Base products are characteristic of 6-coordinate complexes.

5.3.2 *Kinetics of Substitution Reactions*

The rate data at 25° obtained for the substitution of $[Ni(Me_6tren)OH_2]^{2+}$ with Y^-, where Y = Cl, Br, N_3, and $HSeO_3$, are shown in Table 5.1. The data for the Cl^- substitution are compared with the unpublished data of Weatherburn.[2]

Fig. 5.3 Visible Spectra of (A) $[Ni(Me_6tren)OH_2]^{2+}$, (B) with $HSeO_3^-$, (C) with Trizma Base.

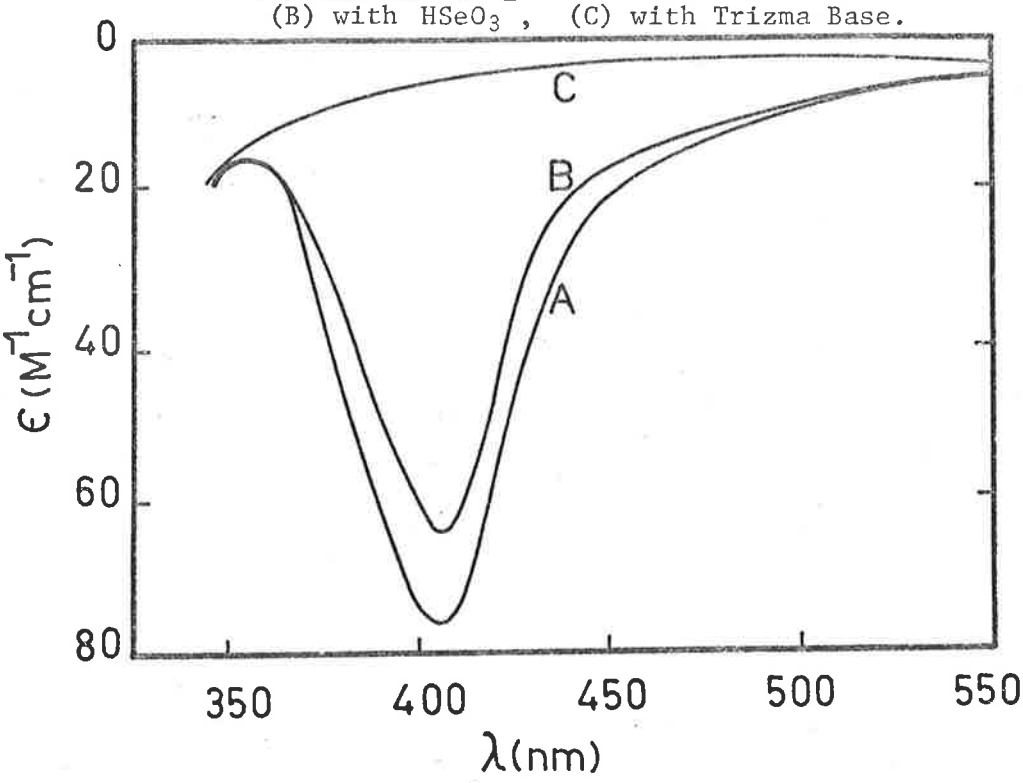

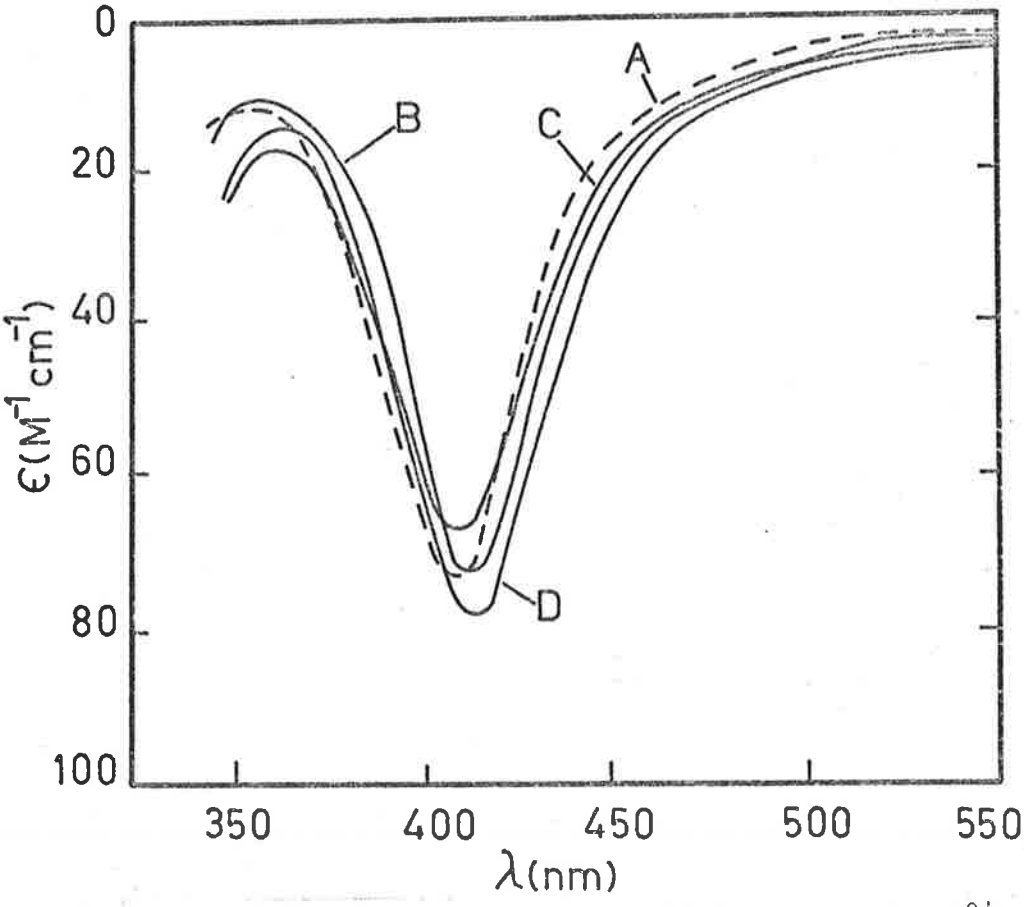

Fig. 5.2 Visible Spectra of (A)$[Ni(Me_6tren)OH_2]^{2+}$, (B) with Cl^- (C) with Br^-, (D) with N_3^-.

Table 5.1 Rate Data for Substitution of $[Ni(Me_6tren)OH_2]^{2+}$ by Y^- at 25°.

$[Y^-]$ (M)	k_{obs} (sec^{-1})			
	Cl^-	Br^-	N_3^-	$HSeO_3^-$
0.05	(8.0) 5.52 ± 0.20	6.25 ± 0.19	27.2 ± 0.6	0.100 ± 0.001
0.1	(8.8) 6.60 ± 0.15	6.57 ± 0.21	32.4 ± 0.6	0.152 ± 0.015
0.2	(8.6) 7.87 ± 0.21	7.46 ± 0.28	43.0 ± 1.5	0.270 ± 0.009
0.3	(9.4) 8.83 ± 0.15	8.76 ± 0.21	52.5 ± 2.8	0.400 ± 0.017
0.4	(10.5)10.1 ± 0.3	9.05 ± 0.15	66.4 ± 2.5	0.506 ± 0.027
0.5	(11.0)11.4 ± 0.4	10.1 ± 0.1	74.6 ± 3.3	0.607 ± 0.022

($[Ni(Me_6tren)OH_2^{2+}] = 5 \times 10^{-3}$ M; μ = 1.0 M, ClO_4^- medium; T = 25.2 ± 0.1°; pH (Cl^-) = 8.40 ± 0.10, pH(Br^-) = 8.35 ± 0.05, pH (N_3^-) = 8.45 ± 0.07, pH($HSeO_3^-$) = 8.55 ± 0.05).

( ) data in brackets from ref. 2.

The plots of k_{obs} vs $[Y^-]$, shown in Fig. 5.4, are linear (slope = k_2) with positive intercepts (= k_1) which differ with the nature of the incoming nucleophile. In order to test whether a D-mechanism was operating, i.e.

$$k_{obs} = \frac{k_1 k_2 [Y^-]}{1+k_{-1}[Y^-]} \quad 5.3 \qquad \text{or} \quad \frac{1}{k_{obs}} = \frac{1}{k_1 k_2 [Y^-]} + \frac{k_{-1}}{k_1 k_2} \quad 5.4$$

$1/k_{obs}$ was plotted as a function of $1/[Y^-]$, as shown in Fig. 5.5. If a D-mechanism is operative such a plot should be linear with an intercept = $k_{-1}/k_1 k_2$ and a slope = $1/k_1 k_2$. The non-linear plots obtained indicate that a D-mechanism is not operative and that rather the kinetics are consistent with the rate law

$$k_{obs} = k_1 + k_2[Y^-] \quad 5.5$$

where k_1 and k_2 are both dependent on the nature of the nucleophile, Y^-. Table 5.2 summarizes the k_1 and k_2 values derived from the plots in Fig. 5.4.

In the case of azide, the initial fast reaction (step I) was followed by a slower reaction (step II). The k_1 and k_2 values listed in Table 5.2 for azide refer to step I. At 25° and $[N_3^-]$ = 0.4 M, k_{obs} = 66.4 ± 2.5 sec^{-1} for step I and k_{obs} = 0.335 ± 0.015 sec^{-1} for step II. For both steps the optical absorbance changes are in the same sense (step I contributes ∿ 90% towards the overall optical absorbance change) with the spectrum of the product corresponding to a 5-coordinate complex.

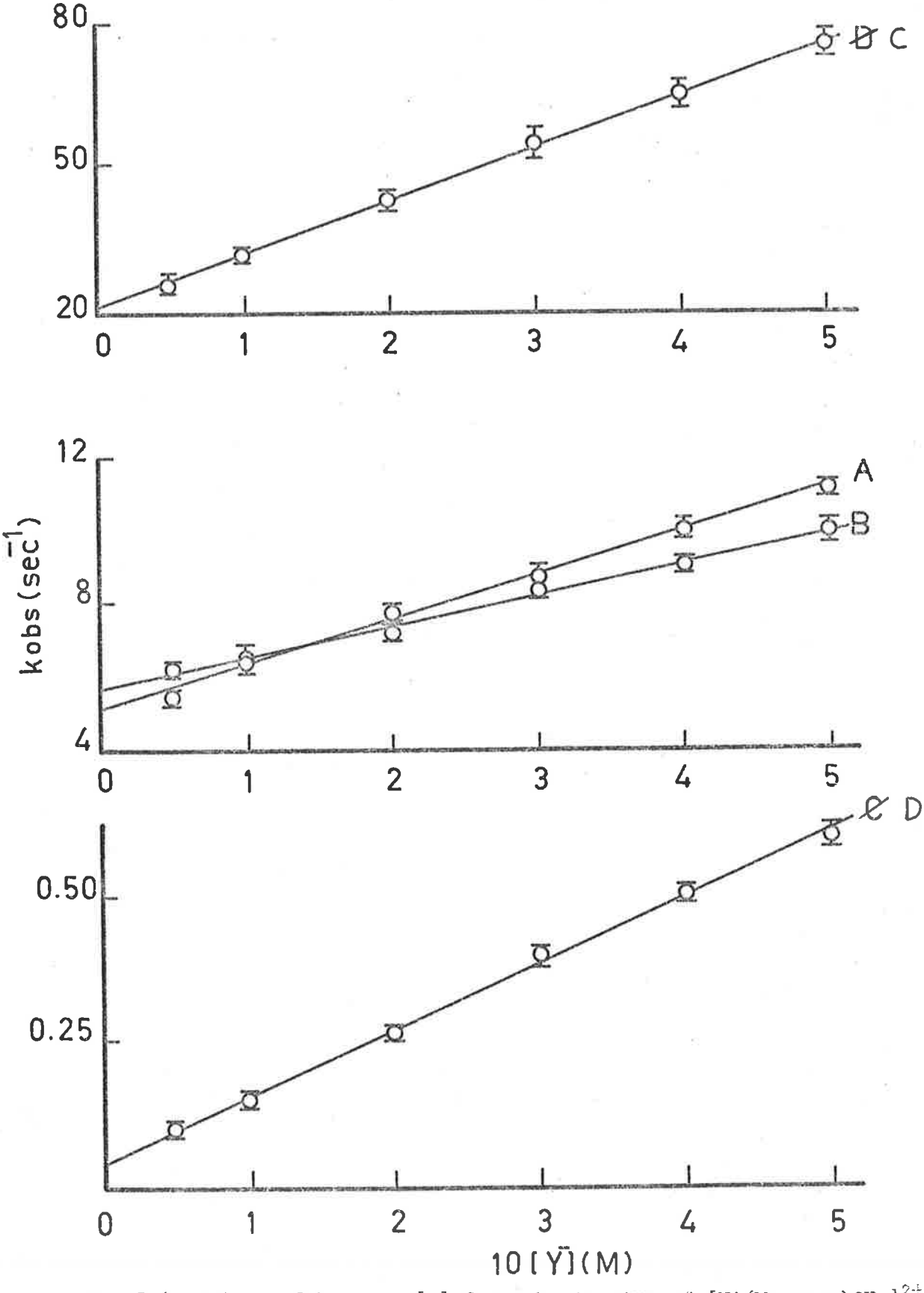

Fig. 5.4 Plots of k_{obs} vs [Y] for Substitution of $[Ni(Me_6tren)OH_2]^{2+}$

(A) $Y = Cl^-$, (B) $Y = Br^-$, (C) $Y = N_3^-$, (D) $Y = HSeO_3^-$.

Fig. 5.5 Plots of $1/k_{obs}$ vs $1/[Y]$ for Substitution of $[Ni(Me_6tren)OH_2]^{2+}$ (A) $Y = Cl^-$, (B) $Y = Br^-$, (C) $Y = N_3^-$, (D) $Y = HSeO_3^-$.

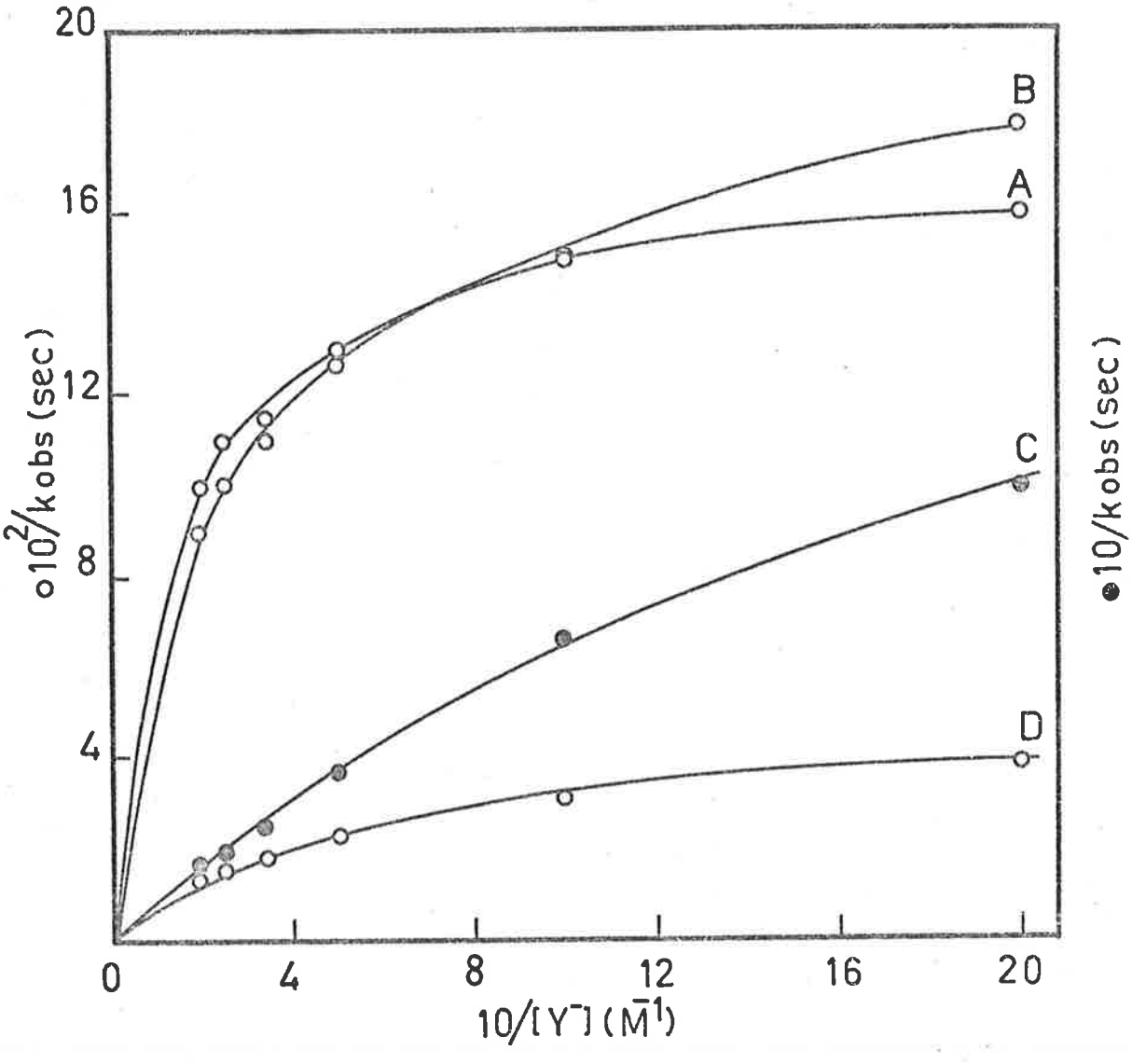

Table 5.2 k_1 *and* k_2 *Terms for* $[Ni(Me_6tren)OH_2]^{2+} + Y^-$

Anion	$k_1(sec^{-1})$	$k_2(M^{-1}sec^{-1})$
Cl^-	5.3 ± 0.3	11.6 ± 1.0
Br^-	5.8 ± 0.3	8.6 ± 0.6
N_3^-	21 ± 1	110 ± 15
$HSeO_3^-$	0.04± 0.01	1.2 ± 0.1

A single kinetic run was performed for $Y^- = SCN^-$. At 25°, $k_{obs} = 34.5 \pm 2.5\ sec^{-1}$, for $[Ni(Me_6tren)OH_2^{2+}] = 5 \times 10^{-3}$ M, $[SCN^-] = 5 \times 10^{-2}$ M, and $\mu = 1.0$ M, adjusted with perchlorate ion. The corresponding value for N_3^- is $k_{obs} = 27.2 \pm 0.6\ sec^{-1}$. A detailed kinetic analysis was prevented because of the rapid crystallization of the thiocyanato complex, presumably as the perchlorate salt, $[Ni(Me_6tren)NCS]ClO_4$.

In the case of $HSeO_3^-$ and Trizma Base only a single slow step could be detected over the entire wavelength range used, although a search was made for a faster step. If such a step occurs it must have a reaction half-time of $t_{\frac{1}{2}} < 5$ msec. A single run was performed for the Trizma Base reaction. At 25°, $t_{\frac{1}{2}} \sim 50$ secs, for $[Ni(Me_6tren)OH_2^{2+}] = 5 \times 10^{-3}$ M, [Trizma Base] = 0.5 M and $\mu = 1.0$ M, adjusted with perchlorate ion. The corresponding value for $HSeO_3^-$ is $t_{\frac{1}{2}} = 1.1$ secs ($k_{obs} = 0.607 \pm 0.022\ sec^{-1}$).

5.4 Discussion

The Cl^- and Br^- substitution reactions follow a simple one-step pathway and the kinetics are consistent with the observed rate law 5.5 where both k_1 and k_2 are dependent on the nature of Y. For octahedral metal complexes in oxidation state II, a single (dissociative) term $k_2[Y]$ is common with k_2 independent of the nature of Y. For square planar complexes, a two-term rate law is common but the k_1 term is characteristic of the solvent path and independent of the nature of Y. The two-term rate law 5.5, with k_1 and k_2 dependent on the nature of Y, has also been found for substitution reactions involving other 5-coordinate metal complexes.

Pearson et. al.[7] studied the rates of substitution in methanol for the 5-coordinate Pt(II) complexes, [Pt X(QAS)]X, where X = Cl^-, Br^-, I^-, SCN^-, and QAS = $(o\text{-}Ph_2As.C_6H_4)_3As$. They attributed the observed two-term rate law 5.5 to a mechanism involving parallel bimolecular attack by the ligand on the complex and an ion-pair of the complex. In order to account for the dependence of the k_1 term on the nature of Y, they examined the plots of k_{obs} vs [Y] at low [Y] and found that there was no longer a linear relation but that the plots curved away to zero. The curved portion of the plot was then identified as the reaction between the complex and the nucleophile and the linear region as the reaction between an ion-pair of the complex and the nucleophile. At high [Y], the rate law then becomes

$$k_{obs} = kc - k_{IP}/K + k_{IP}[Y] \qquad 5.6$$

where K is the equilibrium constant for ion-pairing and kc and k_{IP} are the respective rate constants for the reaction of Y with complex and ion-pair. This mechanism ignores any possible solvent path and proposes a 6-coordinate transition state. The present studies, however, give no evidence for ion-pairing effects in the $k_2[Y]$ term in that even at 0.5 M [Y], no significant deviation from linearity is observed, as can be seen from Fig. 5.4.

Morgan and Tobe[8] have studied the substitution reactions

$$[MX(Qas)]^+ + Y^- \xrightarrow{MeOH} [MY(Qas)]^+ + X^- \qquad 5.7$$

(where M = Pt; X = Cl^-, Br^-; Y = NO_2^-, N_3^-, NCS^-, I^-, $SC(NH_2)_2$, $P\emptyset_3$; M = Pd; X = Cl^-; Y = NO_2^-; Qas = $(o\text{-}Me_2As\ C_6H_4)_3As$).

They question the validity of the ion-pair pathway proposed by Pearson et.al. and suggest an alternative mechanism involving a planar 4-coordinate intermediate in which one or two of the four arsenics of the quadridentate ligand are temporarily uncoordinated. Their reaction scheme is shown below.

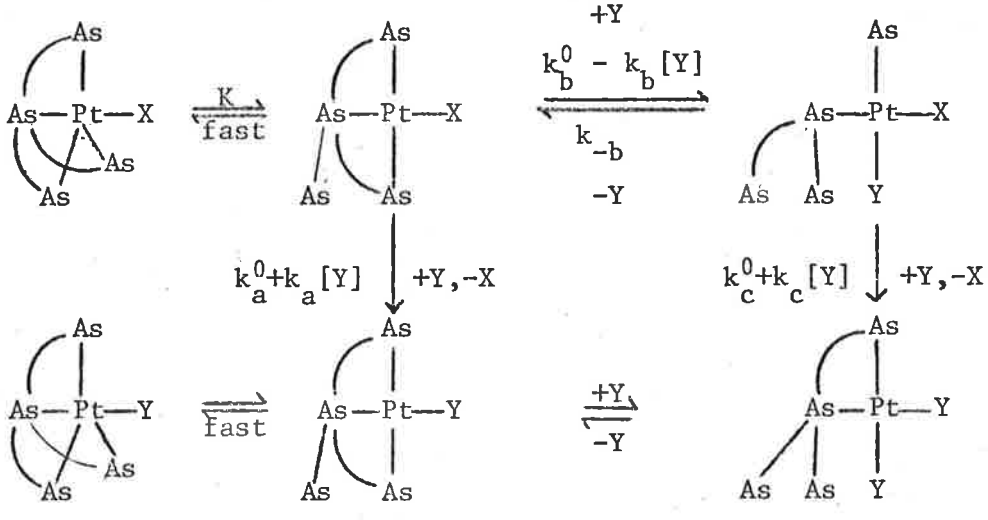

Assuming, (1) K << 1 so that only a small fraction of the complex is in the 4-coordinate form, (2) the square planar substitution follows a two-term rate law, and (3) the replacement of the axial X is irreversible, they define a rate expression which, when $k_c[Y] >> k_{-b} + k_c^0$, simplifies to

$$k_{obs} = K\{(k_a^0 + k_b^0) - k_b k_{-b}/k_c\} + (k_a + k_b)K[Y] \qquad 5.8$$

Thus k_2 from eq. 5.5 can now be equated with $(k_a + k_b)K$, and k_1 with $K\{(k_a^0 + k_b^0) - k_b k_{-b}/k_c\}$. For the k_1 expression, the first term in the brackets represents the solvolytic reactivity of the substrate and is independent of Y, but the second term contains three Y-dependent constants thus making k_1 dependent on Y.

A similar type of mechanism is envisaged for the substitution of $[Ni(Me_6tren)OH_2]^{2+}$ by Y^-, viz.,

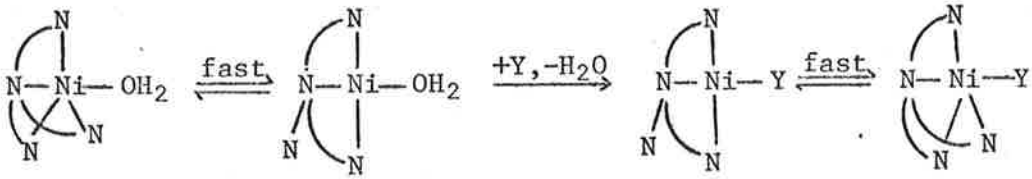

The azide reaction is complicated by the emergence at high N_3^- concentration of a slower second step after the initial fast reaction step. Lincoln[9] has found from equilibrium studies on the $[Cu(Me_6tren)N_3]^+$ and $[Cu(Me_6tren)NCS]^+$ ions that two species are produced in both systems even though both are 5-coordinate and have the same stoichiometry. Also, variation of the $[N_3^-]/[ClO_4^-]$ ratio in the azide system causes a shift in the conformational equilibrium of the Me_6tren ligand. The reason that the conformer equilibrium

arises in the case of N_3^- (and SCN^-) may be attributed to the much faster substitution rates (step I) with N_3^- and the subsequent conformer rearrangement reaction (step II) cannot keep pace, as it presumably can for the slower Cl^- and Br^- reactions.

Although only one reaction step was kinetically detected for the $HSeO_3^-$ reaction, it seems likely that there is a two-step process leading to the formation of a 6-coordinate selenito complex. The first step would then be substitution (step I) to form a monodentate selenito product followed by ring closure (step II) to form a bidentate selenito-complex. The fact that there was no "instantaneous" increase in optical absorbance (corresponding to 5-coordinate complex formation) on commencement of a kinetic run indicates that step I is slow and step II is fast. This means that the stationary concentration of the 5-coordinate monodentate selenito intermediate is very low and hence no spectral effect is observed. As fast as this intermediate is formed it is converted to the 6-coordinate bidentate selenito product. The k_1 and k_2 values listed in Table 5.2 for $HSeO_3^-$ can now be identified with step I. Since $t_{\frac{1}{2}} < 5$ msec for step II, $k_{II} \geq 2 \times 10^4$ sec^{-1}, for ring-closure. The proposed reaction scheme for $HSeO_3^-$ substitution is shown below.

$$[Ni(Me_6tren)OH_2]^{2+} \xrightarrow[\text{slow}]{I} [Ni(Me_6tren)OSeO_2] \xrightarrow[\text{fast}]{II} Me_6tren \quad Ni\begin{smallmatrix}O\\ \diagdown\\ \diagup\\ O\end{smallmatrix}Se = O$$

This mechanism is consistent with the observed rate law 5.5.

It is interesting to note that, unlike the substitution reactions of $[Co(NH_3)_5OH]^{2+}$ and $[Rh(NH_3)_5OH]^{2+}$ with selenite around

pH 8, there is no evidence of any dependence of the substitution rate for $[Ni(Me_6tren)OH_2]^{2+}$ on $[Se(IV)]^2$, even up to [Se(IV)] = 0.5 M, at the pH (8.55 ± 0.05) used for the kinetic investigation.

A similar mechanism can also be tentatively assigned to the Trizma Base substitution reaction. This means that Trizma Base would then be acting as a bidentate ligand coordinating to the metal centre through either two oxygen atoms, as for selenite, or one oxygen and a nitrogen atom. Gillard[10] has proposed the latter case for the structure of the Trizma Base complex, $[Co(en)_2T\text{-}B]^{2+}$, which is shown below.

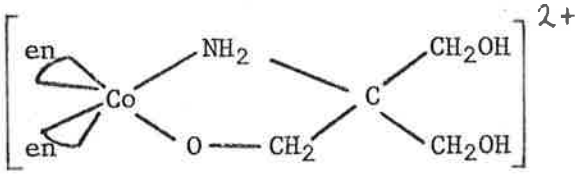

Similar octahedral Ni(II) complexes, such as $[Ni(triol)(CH_3CN)_3]^{2+}$, where triol = 1,1,1- trimethylolethane, and $[Ni(diamol)(CH_3CN)_3]^{2+}$, where diamol = 1,1-dimethylamino-1-methylolethane, have recently been prepared by West.[1] The structures of these complexes are shown below.

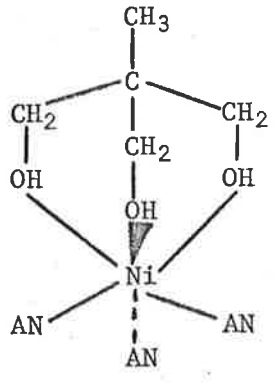

$[Ni(triol)(AN)_3]^{2+}$

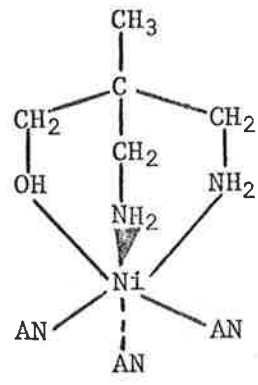

$[Ni(diamol)(AN)_3]^{2+}$

AN = CH_3CN (acetonitrile)

The following structure can therefore be proposed for the Trizma Base complex with $[Ni(Me_6tren)OH_2]^{2+}$.

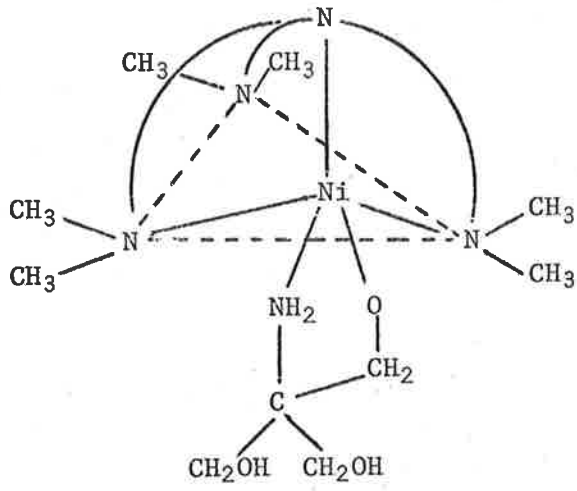

5.5 *Conclusion*

The substitution reactions of $[Ni(Me_6tren)OH_2]^{2+}$ with Cl^-, Br^-, N_3^- (and SCN^-), $HSeO_3^-$, and Trizma Base, all appear to have kinetics which are consistent with the two-term rate law

$$k_{obs} = k_1 + k_2[Y]$$

Although Cl^-, Br^-, and N_3^- (also SCN^-) form the anticipated 5-coordinate products, the potential bidentates, selenite and Trizma Base, have the unusual property of converting the original 5-coordinate Me_6tren species into an apparently 6-coordinate product.

It will be necessary to evaluate activation parameters before the differences in k_1 and k_2 for different nucleophiles can be discussed in detail. A pH study of the selenite substitution reaction and the isolation and characterization of products are also required. To test whether the apparent 6-coordinate species are in fact only intramolecular hydrogen bonded forms without genuine 6-coordination, the reactions of other potential bidentate ligands, such as AsO_4^{3-}, should be studied.

5.6 Results and Discussion for the Aquocobalamin System.

Only a very slight shift in λ_{max} was detected spectrophotometrically on the addition of excess selenite to aquocobalamin in aqueous solution at room temperature. There was no change in the intensity of λ_{max}. No reaction was observed in the millisec-second time range using stopped-flow kinetics.

A qualitative investigation was then performed in which aquocobalamin was mixed with a variety of different ligands including other oxyanions. There was no visually detectable reaction for those ligands which coordinate through oxygen, viz., selenite, selenate, sulphate, phosphate, arsenate, oxalate, carbonate, nitrate, and chromate.

Reactions were immediately observable for nitrogen bonding ligands such as nitrite, azide, and thiocyanate; sulphur bonding ligands such as sulphite and dithionite; halogen bonding ligands, Cl^- and Br^-; and carbon bonding ligands such as cyanide. As mentioned in the introduction, some of these reactions have already been kinetically investigated.

It would appear from the above evidence that the formation constants for coordination of O-bonded ligands are very low or that their coordination has little spectral influence on the cobalamin moiety.

References to Chapter 5.

1. R.J. West, *Ph.D. Thesis, University of Adelaide,* 1973.
2. D. Weatherburn, *unpublished data.*
3. D. Thusius, *J. Am. Chem. Soc.,* 1971, 93, 2629.
4. M. Ciampolini and N. Nardi, *Inorg. Chem.,* 1966, 1, 41.
5. J.H. Coates, *private communication.*
6. J.M. Pratt and R.G. Thorp, *J. Chem. Soc.,* 1966, 187.
7. R.G. Pearson, M.M. Muir, and L.M. Venanzi, ibid., 1965, 5521.
8. T.D.B. Morgan and M.L. Tobe, *Inorg. Chim. Acta.,* 1971, 5, 563.
9. S.F. Lincoln, *private communication.*
10. D.E. Allen, D.J. Baker, and R.D. Gillard, *Nature,* 1967, 214, 906.

Appendix I Stopped-Flow Apparatus

The general layout of the mechanical section of the apparatus is shown on the following pages. This section incorporates the storage and drive-syringes which are linked through two-way taps in block 1, the mixing chamber (blocks 2a, b, c, d, e), the cell-block (block 3), and the stopping-block (block 7) which is linked to the stopping-syringe and the cell-block through a 3-way tap contained in block 8. Blocks 4, 5, and 6 are connecting blocks, and 1a and 9 are pressure-plates.

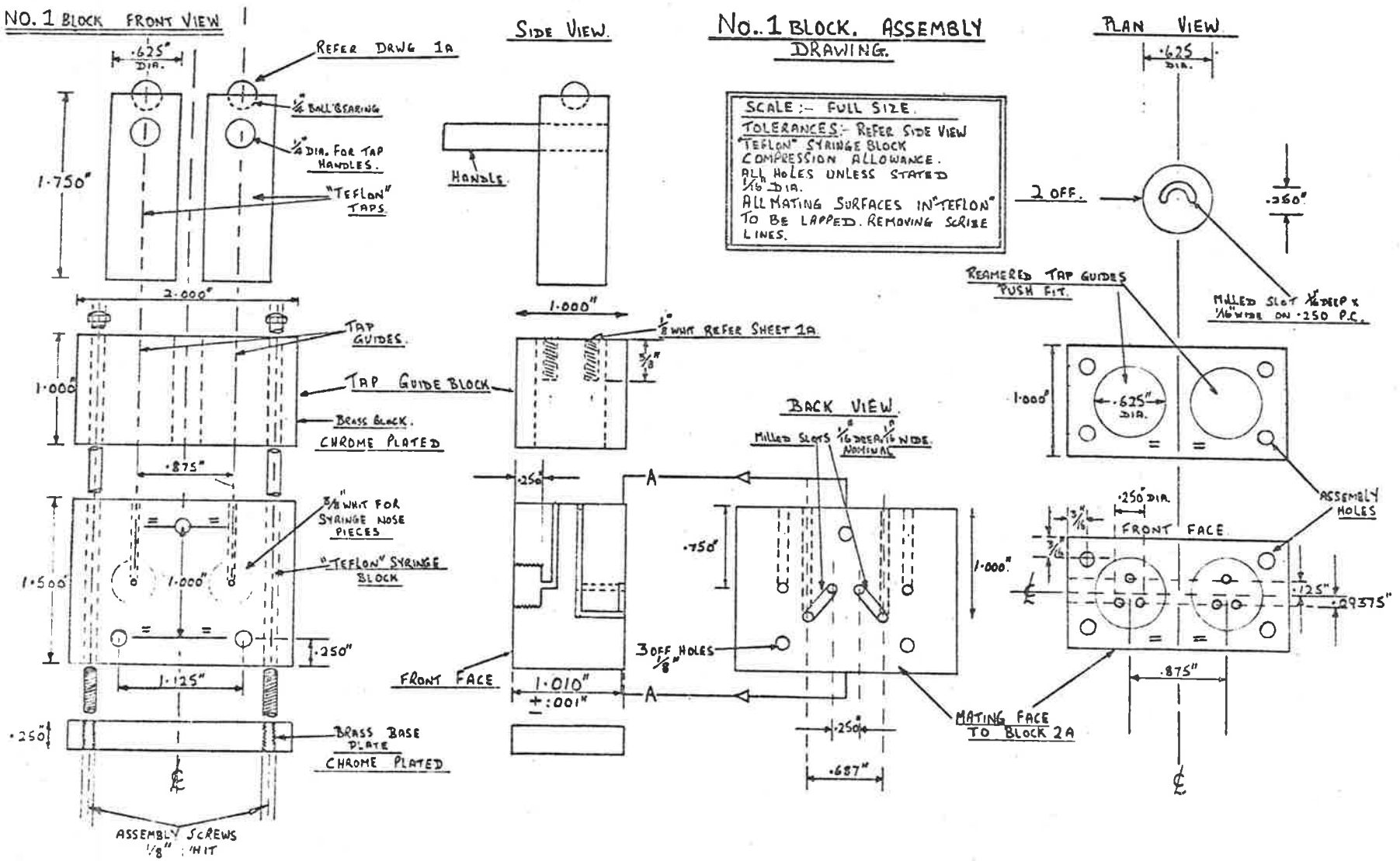
NO. 1 BLOCK FRONT VIEW
SIDE VIEW.
NO. 1 BLOCK. ASSEMBLY DRAWING.
PLAN VIEW
SCALE :- FULL SIZE.
TOLERANCES :- REFER SIDE VIEW
"TEFLON" SYRINGE BLOCK COMPRESSION ALLOWANCE.
ALL HOLES UNLESS STATED 1/16 DIA.
ALL MATING SURFACES IN "TEFLON" TO BE LAPPED. REMOVING SCRIBE LINES.
.625" DIA.
REFER DRWG 1A
1/4" BALL BEARING
1/4" DIA. FOR TAP HANDLES.
"TEFLON" TAPS
1.750"
2.000"
TAP GUIDES.
TAP GUIDE BLOCK
1.000"
BRASS BLOCK. CHROME PLATED
.875"
3/8" WHT FOR SYRINGE NOSE PIECES
"TEFLON" SYRINGE BLOCK
1.500"
1.000"
.250"
1.125"
.250"
BRASS BASE PLATE CHROME PLATED
ASSEMBLY SCREWS 1/8" : WHIT
HANDLE
1.000"
1/8" WHT REFER SHEET 1A
5/8"
FRONT FACE
.250"
1.010" ±.001"
A
A
BACK VIEW.
MILLED SLOTS 1/16 DEEP X 1/16 WIDE NOMINAL
.750"
1.000"
3 OFF HOLES 1/8"
.250"
.687"
MATING FACE TO BLOCK 2A
2 OFF.
.250"
REAMED TAP GUIDES PUSH FIT.
MILLED SLOT 1/16 DEEP X 1/16 WIDE ON .250 P.C.
1.000"
.625" DIA.
.250" DIA.
3/16"
3/16"
FRONT FACE
ASSEMBLY HOLES
.125"
.9375"
.875"

PRESSURE PLATE ASSEMBLY DRAWING BLOCK 1

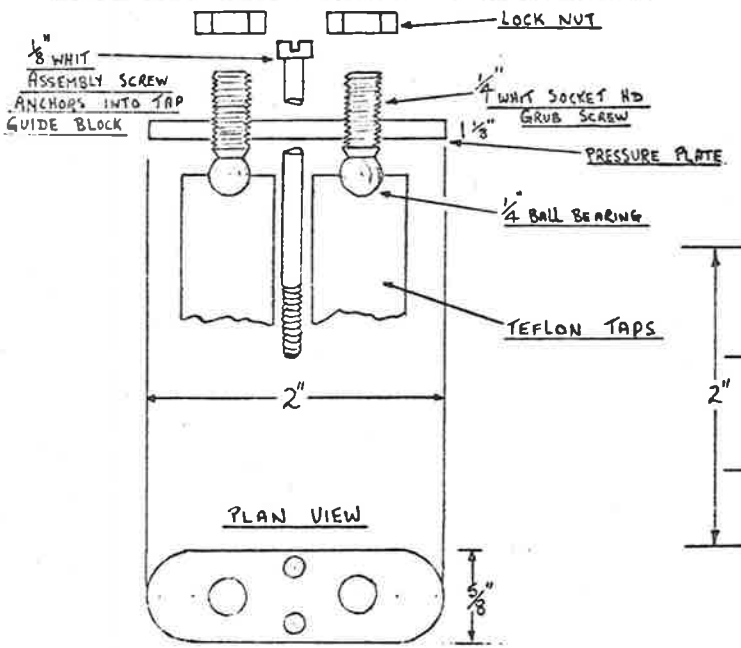

PRESSURE PLATE

FRONT SYRINGE AND ANCHOR PLATE.

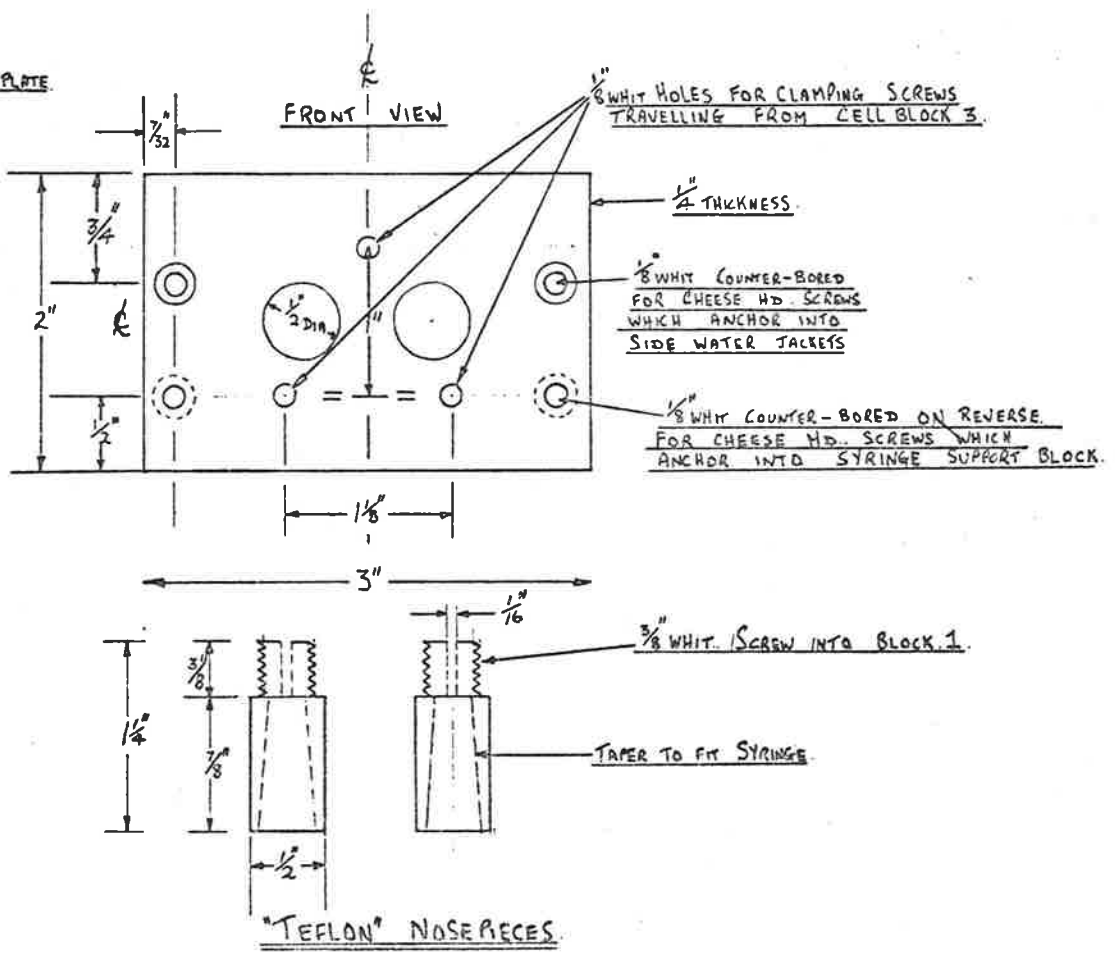

"TEFLON" NOSEPIECES.

PRESSURE PLATE BRASS CHROME PLATED
FRONT SYRINGE PLATE BRASS CHROME PLATED.

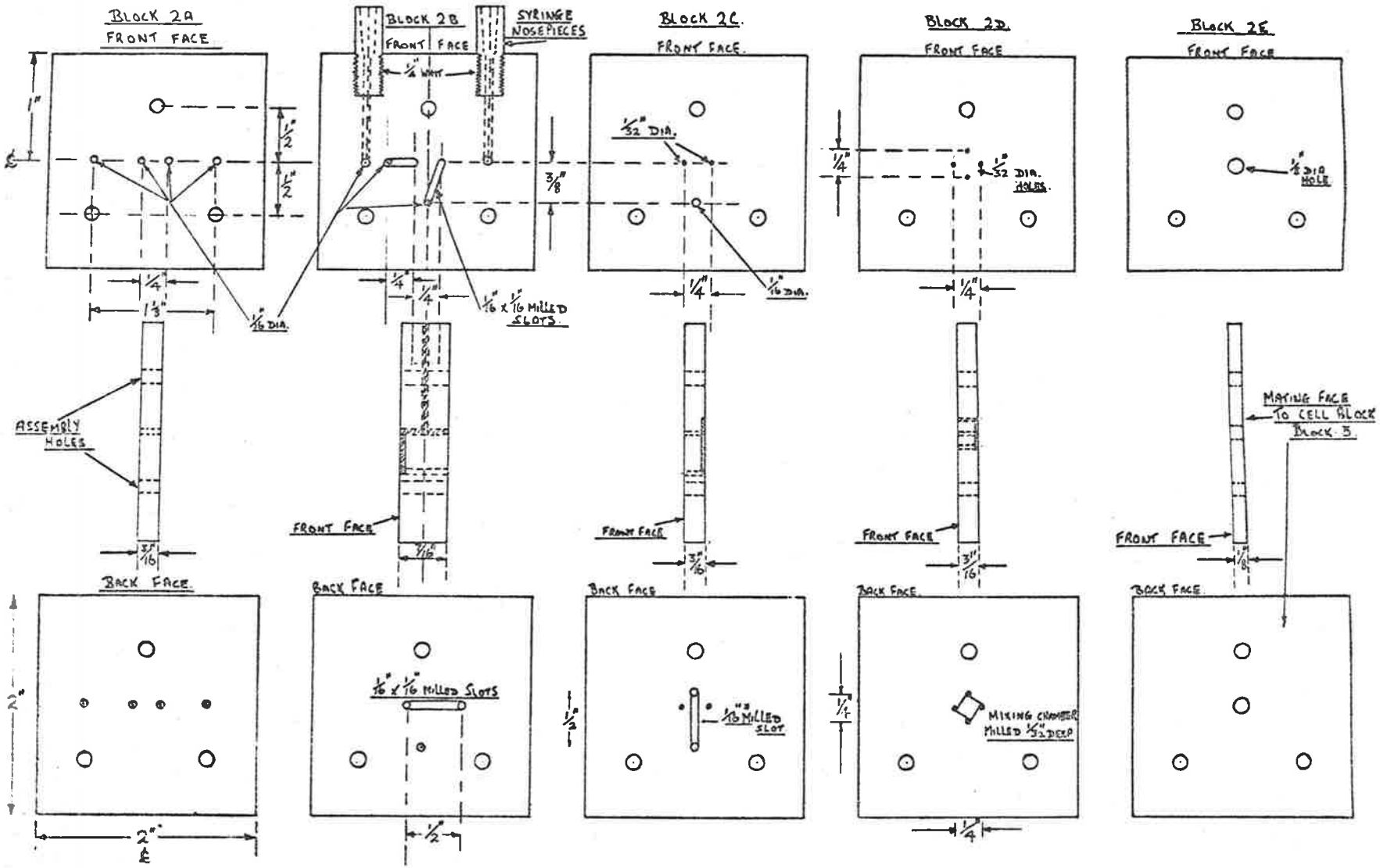
BLOCK 2A
FRONT FACE
BLOCK 2B
FRONT FACE
SYRINGE NOSEPIECES
BLOCK 2C.
FRONT FACE.
BLOCK 2D.
FRONT FACE
BLOCK 2E
FRONT FACE
1"
1/2"
1/2"
1/4"
1 1/3"
1/16 DIA.
1/4"
1/4"
1/16 x 1/16 MILLED SLOTS.
3/8"
1/32" DIA.
1/16 DIA.
1/4"
1/4"
1/32" DIA. HOLES.
1/8" DIA HOLE
ASSEMBLY HOLES
FRONT FACE
FRONT FACE
FRONT FACE
FRONT FACE
MATING FACE TO CELL BLOCK BLOCK 3
3/16"
3/16"
3/16"
3/16"
BACK FACE.
BACK FACE
BACK FACE.
BACK FACE
BACK FACE
2"
2"
1/16" x 1/16" MILLED SLOTS
1/2"
1/16" MILLED SLOT
1/2"
MIXING CHAMBER MILLED 1/32" DEEP
1/4"
1/4"
1/2"

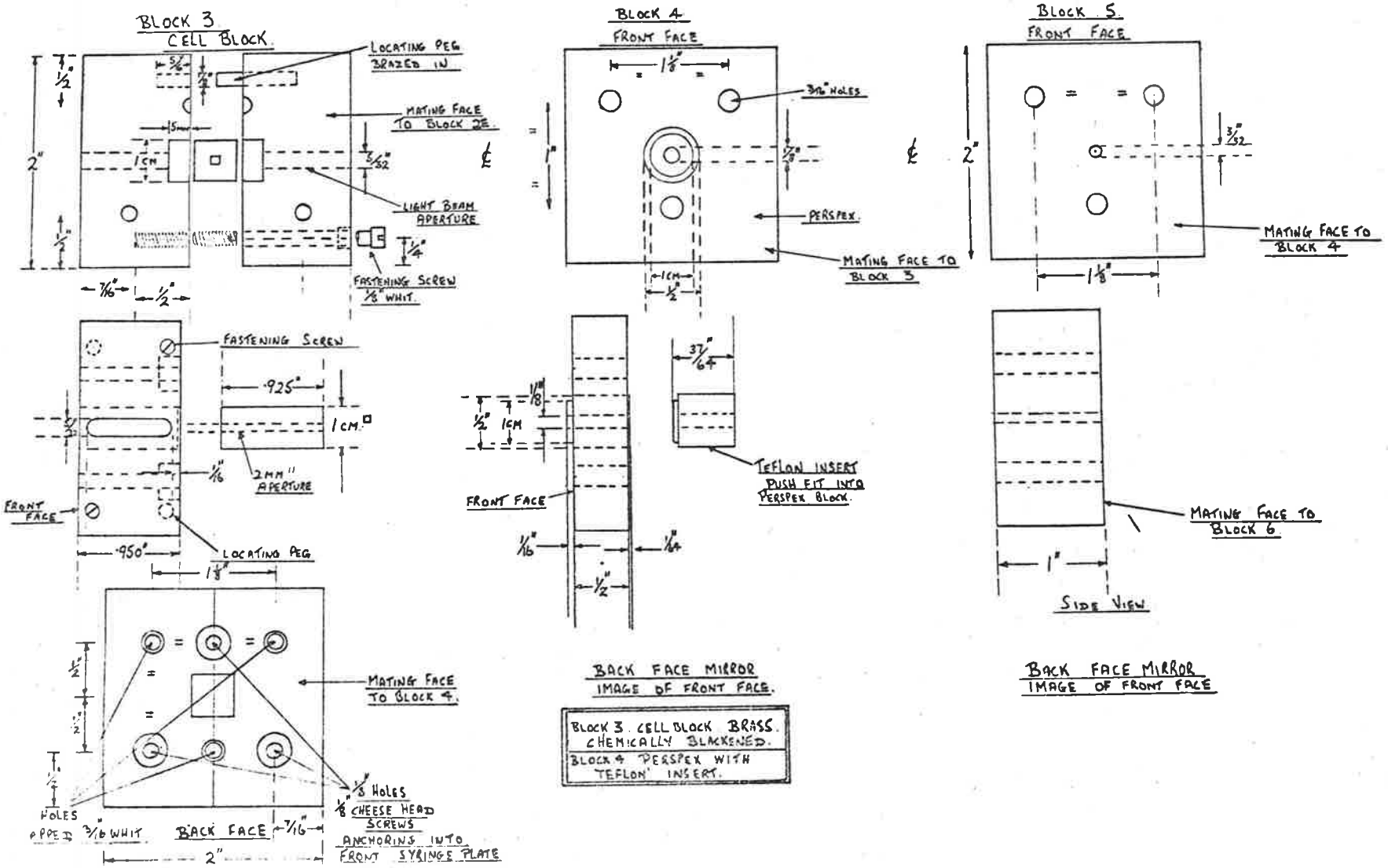
BLOCK 3
CELL BLOCK.
LOCATING PEG BRAZED IN
MATING FACE TO BLOCK 2E.
LIGHT BEAM APERTURE
FASTENING SCREW 1/8" WHIT.
FASTENING SCREW
·925"
1 CM.
2MM" APERTURE
FRONT FACE
·950"
LOCATING PEG
1 1/8"
MATING FACE TO BLOCK 4.
1/8" HOLES
1/8" CHEESE HEAD SCREWS ANCHORING INTO FRONT SYRINGE PLATE
HOLES TAPPED 3/16 WHIT
BACK FACE
2"
BLOCK 4
FRONT FACE
1 1/8"
3/16" HOLES
PERSPEX.
MATING FACE TO BLOCK 3
1 CM
1/2"
TEFLON INSERT PUSH FIT INTO PERSPEX BLOCK.
FRONT FACE
BACK FACE MIRROR IMAGE OF FRONT FACE.
BLOCK 5
FRONT FACE
MATING FACE TO BLOCK 4
MATING FACE TO BLOCK 6
1"
SIDE VIEW
BACK FACE MIRROR IMAGE OF FRONT FACE
BLOCK 3. CELL BLOCK BRASS. CHEMICALLY BLACKENED.
BLOCK 4 PERSPEX WITH TEFLON' INSERT.

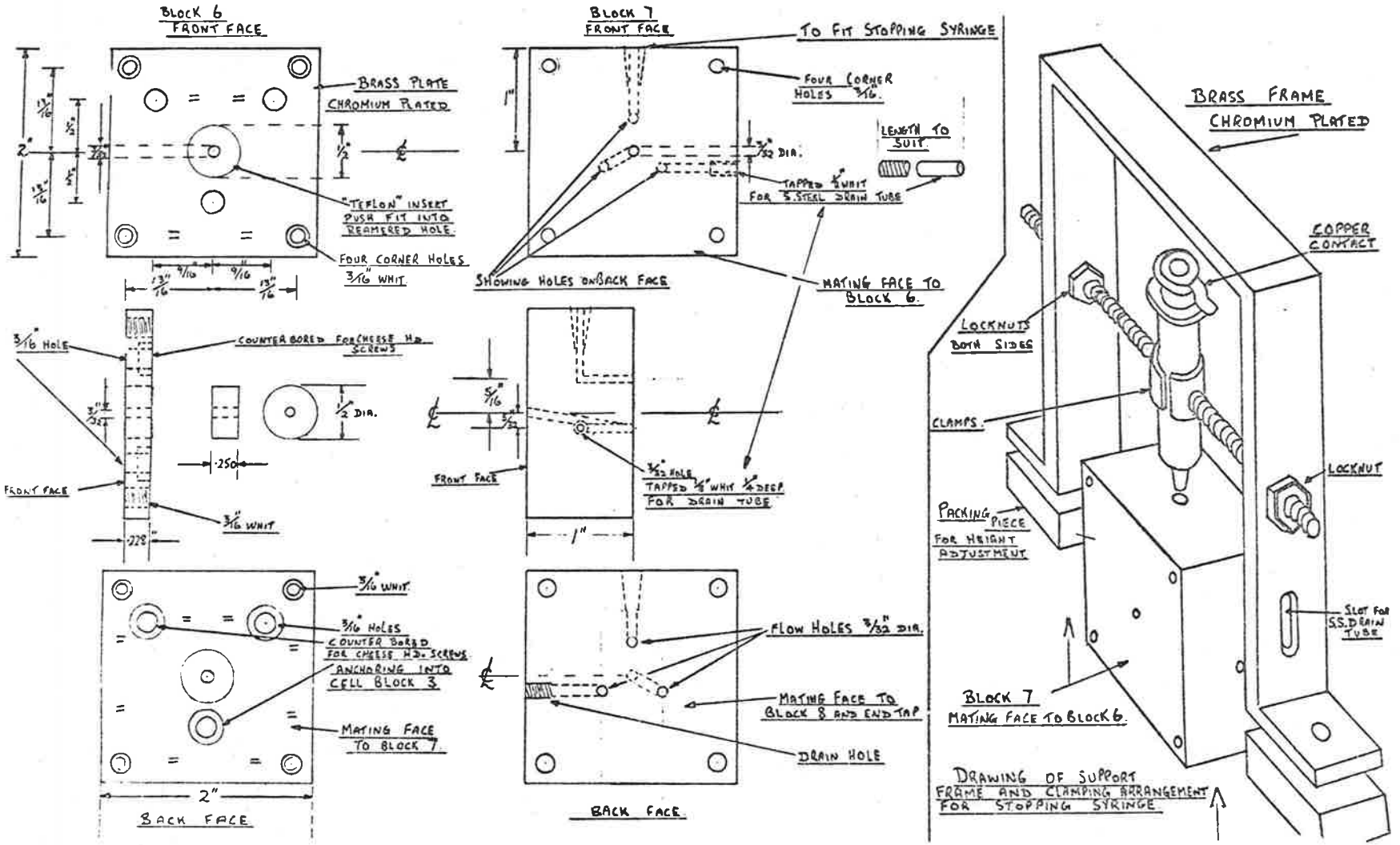
BLOCK 6
FRONT FACE
BRASS PLATE
CHROMIUM PLATED
"TEFLON" INSERT
PUSH FIT INTO
REAMERED HOLE
FOUR CORNER HOLES
3/16" WHIT
3/16" HOLE
COUNTER BORED FOR CHEESE HD. SCREWS
FRONT FACE
3/16" WHIT
3/16" WHIT
3/16" HOLES
COUNTER BORED
FOR CHEESE HD. SCREWS
ANCHORING INTO
CELL BLOCK 3
MATING FACE
TO BLOCK 7
2"
BACK FACE
BLOCK 7
FRONT FACE
TO FIT STOPPING SYRINGE
FOUR CORNER
HOLES 3/16"
LENGTH TO
SUIT
TAPPED 1/4" WHIT
FOR S.STEEL DRAIN TUBE
SHOWING HOLES ON BACK FACE
MATING FACE TO
BLOCK 6.
FRONT FACE
3/32" HOLE
TAPPED 1/8" WHIT 1/4" DEEP
FOR DRAIN TUBE
FLOW HOLES 3/32" DIA.
MATING FACE TO
BLOCK 8 AND END TAP
DRAIN HOLE
BACK FACE
BRASS FRAME
CHROMIUM PLATED
COPPER
CONTACT
LOCKNUTS
BOTH SIDES
CLAMPS
LOCKNUT
PACKING PIECE
FOR HEIGHT
ADJUSTMENT
SLOT FOR
S.S. DRAIN
TUBE
BLOCK 7
MATING FACE TO BLOCK 6.
DRAWING OF SUPPORT
FRAME AND CLAMPING ARRANGEMENT
FOR STOPPING SYRINGE

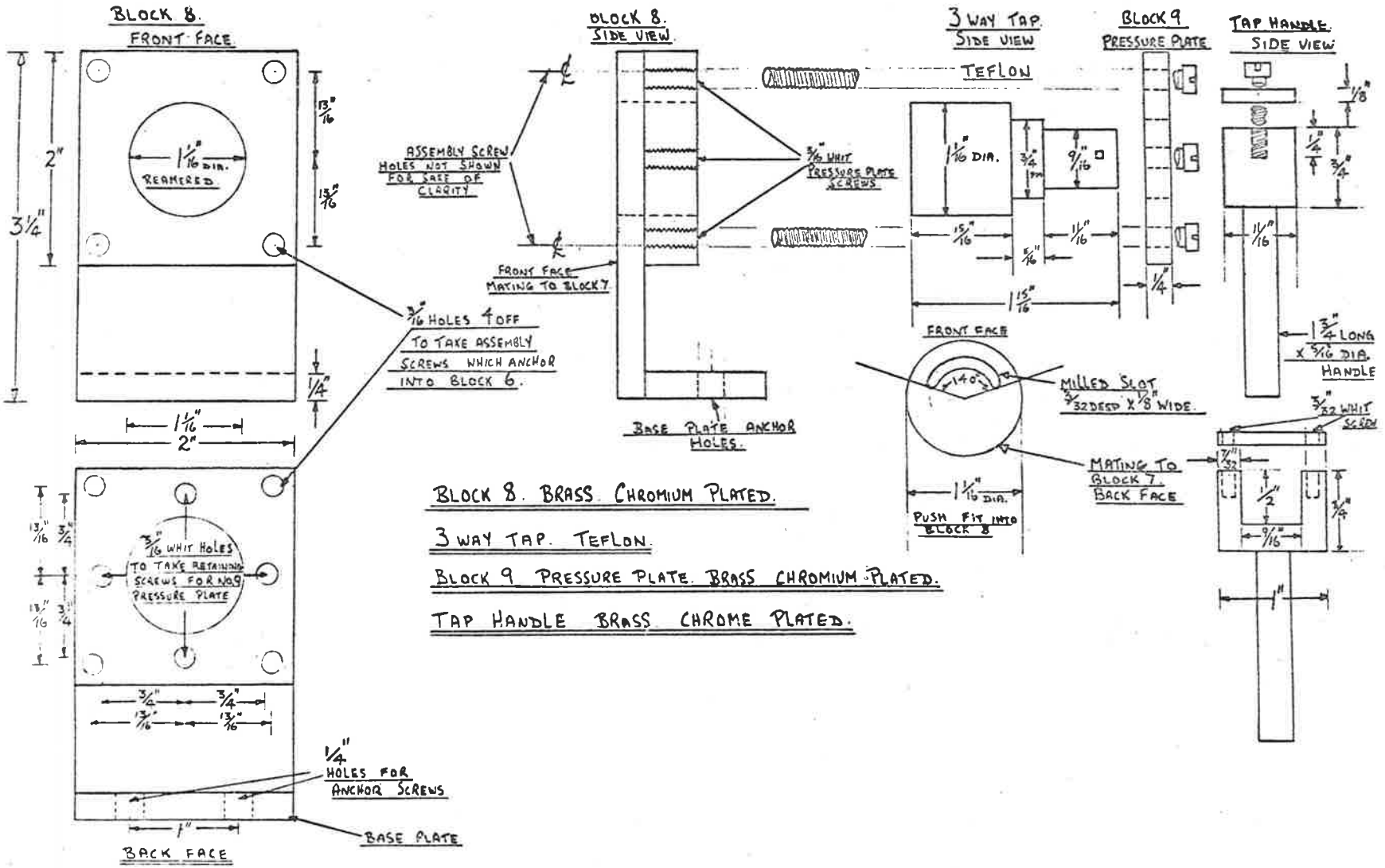

BLOCK 8. BRASS. CHROMIUM PLATED.

3 WAY TAP. TEFLON.

BLOCK 9 PRESSURE PLATE. BRASS CHROMIUM PLATED.

TAP HANDLE BRASS CHROME PLATED.

Appendix II Program Amod

This program was designed to calculate first- and second-order rate constants from plots of $\log_{10}$ C vs t, where C is the concentration (M) and t is the time (secs), using a least squares subroutine. The function, $\log_{10}$ C, is directly proportional to $\log_{10}$ (Vo - Vt), where V is the intensity of transmitted light measured in volts, Vo is the base line voltage, and Vt (= Vo - ΔV) is the voltage at time t. Also incorporated into Program Amod is Subroutine Reader which provides a means for calculating both weighted and unweighted values of the rate constants.

Below is a listing of the input data, and Program Amod.

INPUT DATA

CARD NO.	COLUMNS	CONTENTS
1	1-80	NAME OF JØB
2	1	CHARACTER INDICATES LAST JOB
	2-3	NUMBER OF POINTS (I2)
	7	CHARACTER INDICATES PLOT
3	1-6	VOLTS/DIVISION (F6.3)
	7-13	TIME/DIVISION (F7.6)
	14-18	TIME OF MAXIMUM (F5.2)
	30-35	BASELINE VOLTAGE(F6.3)
	36-38	MAGNIFICATION FACTOR (F3)
	41	CHARACTER INDICATES CARD 4 TO BE READ
	42	0 FOR UNWEIGHTED L.S.; 1 FOR WEIGHTED L.S. 2 FOR BOTH
4	1-5	EXTINCTION COEFF. (F5)
	6-11	CELL LENGTH (CM) (F6.3)

5	1-5	TIME(1)	(F5.2)
	6-10	VOLTAGE(1)	(F5.2)
	11-15	TIME(2)	
	16-20	VOLTAGE(2)	
	ETC.	8 PAIRS OF READINGS/CARD	

```
    PROGRAM AMOD (INPUT,OUTPUT)
    DIMENSION NAME(10),T(100),C(100),C1(100),C2(100),W1(100),W2(100)
    DIMENSION D(100),C3(100,2)
    COMMON/A1/E,CL,TZ
 1  READ 2, (NAME(I),I=1,8)
 2  FORMAT(8A10)
    READ 3, N,NV,LOT
 3  FORMAT(A1,I2,3X,A1)
    CALL READER(T,C,W1,NV,NW)
    TZ = TZ*1000000.
    SW1 = 0.0
    SW2 = 0.0
    DO 4 I=1,NV
    C1(I) = ALOG(C(I))
    C2(I) = 1.0/C(I)
    D(I) = C(I)*E*CL
    W2(I) = C(I)*W1(I)
    SW1 = SW1 + W1(I)
 4  SW2 = SW2 + W2(I)
    L = 0
    IF(NW-1) 41,6,6
41  DO 5 I=1,NV
    W1(I) = 1.0
 5  W2(I) = 1.0
    K =
    GO TO 8
 6  DO 7 I-1,NV
    W1(I) = W1(I)*NV/SW1
 7  W2(I) = W2(I)*NV/SW2
    K = 1
 8  CALL LSQU(T,C1,W1,NV,S1,R1,YI1,SINT1, SS1)
    CALL LSQU(T,C2,W2,NV,S2,R2,YI2,SINT2,SS2)
    L = L + 1
    S1 = ABS(S1)
    IF(L-1) 81,81,121
81  CZ = (T(2) - T(1))/(C2(1)*T(2) - C2(2)*T(1))
    PRINT 9, (NAME(I),I=1,8),E,CL
```

```
  9  FORMAT(1H1,10X,8A10,///,10X,*EXTINCTION COEFFICIENT =*,F5.0,/,10X,
    $ *CELL LENGTH =*,F6.3,///)
     PRINT 10
 10  FORMAT(12X,*TIME*,14X,*CONC*,15X,*LN(CONC)*,15X,*1/CONC*,21X,
    $ *O.D.*,/,10X,*(X1000)*,11X*(X1000)*,38X,*(X.001)*,/)
     DO 101 I=1,NV
     A1 = 1000.*T(I)
     A2 = 1000.*C(I)
     A3 = 0.001*C2(I)
101  PRINT 11, A1,A2,C1(I),W1(I),A3,W2(I),D(I)
 11  FORMAT(10X,F8.4,10X,F8.4,10X,F6.3,* (*,F5.3,*)*,10X,F8.4,* (*,
    $F5.3,*)*,10X,F8.4)
     PRINT 12, TZ,CZ
 12  FORMAT(//,10X,*TIME TO REACH MAX CONC = *,F6,*USEC*,10X,*EXTRAPOL
    $ATED CONCENTRATION AT T=0 IS*,E10.3,*M*)
121  IF(K) 122,122,124
122  PRINT 123
123  FORMAT(///,5X,*UNWEIGHTED LEAST SQUARES PARAMETERS*,//)
     GO TO 126
124  PRINT 125
125  FORMAT(///,5X,*WEIGHTED LEAST SQUARES PARAMETERS*,//)
126  PRINT 13, S1,SS1,YI1,SINT1,R1
 13  FORMAT(10X,*1ST ORDER K =*,F7.3,2X,*+/-*,F7.3,/,10X,*Y INTERCEPT =
    $*,F7.3,2X,*+/-*,F7,3,/,10X,*CORRELATION COEFFICIENT =*,F8.5)
     S2 = 0.001*S2
     SS2 = 0.001*SS2
     YI2 = 0.001*YI2
     SINT2 = 0.001*SINT2
     PRINT 14, S2,SS2,YI2,SINT2,R2
 14  FORMAT(//,10X,*2ND ORDER K =*,F7.3,2X,*+/-*,F7.3,2X,*X1000*,/,10X,
    $*Y INTERCEPT = *,F7.3,2X,*+/-*,7.3,2X,*X1000*,/,10X,*CORRELATION C
    $OEFFICIENT =*,F8.5)
     IF(L-1) 141,141,142
141  IF(NW-1) 142,142,41
142  IF(LOT.EQ.1H ) GO TO 16
     CALL SCALE (C1,C2,C3,NV,FACT,T)
     PRINT 15, (NAME(I),I-1,8),FACT
 15  FORMAT(/,10X,8A10,/,10X,*FIRST ORDER VALUES MADE POSITIVE AND MULT
    $IPLIED BY*,F8)
 16  IF(N.EQ.1H ) GO TO 1
     STOP
     END AMOD

     SUBROUTINE READER(T,V,W,NV,NW)
     DIMENSION T(1),V(1),W(1)
     COMMON/A1/E,CL,TZ
     READ 1, VPD,TPD,TZ,VO,FMAG,N,NW
     IF(N.NE.1H ) 2,4
```

```
1  FORMAT(F6.3,F7.6,F5.2,11X,F6.3,F3,2X,2A1)
2  READ 3, E,CL
3  FORMAT(F5,F6.3)
4  READ 5, (T(I),V(I),I=1,NV)
5  FORMAT(16F5.2)
   VPD = VPD/FMAG
   TPD = TPD/FMAG
   TZ = TZ*TPD
   DO 6 I-1,NV
   VT = VO/(VO -VPD*V(I))
   V(I) = ALOG10(VT)/(E*CL)
   R(I) = TPD*T(I) - TZ
6  W(I) = VT*V(I)
   RETURN
   END READER

   SUBROUTINE LSQU(X,Y,W,N,S,R,YI,SERINT,SERS)
   DIMENSION X(1),Y(1),W(1)
   XY=X2=Y2=CX=CY=0.0
   DO 2 I=1,N
   CX = CX + X(I)*W(I)
   CY = CY + Y(I)*W(I)
   XY = XY + X(I)*Y(I)*W(I)
   X2 = X2 + X(I)*X(I)*W(I)
2  Y2 = Y2 + Y(I)*Y(I)*W(I)
   CX = CX/N
   CY = CY/N
   X2 = X2/N
   SX = SQRT(X2 - CX*CX)
   SY = SQRT(Y2 - CY*CY)
   S = (XY/N - CY*CY)/(SX*SX)
   YI = CY- S*CX
   R = S*SX/SY
   SERY = SY*SQRT((1.0-R*R)/(N-2.0))
   SERS = SERY/SX
   SERINT = SERY*SQRT(X2)/SX
   RETURN
   END LSQU

   SUBROUTINE SCALE(C1,C2,C3,NV,FACT,T)
   RETURN
   END SCALE
```

Appendix III Program Actpar

This program was designed to calculate the activation parameters, E, $\Delta H^{\ddagger}$, and $\Delta S^{\ddagger}$, from plots of $\log_{10}$ k vs 1/T, where k is the rate constant and T is the absolute temperature measured in °K, using the least squares subroutine, LSQU. The entropy of activation term $\Delta S^{\ddagger}$, was determined both from the intercept at 1/T = 0 and by direct substitution of k and $\Delta H^{\ddagger}$ into the transition-state equation.

$$k = \frac{k_B T}{h} \cdot e^{\Delta S^{\ddagger}/R} \cdot e^{-\Delta H^{\ddagger}/RT}$$

where k_B = Boltzmann's constant and h = Planck's constant.

Below is a listing of the input data, and Program Actpar.

INPUT DATA

CARD NO.	COLUMNS	CONTENTS
1	1	CHARACTER INDICATES LAST JOB
	11-12	NUMBER OF POINTS (I2)
2	1-10	PLANCK'S CONSTANT (E 10.3)
	11-20	BOLTZMANN'S CONSTANT (E 10.3)
	21-30	GAS CONSTANT (F 10.0)
	31-40	TEMPERATURE (F 10.0)
	41-50	RATE CONSTANT (F 10.0)
3--	1-10	TEMPERATURE (F 10.0)
	11-20	RATE CONSTANT (F 10.0)
	ETC.	4 PAIRS OF READINGS/CARD

```
      PROGRAM  ACTPAR (INPUT,OUTPUT)
      DIMENSION VT(100),RC(100),X(100),Y(100)
    2 READ1,M,N
    1 FORMAT(A1,9X,I2)
      READ 101,PC,BC,GC,T,RCC
  101 FORMAT(2E10.3,3F10.0)
      READ 100,(VT(I),RC(I),I=1,N)
  100 FORMAT(8F1010)
      DO 3 I=1,N
      X(I)=1/VT(I)    $    Y(I)=ALOG(RC(I))
    3 CONTINUE
      CALL LSQU(X,Y,N,S,R,YI,SERINT,PEI, SERS,PES)
      E=-GC*S
      SEE=PES*E/100.
      H=E-GC*T
      SEH=PES*H/100.
      RK=EXP(S/T+YI)
      EN=GC*ALOG((RK*PC*EXP(H/(GC*T)))/(BC*T))
      EN2=GC*ALOG((RCC*PC*EXP(H/(GC*T)))/(BC*T))
      ENT=GC*(YI-ALOG(BC*T/PC))
      SEENT=PEI*ENT/100.
      PRINT 200
  200 FORMAT(1H1.30X,*ACTIVATION    PARAMETERS*,///)
      PRINT 201
  201 FORMAT(25X,*X*,30X,*Y*,//)
      PRINT 202,(X(I),Y(I),I-1,N)
  202 FORMAT(20X,E10.3,20X,E10.3)
      PRINT 203,S,YI,SERS,PES,SERINT,PEI,R,SEE,SEH
  203 FORMAT(///.*    SLOPE = *,E10.3,/,*    Y INT = *,E10.3,/,*    S,E.
     * SLOPE = *,E10.3,/,*    P.E. SLOPE =*,F6.2,/,*    SLE. INTERCEPT =
     **,E10.3,/,*    P.E. INTERCEPT = *,F6.2,/,*    CORRELATION COEFF =
     **,F8.4,/,*    S.E. ACT. ENERGY =*,E10.3,/,*    S.E. ENTHALPY= *,
     1E10.3)
      PRINT 204,T
  204 FORMAT(///,*    TEMP.= *,F7.2)
      PRINT 207
  207 FORMAT(//,   * ENTROPY CALCULATED BY DIRECT SUBSTITUTION INTO T. S
     1. EQUATION*)
      PRINT 205,E,H,EN
  205 FORMAT(//,*    ACT. ENERGY= *,F7,/,*    ENTHALPY= *,F7,/,
     1*    ENTROPY= *,F6.2)
      PRINT 208
  208 FORMAT(//,   *ENTROPY CALCULATED FROM INTERCEPT*)
      PRINT 206,E,H,ENT,SEE,SEH,SEENT
  206 FORMAT(//,*    ACT. ENERGY= *,F7,/,*   ENTHALPY= *,F7,/,*     ENTR
     1OPY=*,F6.2,/,*     S.E. ACT. ENERGY= *,E10.3,/,*   S.E. ENTHALPY =
     1 *,E10.3,/,*    S.E. ENTROPY= *,E10.3)
      PRINT 205,E,H,EN2
      IF(M.EQ.1H) GOTO 2
      END ACTPAR
```

```
      SUBROUTINE LSQU(X,Y,N,S,R YI,SERINT,PEI,SERS,PES)
      DIMENSION X(100),Y(100)

C     SUBROUTINE LSQU APPLIES LEAST SQUARES METHOD TO V VS X

      XY=X2=Y2=CX=CY=0.
      DO 2 I=1,N
      CX=CX+X(I)
      CY=CY+Y(I)
      XY=XY+X(I)*Y(I)
      X2=X2+X(I)*X(I)
    2 Y2=Y2+Y(I)*Y(I)
      XB=CX/N
      YB=CY/N
      SX=(X2/N-XB*XB)**0.5
      SY=(Y2/N-YB*YB)**0.5
      R=(XY/N-XB*YB)/(SX*SY)

C     CALCULATE SLOPE OF LINE OF BEST FIT

      S=(R*SY)/SX
      YI=YB-S*XB
      SYY=Y2-CY*CY/N
      SXX=X2-CX*CX/N
      SERY=SQRT((SYY-S*S*SXX)/(N-2.0))

C     CALCULATE STANDARD ERROR IN SLOPE AND INTERCEPT

      SERS=SERY/SQRT(SXX)
      SERINT=SERY*SQRT(1.0/N+XB*XB/SXX)
      PCSE=(SERS/S)*100.0
      PES=ABS(PCSE)
      PEI=(SERINT*100.0)YI
      PEI=ABS(PEI)
      RETURN
      END LSQU
```